COMMUNICATIONS

Dear reader,

This issue of the Communications is devoted to the problems of traffic effects on structures and environment. The research activities at the Faculty of Civil Engineering in this field are focused on the research projects solved mainly at the Department of Structural Mechanics, Department of Structures and Bridges, Department of Railway Engineering, and Department of Highway Engineering.

The traditional problems of the engineering construction proposals are complemented with new urgent problems of safety and reliability, energy saving, the environmental protection and problems of structure diagnostics. It is the impressive appeal to design constructions of high quality. The special requests are put on the traffic structures – railway and road engineering structures, bridges, tunnels and especially on their dynamic loading and interaction problems of the system vehicle – construction – environment components.

Ten papers in this Volume are written by authors from the Faculty of Civil Engineering of the University of Zilina and five are written by authors from other work places. The papers cover a broad spectrum of structural engineering problems viewed from theoretical, practical and computational aspects in this field. I am convinced that the papers of this volume adequately reflect the present theoretical and experimental research carried out at the Faculty of Civil Engineering.

Milan Moravcik

Josef Vican – Jozef Gocal – Jozef Jost *

FATIGUE RESISTANCE OF TYPICAL FATIGUE PRONE RIVETED STEEL RAILWAY BRIDGE STRUCTURAL DETAIL

There are still a lot of riveted steel railway bridges built in the first half of 20th century in service, and so it is important to pay attention to their evaluation. Their fatigue resistance represents one of the most determining factors on decision making process oriented to possibility of their further exploitation after finishing their planned service life. The standard method of fatigue assessment according to Eurocode EN 1993-1-9 is based on categorization of structural details, which reflects their predisposition to fatigue failure. The paper deals with laboratory investigation of the riveted connection of stringer to cross beam of a railway bridge deck. This structural detail is typical by frequent occurrence of fatigue cracks, but its categorization according to standard mentioned above is at least questionable. In order to investigate and define the fatigue category of this detail more properly, the laboratory tests on specially adapted specimens were performed.

Keywords: bridge fatigue lifetime, fatigue resistance, fatigue detail categorisation, stringer to cross-beam connection.

1. Introduction

The aim of fatigue assessment is to verify that the fatigue life of the evaluated structure corresponds to its planned service life time. The assessment is based on evaluating critical structural details prone to fatigue failure, which are classified according to corresponding fatigue categories specified in EN 1993-1-9 [1]. When the detail category is known, the fatigue assessment may be done using the appropriate S-N curve expressing the fatigue life of the detail dependent on the constant cyclic stress range caused by variable load. Since the bridges are specific by stochastic character of the traffic load, the S-N curves used for their fatigue assessment were modified in order to consider a variable spectrum of stress ranges. The riveted connections of stringer to cross-beams in the case of railway bridges with open bridge decks are typical details prone to fatigue cracks. Webs of stringer and cross-beam are only connected without flange mutual connecting, so that the joint is usually verified on the shear and normal forces only [7]. Due to connection arrangement and certain bending stiffness, the bending moment is arising and producing normal stresses causing the crack in the form given in Fig. 1.

Fig. 1 Example of fatigue crack in the investigated detail

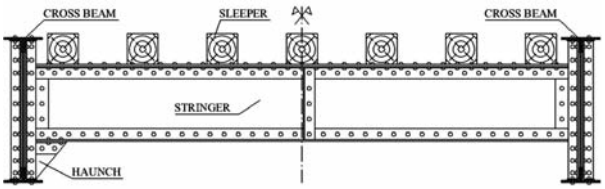

Fig. 2 Arrangement of a typical stringer to cross-beam connection with/without reinforcing haunches

However, in the case of the mentioned type of connection, the fatigue detail categorisation is absent in [1]. Some recommendations for categorization of the riveted details may be found in works of Adamson and Kulak [2] or Matar [3], which deal with riveted details of bridge decks, bracings and connections of bridge decks to main girders, but the detail mentioned above is not able to be categorized even according to these works. Therefore, the laboratory tests of the riveted detail were realized at the Department of structures and bridges to obtain the detail fatigue resistance and to define the detail fatigue categorisation.

* **Josef Vican, Jozef Gocal, Jozef Jost**
Department of Structures and Bridges, Faculty of Civil Engineering, University of Zilina, Slovakia E-mail: josef.vican@fstav.uniza.sk

2. Laboratory specimens

Because of limited possibilities of the applied pulsating device as well as due to the economic aspect, the common static scheme of real stringers as a simply supported beam (supported by cross-beams), loaded by reactions from sleepers (see Fig. 2), could not be applied. Therefore, a cantilever loaded by one force at the free end was used as the static scheme for laboratory testing (see Fig. 3). Six specimens were manufactured of steel S235 in all. All specimens consisted of the web from steel plate of P 10 × 390 – 1115 and flanges made of two angles L 80 × 80 × 8 – 995 mm connected to the web by means of rivets with diameters of 22 mm. Stringer was connected to the hot rolled cross-beam of IPE 700 by means of two angles L 80 × 80 × 8 – 692 mm using 16 bolts of M 24 – 8.8 in the case of specimens of type I and II. Three specimens were reinforced by triangular haunches at the connection to cross-beam (Fig. 3b) and other three specimens were manufactured without the haunches (Fig. 3a).

After testing the six aforesaid specimens, other five specimens of type III (see Fig. 3c) were obtained adjusting the previously tested stringers. The connecting angles were cut off and the new connecting angles L 120 × 120 × 12 – 400 mm were riveted to the free end of the specimens by means of 10 bolts M24 – 8.8. The new connecting angles were shortened compared to previous six specimens in order to situate measuring gauges above the first and below the last rivet, respectively, since the fatigue crack was supposed to develop from this point. Thus, eleven test specimens were tested altogether. One of the specimens was used for destructive tests to determine the material characteristics. The following material characteristics were obtained by testing – the yield strength f_y = 244.92 MPa and the ultimate strength f_u = 360.77 MPa.

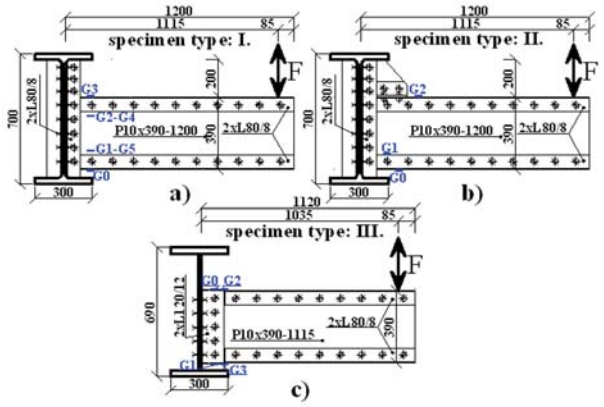

Fig. 3 Configuration of laboratory specimens without haunch (I), reinforced by haunch (II) and new specimens without haunch (III) and specimen gauge arrangement

3. Laboratory testing process

Firstly, the numerical calculations of the tested detail were accomplished using software SCIA Engineer to determine required maximum and minimum forces causing the needed stress ranges. The specimen types I and II were tested in 2009 and the testing process as well as the test results were described in [4]. Other five new specimens were tested in the laboratory of Transport Research Institute in Zilina from January to April 2010.

All the specimens were gradually subjected to fluctuating bending moment through the application of concentrated vertical load situated at the distance 1 115 mm from the supporting cross-beam (see Fig. 3), in the case of specimen type I and II and 1 035 mm, in the case of specimen type III, respectively. For all specimens, the loading force was floating between positive and negative limit values (see Fig. 3). At the start of fatigue test, each specimen was loaded statically at the maximum and minimum values of the loads that would be applied during the fatigue test. In the case of specimens with reinforcing triangular haunches the absolute values of maximum (positive) and minimum (negative) loading forces were different, i.e. the normal stresses in the observed points of the stringer web (see Fig. 3a) oscillated around the mean stress different from zero. In the case of specimens without haunches the absolute values of maximum (positive) and minimum (negative) loading forces were the same, i.e. the normal stresses in the observed points of the stringer web (see Fig. 3b) oscillated around the mean stress close to zero.

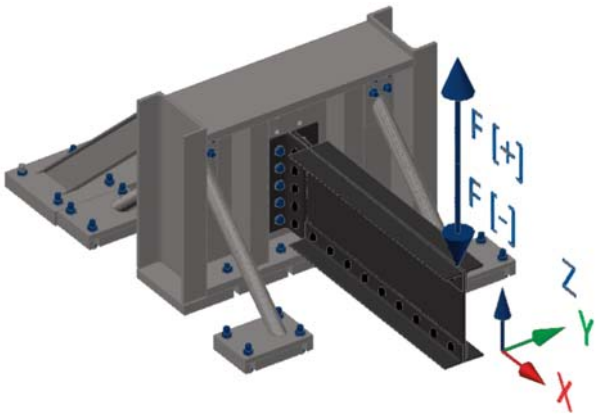

Fig. 4 Configuration of a laboratory specimen and the pulsating forces

Normal stresses in the stringer web were measured by means of gauges LY11-6/120 manufactured by Hottinger–Baldwin Messtechnik [6]. Location of gauges is shown in Fig. 3. Measured data was recorded by measuring equipment Spider 8, controlled by computer software Catman. Fatigue test arrangement is shown in Fig. 5.

4. Experimental results

The results of the experimental fatigue tests of the specimens described above are presented in the form of stress ranges and corresponding numbers of cycles to failure in Table 1. Specimens No. 1 – 6 had been tested previously, specimens of No. 7 – 10 rep-

Fig. 5 Illustration photos from fatigue tests

resent the results of the last tests in 2010. As it was mentioned above, eleven specimens altogether were experimentally investigated, but one specimen failed due to cracks in connecting angle, so that its result had to be rejected. In order to avoid this type of failure, the remaining four specimens were reinforced by means of triangular sheets welded between angle flanges according to Fig. 6.

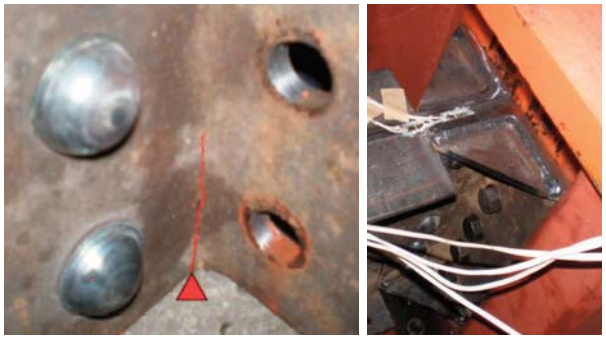

Fig. 6 Failure of specimen due to crack in the angle and reinforcement of this detail

Typical failure of the investigated detail is presented in Fig. 7. Picture on the left side shows the out-of-roundness of the hole diameter due to material cyclic plasticity after which the beam global deflection is rapidly growing. The picture on the right side shows the classic type of fatigue failure in the form of crack starting from the rivet hole.

Since the standard *S-N* curves are derived for fully reversed alternating stresses (stress ratio $R = \sigma_{min}/\sigma_{max} = -1$, mean stress $\sigma_m = 0$), the measured stresses alternating around the nonzero mean stress ($\sigma_m \neq 0$) in the case of specimens of type II had to be modified. The Goodman's mean stress correction relationship

Fig. 7 Types of detail fatigue failures

was applied, which defines the equivalent stress amplitude $\sigma_e = 0$ corresponding to the mean stress $\sigma_m = 0$ by the following equation

$$\sigma_e = \frac{\sigma_a}{1 - \frac{\sigma_m}{f_u}}, \tag{1}$$

where σ_a is stress amplitude corresponding to the mean stress $\sigma_m \neq 0$ and f_u is the ultimate material strength.

Different form of the cracks in the real bridge stringer webs (see Fig. 1) and the ones in tested specimens (see Fig. 7) was caused due to discrepant stringer static system. While stringer in Fig. 1 seems to be quasi simple supported beam, the static system of the tested stringers is cantilever (see Figs. 4 and 5).

These results were subjected to linear regressive analysis (see Fig. 8) according to the Appendix L in STN 73 1401[5], in which log $\Delta\sigma$ represents an independent variable and log N represents a dependent variable with normal probability distribution. Based on the regressive analysis results, the fatigue resistance of investigated detail corresponding to 2×10^6 cycles is $\Delta\sigma_C = 83.9$ MPa.

Results of fatigue tests Table 1

Specimen No.	Equivalent stress range $\Delta\sigma_e$ [MPa]	Number of cycles to failure N [cycles]
1	114.9	1 276 750
2	136.6	571 000
3	88.0	3 653 000
4	97.2	2 218 900
5	147.7	629 000
6	125.4	798 350
7	121.7	1 240 450
8	116.3	1 863 760
9	142.5	1 406 080
10	119.0	1 697 600

Therefore, the detail can be classified to the category 80 with characteristic fatigue strength $\Delta\sigma_C = 80$ MPa in accordance with [1].

5. Conclusion

The paper deals with experimental investigation of the fatigue resistance of the stringer to cross-beam riveted connection representing the common fatigue prone structural detail of existing steel railway bridges with open decks. After collection of all experimental data from tests realized in 2009 and 2010 and based on the obtained results of all performed fatigue tests, the detail could be classified to the category 80 according to EN 1993-1-9 [1].

Acknowledgements

This work was supported by the Scientific Grant Agency of the Slovak Republic under the project 1/0311/09 "Durability of the steel bridge structural members".

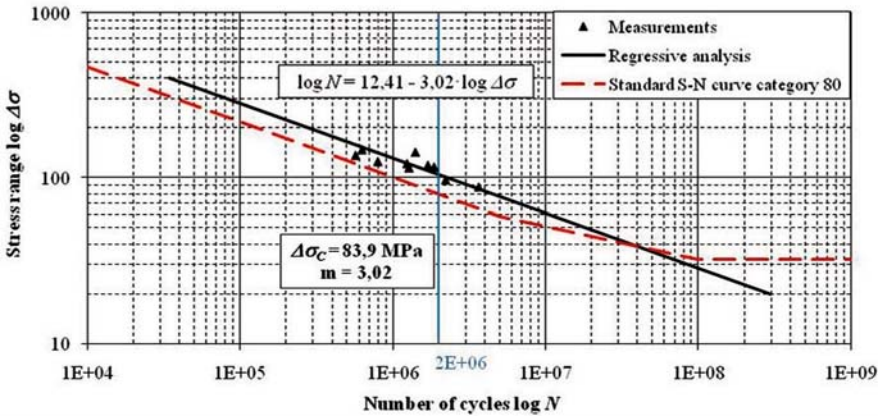

Fig. 8 Results of fatigue tests

References

[1] EN 1993-1-9, Eurocode 3: Design of Steel Structures, Part 1.9, *Fatigue,* Brussels, 2003.
[2] ADAMSON, D., KULAK, G.: Fatigue Tests of Riveted Bridge Girders, *Structural Engineering Report,* No. 210, University of Alberta., 1995.
[3] MATAR, E. B.: Evaluation of Fatigue Category of Riveted Steel Bridge Connections. *Structural Eng. Int'l, No.* 1, 2007, pp. 72-78.
[4] GOCAL, J., VICAN, J., HLINKA, R., JOST, J.: Laboratory Tests of a Typical Fatigue Prone Riveted Steel Railway Bridge Structural Detail, *Procedia Engineering* 2, 2010, ScienceDirect, Elsevier 2010, pp. 1761–1766.
[5] STN 73 1401 Design of Steel Structures, SUTN Bratislava 1998.
[6] TREBUNA, R., SIMCAK, F.: Handbook of Experimental Mechanics, *Edition of the Scientific and Technical Literature,* Kosice, 2007.
[7] VICAN, J., GOCAL, J., MELIS, B., KOTES, P., KOTULA, P: Real Behaviour and Remaining Lifetime of Bridge Structures, *Communications - Scientific Letters of the University of Zilina,* Vol. 2, 2008, ISSN 1335-4205, pp. 30-37.
[8] KALA, Z., PUKLICKY, L., OMISHORE, A., KARMAZINOVA, M., MELCHER, J.: Stability Problems of Steel-concrete Members Composed of High-strenght Materials. *J. of Civil Eng. and Management,* 2010, ISSN 1392-3730 print/ISSN 1822-3605 online, doi: 10.3846/jcem.2010.40, pp. 352–362, http: www.jcem.vgtu.It.

Jan Bujnak – Kazimierz Furtak *

INVESTIGATION ON CRACKS CREATION AND PROPAGATION IN CONCRETE SLAB OF COMPOSITE BEAMS

Analytical and experimental research have illustrated initiation of cracks in concrete deck immediately after its casting and placing on the upper flange of steel beams, especially prior to application of additional permanent load on composite element. Not only value of concrete shrinkage strain may influence creation and propagation of cracks in concrete. However ratio of deck reinforcement, cross-sectional area of reinforcement steel and strength of concrete can modify the process. Moreover, the ratio of steel beam flexural stiffness and flexural stiffness of concrete deck can be significant. Important shrinkage strains can occur at the lower concrete surface in the steel and concrete interface. Parametrical studies have provided the relationships illustrating impact of above parameters on crack aspect. The aim of the paper is to provide further details.

1. Introduction

Steel-concrete composite bridges are nowadays considered to be an appropriate structural system for the bridge engineering (Fig. 1). The innovative systems using concrete deck can act both as a roadway resisting local traffic loads and as an integral part of the bridge girders or trusses. In such a design, the concrete slab may act also as an integral part of the compression flanges of the stringers, and cross-beams. The contribution presents problems with rheological effects estimation and concrete cracking consideration, which can be found in the design of especially continuous type composite girders of the steel and concrete. Detail requirements for advanced design of concrete members of these composite steel and concrete structures as outputs of our investigation are given in graphic form.

Fig. 1 View of a continuous composite bridge concrete deck

2. Failure of the concrete slab by cracking

Composite slab of steel and concrete structural members as shown in Fig. 2 can be affected by tensile cracking induced by shrinkage. The strength degradation may be significant, if there were not enough reinforcing bars crossing the planes of cracking. Shrinkage of the concrete element depends on the environment and the constituents of the concrete. Corresponding strains can reach values accessing of 500 microstrains. Furthermore, shrinkage is time-dependent, and therefore the forces that are created will cause creep. Longitudinal strains can be induced in composite beam due to thermal gradients. The changes in strains are the similar as for shrinkage. The tensile cracking can also be initiated by effects of concrete hydration.

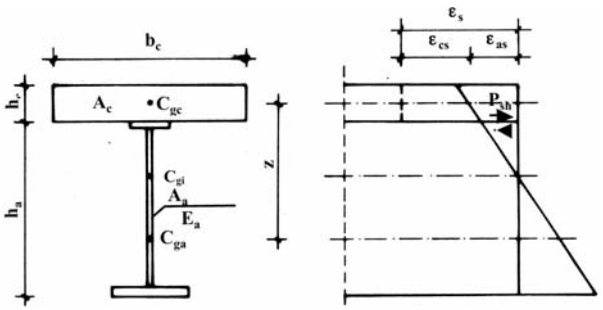

Fig. 2 Dimensions, forces in cross-section and longitudinal layout

The problem of tensile failure of the slab has not been subject of any extra fundamental investigation, because this question was

* **Jan Bujnak[1], Kazimierz Furtak[2]**
[1] Faculty of Civil Engineering, University of Zilina, E-mail: jan.bujnak@fstav.uniza.sk
[2] Kazimierz Furtak, Cracow University of Technology, Krakow, Poland

considered only subsidiary. The main attention is generally paid to the ultimate strength analyses. Design, analysis and detailing of the bridge concrete deck are actually just in general given in Eurocode 4 [1]. Primary, the slabs are required to be designed to transmit in-plane forces as well as bending moments and shears. Where composite action becomes effective as concrete hardens, effects of heat of hydration of cement and corresponding thermal shrinkage should be taken into account during the construction stage in areas where tension is expected. Specific measures should be provided to limit the effects of heat of hydration of cement. For simplification a constant temperature difference between the concrete section and the steel beam as concrete cooler can be assumed for the determination of the cracked regions. Unless a more accurate method is used, minimum reinforcement area for the slabs of composite beams is essential for limitation of crack width.

Factor specifying capacity of composite steel and concrete beams to prevent slab cracking due thermal effects can be expressed by the ratio of cross-sectional area of the structural steel beam A_a to cross-sectional area of concrete slab A_c, i.e. $\beta = A_a/A_c$. In fact this factor can be only approximate, because the beam shape or proportion of the flanges is not taken into account.

Based on results of the investigation [2, 3, 4], it can be supposed that thermal stresses created by effects of hydration of cement can be neglected for the values of ratio $\beta \leq 0.5$. Moreover, this effect occurs only during concrete casting and its curing, when magnitude of concrete modulus is rather smaller. Contraction of the concrete through shrinkage is of prime importance for tensile cracking in the case of a composite beam design. These short time-varying deformations of concrete affect greatly serviceability limit state. In hogging region, cracks due to concrete shrinkage during the hydration process have also a significant effect on the ultimate flexural capacity of composite beams. The magnitude and rate of development of the shrinkage strain depend on such characteristics as the relative humidity, temperature, mix proportions as well as shape and size of members. With time increasing, the rate of shrinkage decreases and the shrinkage strains approach its limit value ε_{sh} at the period obviously 28 days.

3. Stresses and strains in concrete slab produced by shrinkage

In the absence of shear connection, the concrete shrinkage in the sagging region would produce the contraction of the slab and slip at the steel-concrete interface. In reality, the shear connectors resist this lack of slip. Contraction of the concrete through shrinkage will induce deflections and flexural stresses in the steel that are in the same direction as those induced by gravity loads. In order to prevent slip and hence the lack of fit, an axial force P_{sh}, shown in Fig. 2, has to be applied at the steel-concrete interface. This force acts at eccentricities from the shear connection plane to the centroids of both structural parts.

As the force in the shear connection induced by shrinkage acts on the concrete rectangular slab at the vertical distance $h_c/2$ from the plane of application of force P_{sh} to the slab centroid concerned, the strains at the top and bottom fibre of concrete slab in Fig. 3 are given from elementary mechanics by

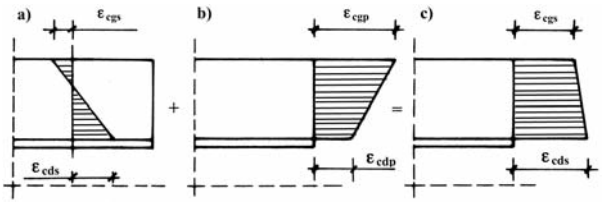

Fig. 3 Strains at the top and bottom fibre of concrete slab

$$\varepsilon_{cgs} = -\frac{2P_s}{E_c b_c h_c}, \quad \varepsilon_{cds} = \frac{4P_s}{E_c b_c h_c}. \tag{1}$$

where E_c is modulus of elasticity for concrete, b_c width and h_c thickness of the concrete slab.

The axial force in the concrete element $N_c(t)$ as well as the axial force in the steel element $N_a(t)$, which are generally time-dependent, should be equal to the axial force P_{sh}

$$P_{sh} = P_{sh}(t) = N_c(t) = N_a(t) \tag{2}$$

with $N_c(t)$ and $N_a(t)$ as axial forces variable in time t acting in concrete slab and steel beam at the level of the shear connection interface.

The force corresponding to shrinkage strain of concrete $\varepsilon_s(t)$ applied at the interface plane (Fig. 2) is given by:

$$N_c(t) = \varepsilon_s(t)\, E_c(t)\, A_c,\ N_a(t) = \varepsilon_{as}(t)/\delta_a \text{ and}$$

$$\varepsilon_{cs}(t) + \varepsilon_{as}(t) = \varepsilon_s(t). \tag{3}$$

where $\varepsilon_s(t)$ is value of shrinkage strain, $\varepsilon_{as}(t)$ conventional strains produced by steel beam at the level of concrete slab neutral axis, $\varepsilon_{cs}(t)$ strains in concrete caused by steel beam prevention to the concrete shrinkage, $E_c(t)$ modulus of elasticity for concrete, A_c cross-sectional area of concrete, z distance between the centroid of concrete slab and the centroid of the beam steel section, E_a modulus of elasticity of structural steel, A_a cross-sectional area of the structural steel section, I_a second moment of area of the structural steel section and conventional factor of flexural stiffness of the steel beam section can be expressed by

$$\delta_a = \frac{1}{E_a A_a} + \frac{z^2}{E_a I_a}. \tag{4}$$

For the strains, the following relationships can be derived:

$$\varepsilon_{as}(t) = \frac{\delta_a}{\delta_a + \delta_c}\varepsilon_s(t) \text{ and } \varepsilon_{cs}(t) = \frac{\delta_c}{\delta_a + \delta_c}\varepsilon_s(t). \tag{5}$$

with δ_c coefficient of longitudinal stiffness of concrete slab given by $\delta_c = 1/(E_c A_c)$.

Applying relationships from (1) to (3), the strains in the top and bottom reference fibres may be written as

$$\varepsilon_{cds}(t) = \frac{4N_c(t)}{E_c(t)A_c} = \frac{4\delta_c}{\delta_a + \delta_c}\varepsilon_s(t)$$

and

$$\varepsilon_{cgs}(t) = \frac{2\delta_c}{\delta_a + \delta_c}\varepsilon_s(t). \tag{6}$$

4. Stresses and strains in concrete slab due to direct load actions

The flexure obviously causes compression in concrete element. For the standard forms of composite beams as shown in Fig. 2, the reduction in the flexural rigidity that can occur through accidental cracking is very small. Possible tensile cracking in bottom fibres of slab can exist if the neutral axis is found to lie in the concrete element. Composite beams with full shear connection are assumed to have full shear interaction so that slip and hence slip strain are ignored. The linear strain profile without any step change is shown in Fig. 2 for this configuration. The steel modulus E_a and the short-term concrete modulus E_c can be considered to be elastic, and for the case of obvious analysis transformed area principles may be adopted. The composite section can be changed into a concrete section by increasing the components of steel elements by the modular ratio of the constituent materials $n = E_a/E_c$. The composite beam is supposed to be subjected to positive bending so that the top fibre of the concrete is in compression. The size and position of all elements are obviously known so that the position of the neutral axis lies at the centroid of the transformed section. Once the neutral axis has been located, the stresses and deformations at top and bottom fibre of the concrete slab may be calculated easily.

$$\varepsilon_{cgp} = \frac{M}{W_{cg}E_c} = \frac{M}{E_cI_{zc}}z_c$$

and

$$\varepsilon_{cdp} = \frac{M}{W_{cd}E_c} = \frac{M}{E_cI_{zc}}(z_c - h_c). \tag{7}$$

With the second moment of area of the effective composite section transformed into the concrete section $I_{zc} = nI_a + I_c + nA_aa_a^2 + A_ca_c^2$, modular ratio of the constituent materials defined as $n = E_a/E_c$, z_c distance between the centroid of the composite section to the extreme fibre of the composite slab in compression, hc thickness of the concrete slab, a_c distance between the centroid of concrete slab to the neutral axis of composite beam, a_a distance between the centroid of steel beam to the neutral axis of composite section, I_c second moment of area of the un-cracked concrete slab, flexural rigidity of the composite beam with full interaction as the sum of flexural rigidities of the individual elements $E_cI_{zc} = B_{zc} = E_aI_a + E_cI_c + E_aA_aa_a^2 + E_cA_ca_c^2$.

5. Control of cracking due to concrete shrinkage

Concrete slab would crack when shrinkage strain satisfies the following criterion:

$$\varepsilon_{cds}(t) = \frac{4N_c(t)}{E_{c(t)}A_c} > \varepsilon_{ct,\lim}. \tag{8}$$

Substituting relations (6), this crack initialization principle, when cracks may first be expected to occur, can be rewritten in the following form:

$$\frac{\varepsilon_{ct,\lim}}{\varepsilon_s(t)} < \frac{4\delta_c}{\delta_a + \delta c}. \tag{9}$$

The limit value of the axial tensile strain of concrete could be calculated from $\varepsilon_{ct,\lim} = \eta_\phi \cdot f_{ctm}/E_{ct}$, with f_{ctm} as mean value of the axial tensile strength of concrete, E_{ct} modulus of elasticity for concrete in tensions, ρ_r percentage of reinforcement related to the area of the tensile cracked zone of the slab cross section, ϕ diameter of reinforcement bar and

$$\eta_\phi = 1 + \frac{0.08\rho_r}{\phi^{1.5}}. \tag{10}$$

With $\eta_c(t) = \frac{f_{ctm}}{E_c\varepsilon_s(t)}$ and $\beta_0 = \frac{1}{\delta} = \frac{\delta_c}{\delta_a}$, the condition for crack initialisation can be expressed in the following more general form

$$\omega = \frac{\eta_c(t)\eta_\phi}{4\beta_0}(1 + \beta_0) < 1, \text{ with } \eta_{c\phi} = \eta_c(t)\eta_\phi \tag{11}$$

6. Cracking produced by concrete shrinkage together with direct load actions

From the relations for determinations of strains ε_{cg} and ε_{cd} is not evident, which of two strains would reach faster the limit strain $\varepsilon_{ct,\lim}$. Crack initialisation depends on the magnitude of shrinkage strains, the dimensions of the elements, the composition of the concrete and on the factor β_0, as well as concrete strength classes and reinforcing steel. The resulting strain diagram shown in Fig.3 indicates that the ultimate or crushing values of extreme strains are at the slab surfaces. The strain profile is thus determined. The top and bottom fibre strains in the slab section, because of the linearity, allow expressing the curvature by the simplified formula

$$\kappa_s = \frac{\varepsilon_{cds} - \varepsilon_{cgs}}{h_c} = \frac{6\delta_c}{(\delta_a + \delta_c)}\varepsilon_s(t), \tag{12}$$

The curvature for resulting strains is similarly

$$\kappa_p = \frac{\varepsilon_{cg} - \varepsilon_{cd}}{h_c} = \frac{M}{B_{zc}}. \tag{13}$$

If $\varepsilon_{cds} < \varepsilon_{ct,\lim}$, cracking in the concrete slab due to shrinkage will not occur. In this case, the strains due to direct load actions to produce slab cracking might reach the magnitude

$$\Delta\varepsilon_{ct}(t) = \varepsilon_{ct,\lim} - \varepsilon_{cds}(t) = \varepsilon_{ct,\lim} - \frac{4\delta_c}{\delta_a + \delta_c}\varepsilon_s(t) \quad (14)$$

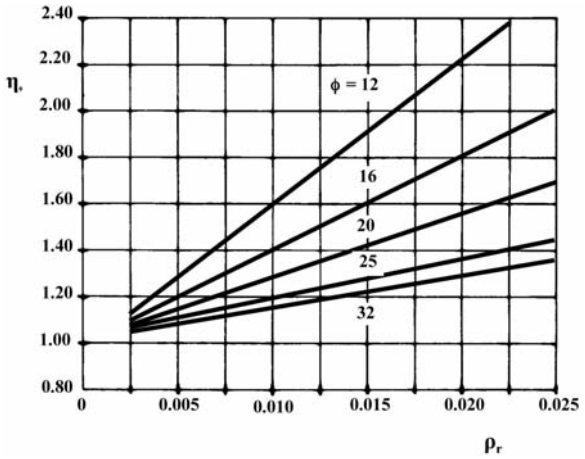

Fig. 4 Percentage ρ_r and diameters ϕ impact on limit strain $\varepsilon_{ct,\lim}$, expressed η_ϕ (10)

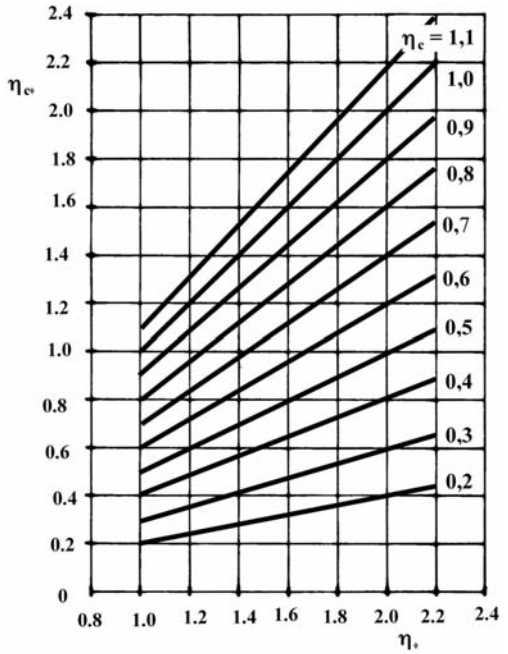

Fig. 5 Factor η_{c_ϕ} variation with diameters ϕ and shrinkage strain ε_s, expressed η_ϕ (11)

This relationship can be written with the ration of both strains $\eta_s = \varepsilon_s(t)/\varepsilon_{ct,\lim}$ as

$$\lambda = \frac{\Delta\varepsilon_{ct}(t)}{\varepsilon_{ct,\lim}} = 1 - \frac{4\beta_0\,\varepsilon_s(t)}{(1+\beta_0)\varepsilon_{ct,\lim}} = 1 - \frac{4\beta_0}{1+\beta_0}\eta_s \quad (15)$$

7. Parametrical study

Influence of the above variable parameters on the concrete slab cracking is shown in Figs.4 – 7. The impact of reinforcement percentage ρ_r and diameters of reinforcement bar ϕ on limit value of the axial tensile strain of concrete $\varepsilon_{ct,\lim}$ is summarised in Fig. 4. The variable parameter is chosen the value η_ϕ.

Relative influence of reinforcement bar diameters and values of the axial tensile strength of concrete is illustrated in Fig. 5. Factors η_ϕ and η_c according to formulae (10) and (11) are taken as variables. Rather large intervals of these factors are studied. Their magnitudes correspond to the actual forms of composite steel and concrete composite structural elements.

The analysis of conventional factor β_0 is shown in Fig. 6. The previously investigated parameters (ϕ, ε_s, f_{ctm}, E_c) are about the concrete slab. The factor β_0 takes into account the steel beam and in the same time the total composite section. When the design value of factor κ in Fig. 6 is superior to one, shrinkage cracks occur without effect of external actions. Cracking starts at the bottom fibre in the shear connection plane. The variation of strains $\Delta\varepsilon_{ct}(t)$ reducing shrinkage for different values of the ratio η_s is shown in Fig. 7. The magnitudes of variable λ could express shrinkage cracking occurring before applications of external load

8. Concluding remarks

The investigations have illustrated possibilities of shrinkage crack occurring in a concrete slab of composite beams even prior to the application of external actions. Except for shrinkage concrete strain, important influence is also presented by percentage of reinforcement, diameter of reinforcement bar, tensile strength of concrete and furthermore the factor β_0, which means a ratio of the stiffness of steel beam and concrete slab. Larger values of concrete strains due to shrinkage arise at the bottom slab surface. Consequently, shrinkage cracking can be initiated primarily at the bottom concrete fibre in the shear connection plane with steel beam flange. For real composite structures, the ratio β_0 can be extremely variable. However, it may be concluded that shrinkage crack would not be initiated, when $\beta_0 < 0.25$. The cracking can be avoided by rational concrete slab reinforcement (percentage of reinforcement ρ_r and bars diameter ϕ). The results of analyses in Figs. 4 to 7 may be useful for control of potential cracking during composite steel and concrete design.

Acknowledgment

This work has been to some extent supported by the Slovak Grant Agency within the scope of Grant No. 1/0311/09.

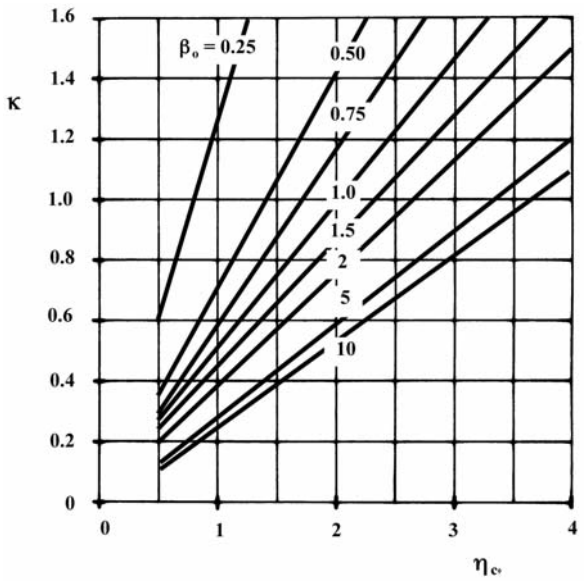

Fig. 6 Impact of factor $\beta_0 = \delta_c/\delta_a$ on the slab curvature κ

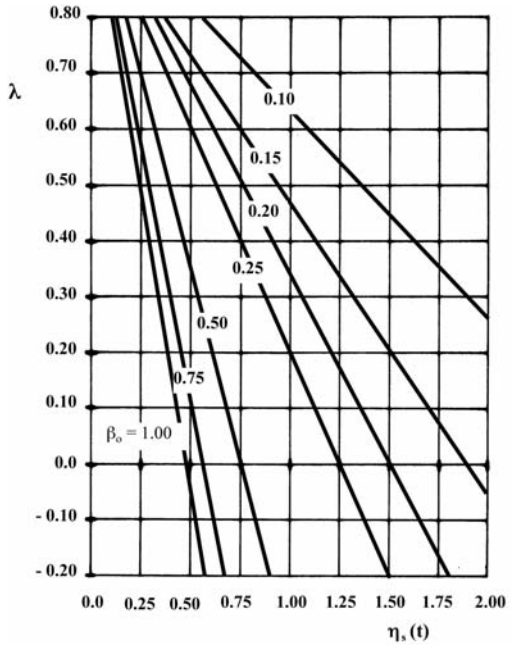

Fig .7 Dependence of strain ratio on λ factor $\beta_0 = \delta_c/\delta_a$

References

[1] Eurocode 4: Design of Composite Steel and Concrete Structures: Part 1-1. General Rules and Rules for Buildings; Part 2. Bridges.
[2] DUCRET, J.M., LENET, J., P.: Effects of Concrete Hydration on Composite Bridges. Conference Report: Composite Construction o Conventional and Innovative. Innsbruck. September, 1997.
[3] BUJNAK, J., FURTAK, K., VICAN, J.: *Design of Structures according to Eurocodes (in Slovak)*, Course book, 6/2003, Zilina, p. 282.
[4] BUJNAK, J., FURTAK, K.: *Steel and Concrete Structural Elements (in Slovak)*, Monographe, Zilina, 1999.
[5] JAREK, B.: *Cracking of Reinforce Concrete Slab in Beams of Composite Steel and Concrete Type (in Poland)*, Doktorand thesis, Politechnika Krakowska.

Gabriela Lajcakova – Jozef Melcer *

DYNAMIC EFFECT OF MOVING VEHICLES ON THE ROAD CONCRETE SLABS

The road concrete slabs represent the typical transport structure exposed to dynamic effects of moving vehicles. Numerical simulation methods demand to pay attention to the proposal of the computing model of the vehicle and the computing model of the road concrete slab. The models must be mathematically described and the equations of motion must be solved in a numerical way. For the solution of such a problem the specialized computer program must be created. It is suitable to use the possibilities of the higher level programming languages as MATLAB. The influence of some important factors on dynamic response of the structure is numerically tested.

1. Introduction

The road structure is the typical transport structure exposed to dynamic effects of moving vehicles. The classic road structures are designed as bitumen pavements. At the present time also the concrete pavements are sometimes utilized in the form of concrete slabs. From the practical point of view it is needed to known the dynamic response of the slab structure on the effect of moving vehicles [1], [2], [3], [4]. One possibility of dynamic analysis is to utilize the methods of numerical simulation. This approach demands to pay attention to the proposal of the computing models of vehicle and the computing models of the road concrete slab. The dynamic response of the road concrete slab is dependent on the parameters of vehicle, the parameters of the slab and the parameters of subgrade. The submitted paper presents the influence of some parameters of the truck and the slab on the dynamic response of analysed structure.

2. Computing model of vehicle

Generally the one two or three dimensional computing model of the vehicle can be adopted for the modelling of dynamic effect of moving vehicles on the road structures. For the purpose of the task presented in this paper the plane computing model of the truck TATRA was adopted, Fig. 1.

The computing model of vehicle has 8 degrees of freedom – 5 mass and 3 massless. The massless degrees of freedom correspond to the vertical movements of the contact points of the model with the surface of the runway. The vibration of the mass objects of the model is described by the 5 functions of the time $r_i(t)$, (i = 1, 2, 3, 4, 5). The massless degrees of freedom are coupled by contact forces $F_{RV,i}(t)$, (i = 6, 7, 8,) acting at the contact points. The equations of motions and the expressions for contact forcers have the following form:

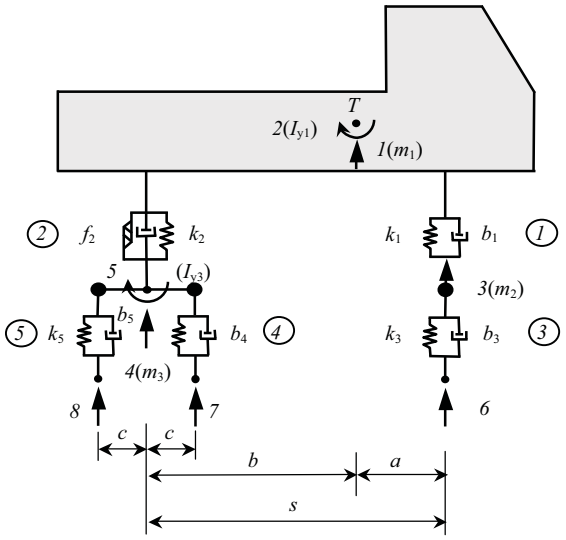

Fig. 1 Plane computing model of the truck TATRA

The meaning of the used symbols is as follows (Fig. 1): k_i, b_i, f_i are the stiffness, damping and friction characteristics of the model, m_i, I_{yi} are the mass and inertia characteristics of the model, a, b, c, s are the length characteristic of the model, g = 9.81 m.s^{-2}, G_i are the gravity forces acting at the contact points with the surface of the runway. The deformations of the spring elements are $d_i(t)$ and the derivation with respect of time is denoted by the dot over the symbol.

* **Gabriela Lajcakova, Jozef Melcer**
Department of Structural Mechanics, Faculty of Civil Engineering, University of Zilina, E-mail: gabriela.lajcakova@fstav.uniza.sk

$$\ddot{r}_1(t) = -\left\{+k_1 \cdot d_1(t) + b_1 \cdot \dot{d}_1(t) + k_2 \cdot d_2(t) + b_2 \cdot \dot{d}_2(t) + f_2 \cdot \dot{d}_2(t)/\dot{d}_c\right\}/m_1,$$

$$\ddot{r}_2(t) = -\left\{-a \cdot k_1 \cdot d_1(t) - a \cdot b_1 \cdot \dot{d}_1(t) + b \cdot k_2 \cdot d_2(t) + b \cdot b_2 \cdot \dot{d}_2(t) + f_2 \cdot \dot{d}_2(t)/\dot{d}_c\right\}/I_{y_1},$$

$$\ddot{r}_3(t) = -\left\{-k_1 \cdot d_1(t) - b_1 \cdot \dot{d}_1(t) + k_3 \cdot d_3(t) + b_3 \cdot \dot{d}_3(t)_2\right\}/m_2, \tag{1}$$

$$\ddot{r}_4(t) = -\left\{-k_2 \cdot d_2(t) + b_2 \cdot \dot{d}_2(t) + f_2 \cdot \dot{d}_2(t)/\dot{d}_c + k_4 \cdot d_4(t) + b_4 \cdot \dot{d}_4(t) + k_5 \cdot d_5(t) + b_5 \cdot \dot{d}_5(t)\right\}/m_3,$$

$$\ddot{r}_5(t) = -\left\{-c \cdot k_4 \cdot d_4(t) - c \cdot b_4 \cdot \dot{d}_4(t) + c \cdot k_5 \cdot d_5(t) + c \cdot b_5 \cdot \dot{d}_5(t)\right\}/I_{y_3},$$

$$F_6(t) = G_6 - k_3 \cdot d_3(t) - b_3 \cdot \dot{d}_3(t) = +g \cdot \left(m_1 \cdot \frac{b}{s} + m_2\right) - k_3 \cdot d_3(t) - b_3 \cdot \dot{d}_3(t),$$

$$F_7(t) = G_7 - k_4 \cdot d_4(t) - b_4 \cdot \dot{d}_4(t) = +\frac{1}{2} \cdot g \cdot \left(m_1 \cdot \frac{a}{s} + m_3\right) - k_4 \cdot d_4(t) - b_4 \cdot \dot{d}_4(t), \tag{2}$$

$$F_8(t) = G_8 - k_5 \cdot d_5(t) - b_5 \cdot \dot{d}_4(t) = +\frac{1}{2} \cdot g \cdot \left(m_1 \cdot \frac{a}{s} + m_3\right) - k_5 \cdot d_5(t) - b_5 \cdot \dot{d}_5(t).$$

3. Computing model of the road slab

The space computing model of the road concrete slab is based on the Kirchhoff theory of the thin slab resting on Winkler elastic foundation. The equation of the slab is

$$D\left(\frac{\partial^4 w}{\partial x^4} + 2\frac{\partial^4 w}{\partial x^2 \partial y^2} + \frac{\partial^4 w}{\partial y^4}\right) + K \cdot w + \mu\frac{\partial^2 w}{\partial t^2} + 2\mu\omega_b\frac{\partial w}{\partial t} = p(x,y,t). \tag{3}$$

It is the partial differential equation for the unknown function $w(x, y, t)$ representing the bending surface of the slab centre plane. The solution of the differential equation will be realised in the sense of Fourier method. The wanted function $w(x, y, t)$ will be expressed as the product of two functions

$$w(x, y, t) = w_o(x,y) \cdot q(t). \tag{4}$$

The function $w_o(x,y)$ figures as known function and it is dependent on the coordinates x, y only and the function $q(t)$ figures as unknown function and it is dependent on the time t. The function $q(t)$ has the meaning of generalized Lagrange coordinate. With the respect to the goal of the solution the assumption about the shape of the function $w_o(x,y)$ was adopted

$$w_o(x,y) = \frac{1}{4}\left(1 - \cos\frac{2\pi x}{l_x}\right)\left(1 - \cos\frac{2\pi y}{l_y}\right). \tag{5}$$

The meaning of the other symbols is as follows: D is the slab stiffness [N.m], K is modulus of foundation in [N.m^{-3}], μ is the mass intensity [kg.m^{-2}], ω_b is damping circular frequency [rad.s^{-1}], $p(x, y, t)$ represent the continuous load in [N.m^{-2}], l_x, l_y are the length and width of the slab in [m]. With the respect to the assumption (5) for $x = l_x/2$, $y = l_y/2$ the equation (3) can be rewritten to the form

$$\ddot{q}(t) \cdot \mu + \dot{q}(t) \cdot 2\mu \cdot \omega_b + q(t) \cdot \frac{D}{2}\left[\left(\frac{2\pi}{l_x}\right)^4 + \left(\frac{2\pi}{l_x}\right)^2\left(\frac{2\pi}{l_y}\right)^2 + \left(\frac{2\pi}{l_y}\right)^4 + 2\frac{K}{D}\right] = p(x,y,t). \tag{6}$$

In the case of plane computing model of vehicle the $p(x, y, t)$ can be expressed as

$$p(x,y,t) = \sum_{j=6,7,8} F_j(t) \cdot \frac{1}{l_x l_y} \cdot \left(1 - \cos\frac{2\pi x_j}{l_x}\right)\left(1 - \cos\frac{2\pi y_o}{l_y}\right). \tag{7}$$

$F_j(t)$ is the contact force under the j-th axle of vehicle at the position x_j and y_o.

4. Numerical analysis

For the purpose of numerical analysis the following slab construction was considered, Fig. 2:

1. CS – concrete slab,
   $h_1 = 240$ mm, $E_1 = 37\,500$ MPa, $v_1 = 0.20$
2. CA II – coating aggregate, quality class II,
   $h_2 = 40$ mm, $E_2 = 4\,500$ MPa, $v_2 = 0.21$
3. SC I – soil cement, quality class I,
   $h_3 = 200$ mm, $E_3 = 2\,000$ MPa, $v_3 = 0.23$
4. PC – protective coat, gravel sand,
   $h_4 = 250$ mm, $E_4 = 120$ MPa, $v_4 = 0.35$
5. SS – sub-soil,
   $h_5 = \infty$ mm, $E_5 = 30$ MPa, $v_5 = 0.35$

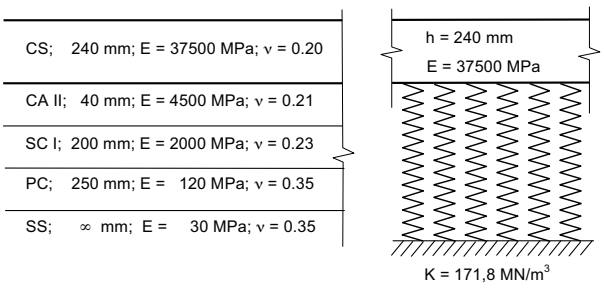

Fig. 2 Model of the slab on elastic foundation

The 1st layer of the computing model is the concrete slab of the thickness h = 240 mm, the length l_x = 6.0 m, the width l_y = = 3.75 m, modulus of elasticity E = 37 500 MPa, Poisson coefficient v = 0.20. The layers under the slab are integrated in the computing model as Winkler foundation. Modulus of foundation K was calculated by the computer program LAYMED. The parameters of computing model of vehicle correspond to the vehicle TATRA 815. Total mass of the computing model of vehicle was 13 tons. For the numerical solution of the mathematical apparatus the computer program in program language MATLAB was created. The program enables to calculate the time courses of all kinematic values (deflection, speed, acceleration) at midspan of the slab and the time courses of contact forces under individual axles. The demonstrations of the form of obtained results are in Figs. 3, 4, 5, 6.

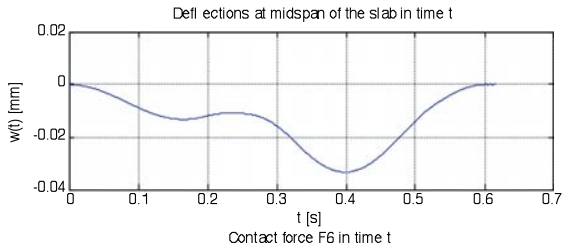

Fig. 3 Time course of the deflection at midspan of the slab

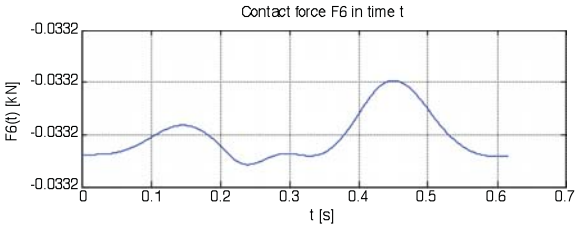

Fig. 4 Time course of the contact force F6 under front axle

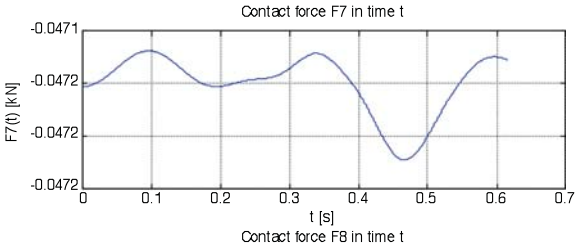

Fig. 5 Time course of the contact force F7 under front wheel of the rear axle

The results of solution are influenced by various parameters of the considered system. In this paper the influence of the speed of vehicle motion and the influence of the modulus of foundation

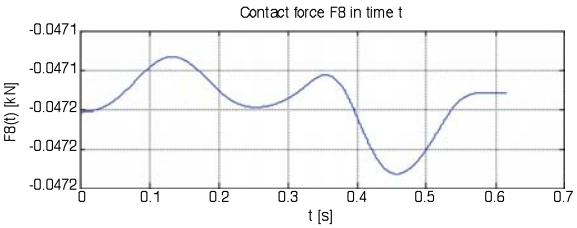

Fig. 6 Time course of the contact force F8 under rear wheel of the rear axle

are analyzed. With the goal to clarify the influence of these two parameters the parametric studies were realized. The influence of the speed of vehicle motion was analyzed in the interval of speeds V = 0 – 120 km/h with the step 5 km/h. The maximums of vertical deflections at the midspan of the slab versus speed of vehicle motion are plotted in Fig. 7. Similarly the extremes (maximum, minimum) of contact forces under front and rear axles versus speed of vehicle motion are plotted in Figs. 8, 9, 10.

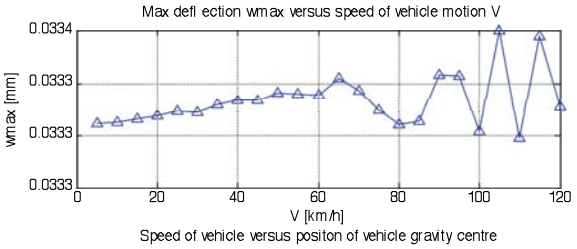

Fig. 7 Maximal deflections at midspan of the slab versus speed of vehicle motion

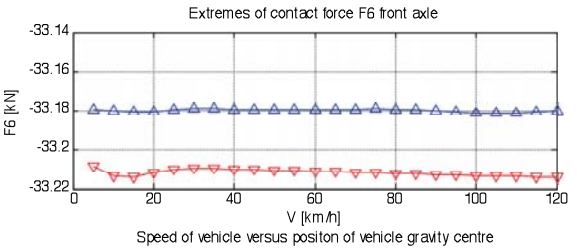

Fig. 8 Extremes of contact force F6 under front axle versus speed of vehicle motion

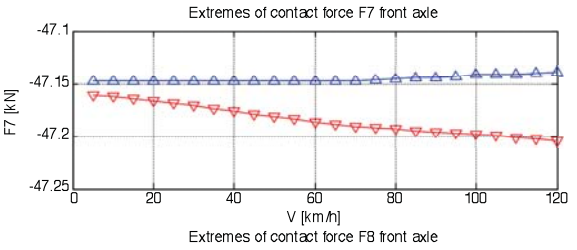

Fig. 9 Extremes of contact force F7 under front wheel of rear axle versus speed of vehicle motion

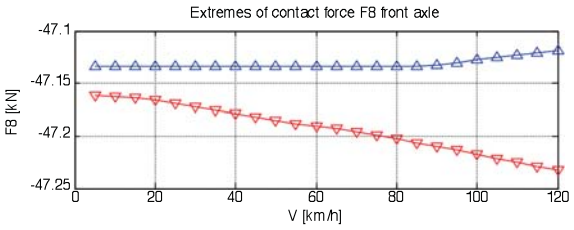

Fig. 10 Extremes of contact force F8 under rear wheel of rear axle versus speed of vehicle motion

The influence of the modulus of foundation K was analyzed in the interval 50.10^6 – 200.10^6 MN/m^3 with the step 25.10^6 MN/m^3 and in the interval 200.10^6 – 500.10^6 MN/m^3 with the step 50.10^6 MN/m^3. The speed of vehicle motion was $V = 65$ km/h. The maximums of vertical deflections at the midspan of the slab versus modulus of foundation are plotted in Fig. 11. Similarly the extremes (maximum, minimum) of contact forces under front and rear axles versus modulus of foundation are plotted in Figs. 12, 13, 14.

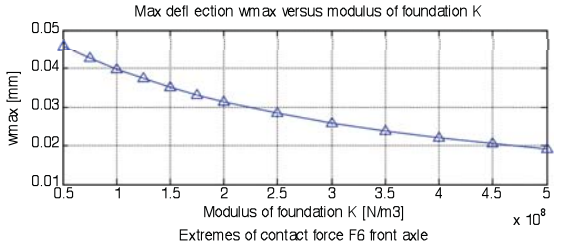

Fig. 11 Maximal deflections at midspan of the slab versus modulus of foundation

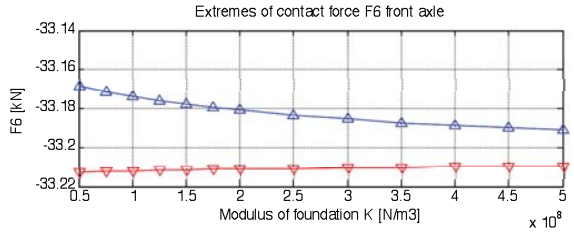

Fig. 12 Extremes of contact force F6 under front axle versus modulus of foundation

5. Conclusion

Vehicle–road dynamic interaction is a topical engineering problem. The basic assumption of numerical solution is the creation of computing models. The computing models of vehicles are usually created as discrete computing models described by the system of ordinary differential equations. Minor attention is dedicated to the creation of pavement computing models. One possibility is to model the pavement as the slab on elastic foundation. Such computing

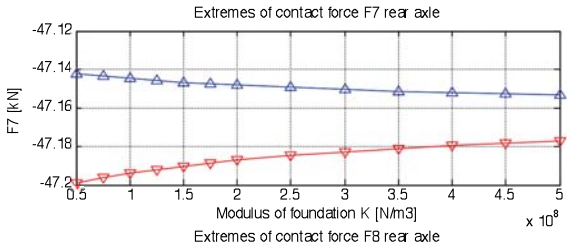

Fig. 13 Extremes of contact force F7 under front wheel of rear axle versus modulus of foundation

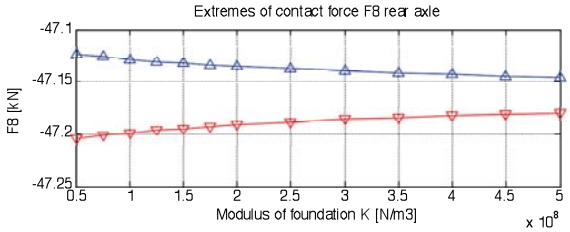

Fig. 14 Extremes of contact force F8 under rear wheel of rear axle versus modulus of foundation

model is suitable for modeling the dynamic effect of moving vehicles on the concrete pavements. When we want to follow the dynamic effect of moving vehicles in one point only we can adopt the assumption about shape of deflection surface of the slab. On the basis of this assumption we can replace the partial differential equation of the slab by ordinary differential equation. Such a computing model enables to analyze all kinematic values (displacement, speed, acceleration) of vehicle and the slab and contact forces acting on the slab. Various parameters come into the analysis. In this paper the influence of speed of vehicle motion and influence of modulus of foundation on the obtained results were analyzed. The deflections of the slab and the extremes of contact forces grow with the speed of vehicle motion. When the slab has good surface without evident unevenness the influence of the speed of vehicle motion on the kinematical and force quantities is very small. The influence of foundation modulus has the opposite tendency as the influence of speed of vehicle motion. The deflections of the slab and the extremes of contact forces fall with the grow values of foundation modulus. The analysis in time domain can be extended on the analysis in frequency domain. The results in frequency domain can serve for the analysis of noise emissions around the roads [5] or for the analysis of seismic problems due to transport [6].

Acknowledgements

This work was supported by the Slovak Grant National Agency VEGA, grant G1/0031/09.

This contribution is the result of the project implementation: "Centre of Excellence in Transport Engineering" (ITMS: 26220120027) supported by the Research & Development Operational Programme funded by the ERDF.

References

[1] MARTINCEK, G.: *Dynamic Diagnostics of Pavements (in Slovak).* VEDA, Bratislava, 1983.
[2] MARTINCEK, G.: Dynamics of Pavement Structures, *E & FN Spon and Ister Science Press,* London/Bratislava, 1994.
[3] CEBON, D.: Handbook of Vehicle – Road Interaction, *Swets&Zeitlinger Publishers,* Lisse, Netherlands, 1999.
[4] KULAKOWSKI, B. T., GARDNER, J. F., LOWEN, S. J.: *Dynamic Modeling and Control of Engineering Systems,* The 3rd edition, Cambridge University Press, New York, 2009.
[5] PANULINOVA, E.: The Influence of the Road Surface Unevenness on the Noise Level from Automobile Transport (in Slovak). *Silnicni obzor,* Vol. 62, No. 11,12, 2001, Praha, ISSN 0322-7154, p. 275–279.
[6] KOTRASOVA, K.: Seismic Proposal of Rectangular Tanks Filled by Water (in Slovak). *Civil and Environmental Engineering,* Vol. 4, No.1, 2008, ISSN 1336-5935, p. 46–53.

Martin Moravcik – Petra Bujnakova *

NEW PRECAST BRIDGE GIRDER WITH COMBINED PRESTRESSING

Traditionally, the major part of highway bridges in Slovakia is realized using the precast concrete technology. The common Slovak precast girders are produced to the34 m length as one element. Nowadays, there is an increasing demand for more economical and resisting bridge structures with longer spans. The company Vahostav-Sk-PREFA, Ltd as the main supplier of precast elements for highwaybridge 207, in cooperation with theUniversity of Zilina and the designer company Dopravoprojekt Inc. Liptovsky Mikulas, developed a new precast girder MDP for the span 38 m with combined prestressing. Some experiences and results of verifying flexural test with numerical analysis of that girder are presented in this paper.

1. The Basic Parameters of the Bridge Girder

The majority of Slovak highway bridges are made of standardized "I" and "T" – shaped precast prestressed girders with cast-in place concrete deck slab. The innovative features allow for spans up to 38 m and increasing girder spacing up to 1680 mm. The girders have a construction depth 1900 mm, with constant top and bottom flange 800 mm wide. The girder's cross section is shown in Fig. 1. The MDP 38 girder has a combined prestressing. The girders are pre-tensioned with 28 strands ϕ15.5 mm/1800 MPa with low relaxation (and 2 strands in top flange). The spacing between prestressing strands is 50 mm. The post-tensioning is realised by three tendons consistings of 4 strands ϕ15.5 mm (A_p = 141.5 mm^2). Reinforcement was realised using ordinary steel BS 500. The designed concrete strength class of girders is C 45/55.

The precast bridge superstructure is built by girder placing on the abutments and next the cross beam and the cast-in-place reinforced concrete deck with a depth of 200 mm is cast.The composite deck is designed from concrete strength class C 30/37. The prestressed girder MDP 38 was designed according toSlovak design code STN 73 1251 [1], CSN 73 6207 [5] and STN 73 6203 [4]. The FEM computer system "Nexis2" was applied to determine the load effect to the shell-beam continual FE model. The material properties for the concrete cross-section model as well as the criteria for the steel bar distance at the concrete cover were applied according to the Europan standard STN EN 1992-1-1 for the design precedure.

2. Mechanical and Rheological Properties of Concrete

The properties of concrete were evaluated in the preparation stage with special care, since they have a decisive influence on the structural properties of the girder. Another important feature is the time development of the concrete compressive strength that determines the time in which the prestressing force transfer into the girder can be started. The prestress force in practice is implemented in the time period from 15 to 48 hours after girder casting. The criteria for the release of prestressing require the minimal compressive strength, the modulus of elasticity and rheological properties of the young concrete. Therefore, the concrete properties in time were analyzed. The measurements of concrete strength and the modulus of elasticity were performed at concrete age of 26 – 36 – 48 – 186 hours (7.7 days), and 690 hours (28.7 days). The specimens were tested in a curing room with temperature of 20 ± 2 °C and relative humidity of 80%. Thecube compressive strengths were measured on 150 × 150 × 150 mm specimens. Three specimens were tested at different time and the average value was taken to the next analysis. The modulus of elasticity of concrete was measured on a specimen of 100 × 100 × 400 mm. The modulus of elasticity was measured by static and dynamic testing. The total 20 concrete prisms were tested. Three prisms were used for measurement of shrinkage. Fig. 2 shows time development of the concrete strength and the modulus of elasticity.

Starting cambers of the girder were calculated from real parameters of concrete at the important construction stage. Table 2

Starting cambers of the girder in building phases Tab.1

Phase No.	Phase definition	Time (hour)	ftest (mm)	fmodel (mm)	fcalc (mm)
1.	Prestressing transfer to the concrete	48	28.50	26.30	32.15
2.	Post-tensioning of added strands	168	50.80	50.16	57.02

* **Martin Moravcik, Petra Bujnakova**
Facultyof Civil Engineering, UniversityofZilina, , Slovakia, E-mail: martin.moravcik@fstav.uniza.sk

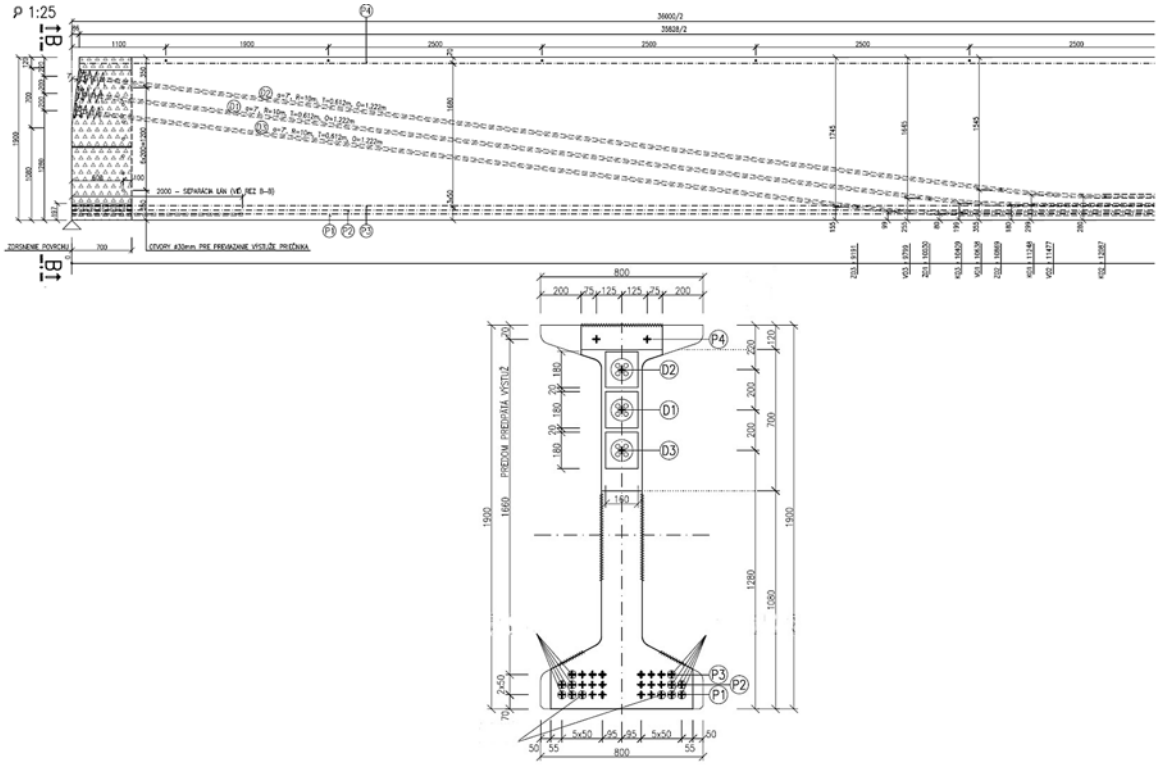

Fig. 1 The longitudinal section and front view of the girder MDP 38

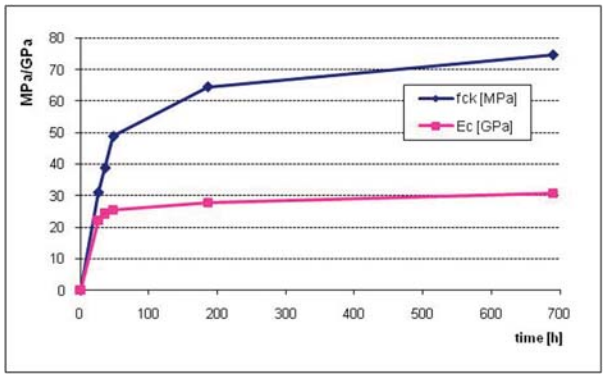

Fig. 2 The development ofmodulus of elasticity and the compressive strength

compares the experimental and calculated values of the camber at the pre and post- tensioning phases.

3. Static Load Test

The MDP 38 prestressed girder was tested using three-point flexure set-up to determine a flexural cracking moment and a ultimate moment capacity. The test setup is illustrated in Fig. 3. The tested girder was supported by rubber bearings placed on concrete panels (l_{eff} = 37.3 m). The load force was manually applied using the prestressing compacting machine. The 60 × 60 × 30 mm rubber pad was placed between the hydraulic jack "PAUL" and the girder to create a distributed contact area. Concrete blocks over the tested girder were used as a counterweight during the loading process. Such non-traditional set-up was chosen to achieve a high ultimate capacity of the hydraulic jack (4000 kN). The load was applied incrementally step by step and monitored using a dynamometer type PROSEQUE.

The prestressing force was recorded by four elastomagnetic sensors, using PROJSTAR system PSS20. One sensor was located on the top of the prestressing strand and three sensors were fixed on bottom strands. The prestressing was controlled permanently – after release of prestressing (2 days), after post-tensioning (7 days), and before the static load test (14 days).

The concrete strain was controlled at the mid span using strain gauges. Three strain gauges were installed on both sides of the girder at the bottom, in the middle and at the top. Deformation was measured using a vertical displacement transducer at the quarter of span, at the mid of span, and close at the support. Possible settlements of abutments were checked geodetically.

Basic mechanical properties of the concrete and prestressing strands were verified before the static load test. The concrete specimens reached the following vallues of the important parameters:
- The mean compressive strength f_{cm} = 44.71 MPa.
- The mean tensile strength f_{ctm} = 2.23 MPa.
- The mean modulus of elasticity E_c = 28989 MPa.

The measured parameters of prestressing strands:
- The minimum value of ultimate strength $f_p = 1851$ MPa.
- The minimum value of yield strength $f_{p0,2} = 1686$ MPa.
- The modulus of elasticity $E_p = 189$ GPa.

Load steps of the structure were realised incrementally with unloading steps at the level of the first visible bending crack and the predicted Ultimate Limit State (ULS), see Table 2. After each load increment, loading was stopped to record the deformation, the concrete strain and to check any visible cracking. At the point of the first visible crack, the loading was noted and all cracks were mapped.

Characteristic deflection during the load test Tab. 2

Phase No.	Phase definition	Load P (kN)	Experiment f_{exp} (mm)	Analysis f_{model} (mm)
1.	Self-weight of the bridge deck	177.40	−15.86	−15.97
2.	Other self-weight and permanent load[a)]	400.60	−44.42	−44.94
3.	Predicted cracking moment	595.70	−75.47	−70.0
4.	The first visible crack	750.00 794.20	−88.35 /	−89.87 −95.86
5.	Ultimate girder bending capacity	1183.2	−129.33	−156.06

[a)] *moving load scheme ZZI according to Slovak standard STN 73 6203*

Fig. 3 The test seting up

4. Numerical Analysis

The FE numerical analysis was performed to simulate the previously described bending test. The numerical model of the tested girder was created in computing system ATENA 2D that allows to perform a nonlinear finite element analysis of the prestressed structures under static loads. The system enables to consider material and geometrical nonlinearities of the concrete structure and nonlinear solution principles. The constitutive relations are formulated for the plane stress state. A smeared approach was used to model the material properties for fixed cracks and the longitudinal and transversal reinforcement. Prestressing strands are modelled as discrete elements and for all reinforcement the bilinear stress-strain relationship was used. The prestressing force applied to the model was reduced considering the calculated prestress losses. Concrete is represented by the material model SBETA with characteristic values of the compressive strength and the modulus of elasticity from the experimental testing. Perfect bond between the concrete and reinforcement is assumed applying the smeared concept.

Loading is applied by prescribing the vertical displacement at the middle of the loading plate with constant increments of 0.1 mm. The overall response is recorded at two monitoring points – loading as the reaction at the top point and the deflection at the bottom of the girder.

5. Some Results of the Static Test

Results of the FEM analysis were compared with results obtained by experimental testing. The maximum value of the camber along the longitudinal axis gained immediately after the pre- tensioning phase (around 48 hours) was observed as well as the value of camber after the post-tensioning phase (around 168 hours), see Tab. 1. There can be seen a good coincidence between experimental and theoretical values of starting camber. The defined material model of the girder well corresponded with real concrete parameters.

The characteristic load vs. the midspan deformation of the girder is shown in Tab. 2. As can be seen the predicted relationship of strain courses in fibres of concrete cross-section and tension force increments in the strands shows a good agreement with the measured structural response, see Figs. 4, 5. The typical stiffness reduction in load steps after cracking was not significant and the short-term load response of that girder was almost linear.

Cracking of the girder during flexural test was propagated as follows. The first visible crack was noted near the midspan at the load level of 750 kN. Additional cracks developed along the span as the load was increased. The real crack propagation in the ULS is shown in Fig. 6. The critical crack width 0.2 mm was observed on the load level around 1000 kN that means aproximately 82 % of the exploitation of cross-section capacity. The recorded spacing of cracks well coincided with calculated values in load steps.

6. Application

Nowadays, the precast prestressed bridge composed of MDP 38 girders, made in continuos structural system is the longest bridge

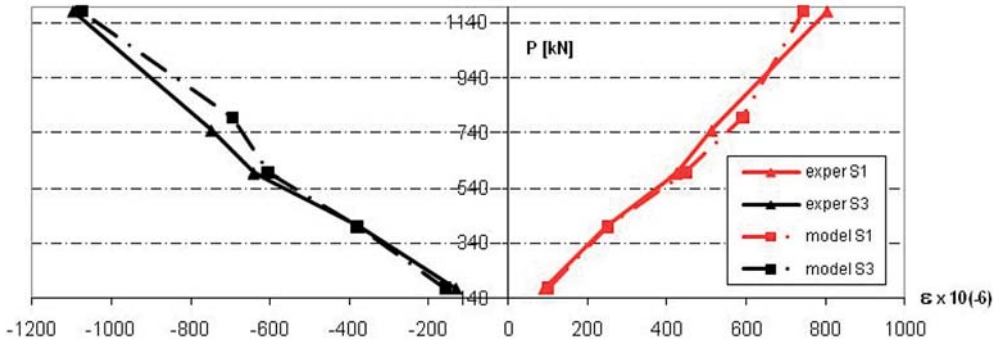

Fig.4 Strain in compressed and tensioned fibres of concrete cross-section in $l_{eff}/2$

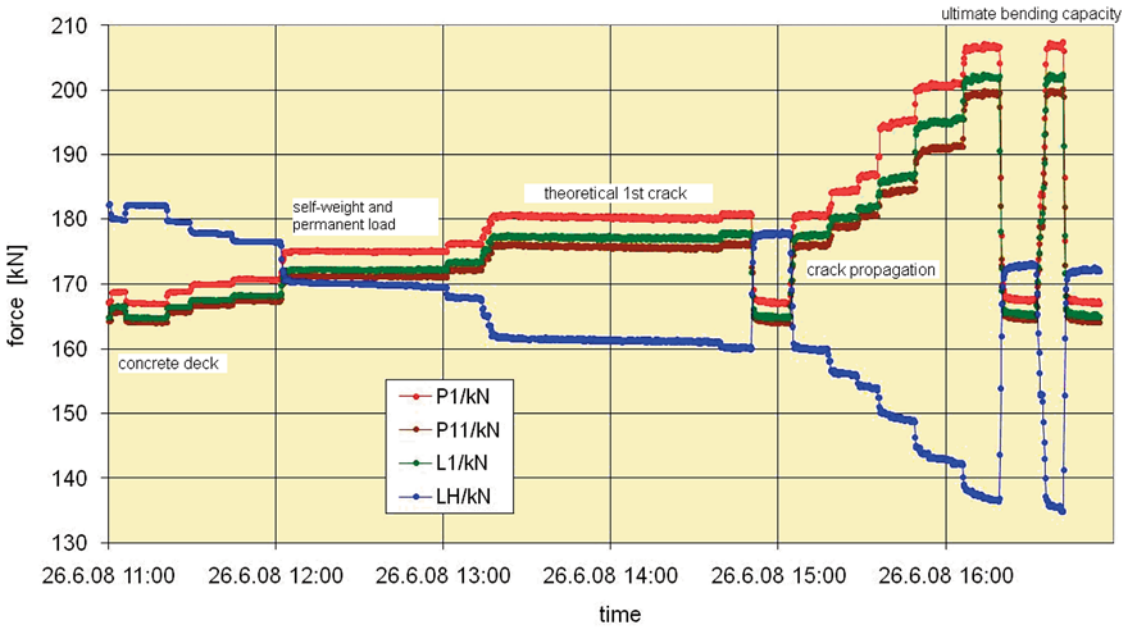

Fig. 5 Development of forces in observed strands in $l_{eff}/2$

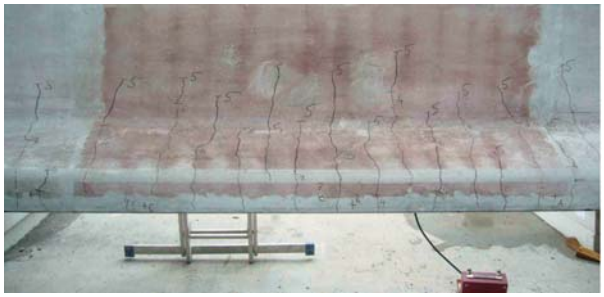

Fig. 6 Crack propagation at the bottom flage in the middle cross-section

Fig. 7 Construction of the highway bridge 207

in Slovakia. Transportation and erection of these bridge girders during construction of highway bridge 207, "Sverepec – Vrtizer" is illustrated in Fig. 7.

7. Conclusion

The experimental analysis showed that the structural behaviour of the girder corresponded to the requirements of design assumptions. The sufficient load carrying capacity was approved

and the manufactured girder can serve reliably and can be used in practice. Neither a structural destruction nor the load on predicted resistance level was reached. The performed FEM model well simulated the behaviour of real precast girder. Experimental and theoretical values of the starting camber, deformations (in $l_{eff}/2$, and $l_{eff}/4$), concrete strains and forces in strands showed a good coincidence. This kind of model can be used for development of other commercial types of precast bridge girders in the future.

Acknowledgement

This research work has been supported by the VEGA agency, 1/0461/10 and as the result of the project implementation: "Support of Research and Development for Centre of Excellence in Transport Engineering" (ITMS: 26220120031) supported by the Research& Development Operational Programme funded by the ERDF.

References:

[1] STN 73 1251, Design of Structures of Prestressed Concrete.
[2] STN EN 1992-1-1, Design of Concrete Structures, Part 1, General Rules
[3] STN EN 1992-1-2, Design of Concrete structures, Part 2. Concrete Bridges
[4] STN 73 6203, Loading on Bridges.
[5] CSN 73 6207, Design of Prestressed Bridges.
[6] MORAVCIK, M., CHANDOGA, M., JAROSEVIC, A. et al.: Load Test of Prestressed Girder MDP 38 m, *Report,* Zilina, Slovakia, 2008.

Milan Moravcik – Martin Moravcik *

DYNAMIC BEHAVIOUR OF THE ARCH BRIDGE – THE FULL-SCALE TESTING

In the paper the full-scale dynamic testing procedure for highway bridges is presented. The procedure is applied on the new highway steel arch bridge in highway R1 at the locality Nitra - Selenec. After a general description of the bridge, some results relative to inspection and the spectral analysis are reported. The testing equipment, methods of evaluating and processing obtained records utilised during the forced vibration of the bridge are described.

1. Introduction

Dynamic testing of bridges has been widely used for the appraisal of the correct structural performance in front of its service loading. Several dynamic testing procedures for highway bridges are reported in literature and national codes. The Slovak National Standard STN 73 6209 "Loading tests of bridges" [1] determines conditions for the performance of dynamic tests for highway bridges. The tests are designed to obtain the basic characteristics of dynamic response:

1. Vibration frequencies and mode shapes for a loaded and unloaded bridge structure calculated from a frequency analysis of the measured data, which are compared with the theoretical amplitudes from a finite–element model of the bridge.
2. The dynamic coefficient (DC) $\delta_{obs}(x)$ (the dynamic amplification factor) in characteristic locations (x) of the bridge structure for passages of the testing vehicle:

$$\delta_{obs}(x) = \frac{S_{\max}(x)}{S(x)} \tag{1}$$

where:
$S_{\max}(x)$ is the maximum measured dynamic response of the bridge - the deformation or force measured quantity in the place (x),
$S(x)$ is the static (quasi-static) response quantity of the bridge in the place (x) that can be defined as:
- $S(x) = S_{fil}(x)$ - is the static response obtained by measured filtering the dynamic response,
- $S(x) = S_{craw}(x)$ - is the maximum static response obtained from the passage of the testing car at a crawl speed over the bridge,
- $S(x) = S_{(thear)}(x)$ - is the maximum theoretical static response obtained from a passage of the testing car over the bridge.

3. The logarithmic decrement coefficient ϑ

$$\vartheta = \frac{1}{i} \ln \frac{S_{found}}{S_i} \tag{2}$$

where:
S_{found} is the primer vibration amplitude of the quantity S of the unloaded bridge,
S_i is the i-th amplitude counted from the primer amplitude.

The characteristics of the dynamic response of a bridge are measured with various displacement transducers (LVDT – Linear Vertical Displacement Transducers), accelerometers and strain gauges. Hereinbefore dynamic characteristics are the base for the study of the effects of changes in the stiffness of structural elements and the influence on the dynamic response. An alternative to the DC is to carry out complex dynamic analysis of the bridge using the finite element method.

Many sources of dynamic excitations are used to evaluate the dynamic characteristics of bridges:

- Passages of a testing vehicle over the bridge at various speeds as:
  - simple smooth passages of the testing vehicle,
  - passages over the bridge instrumented by the normalised (6 cm high) roughness.
- Use of the normal traffic conditions.
- Impact tests on a characteristic place of the bridge – for example by the impact generated by the back axes of the vehicle from a defined high; or sudden release of static loads.
- Eccentric mass shakers or exciters allowing the excitation of a bridge at predetermined frequencies.

* **Milan Moravcik[1], Martin Moravcik[2]**
[1] Department of Mechanics, Faculty of Civil Engineering, University of Zilina, E-mail: milan.moravcik@fstav.utc.sk
[2] Department of Structures and Bridges, Faculty of Civil Engineering, University of Zilina,

The paper presents the testing procedure used at the Department of Structural Mechanics, the University of Žilina, applied to the new highway arch bridge in highway R1 at the locality Nitra – Selenec, see Fig. 1. The theoretical vibration frequencies and mode shapes for the bridge were calculated using a finite-element model for the bridge [2]. These calculated frequencies were compared with the measured data. It should be noted that the performed analysis can be applied to further important highway bridges.

2. Description of the bridge

The tested structure is a two-lane steel arch bridge whose total length is 88.85 m and its height is 9.59 m. The construction system includes two separated steel arches on which bridge platform is hanged. The platform consists of two main steel girders connected by transverse beams and is stiffed with a reinforced concrete slab 200 ÷ 300 mm thick. The platform is hanged on arches by means of 15 hang bars and its ends are fixed into arches by stiff transverse beams. Fig. 1 shows the bridge model and its cross section.

3. Numerical analysis – Dynamic properties of the bridge

In order to evaluate the response under specified loading and standards design loads and dynamic characteristics (frequencies, mode shapes) of the bridge, the complete three-dimensional numerical FEM was set up. The analysis was carried out in the linear elastic range using the computer code ANSYS [2]. Tab. 1 gives analytical natural vibration frequencies – the first ten natural frequencies for the bridge loaded by testing vehicle of the type Tatra 815 (22,0 t)

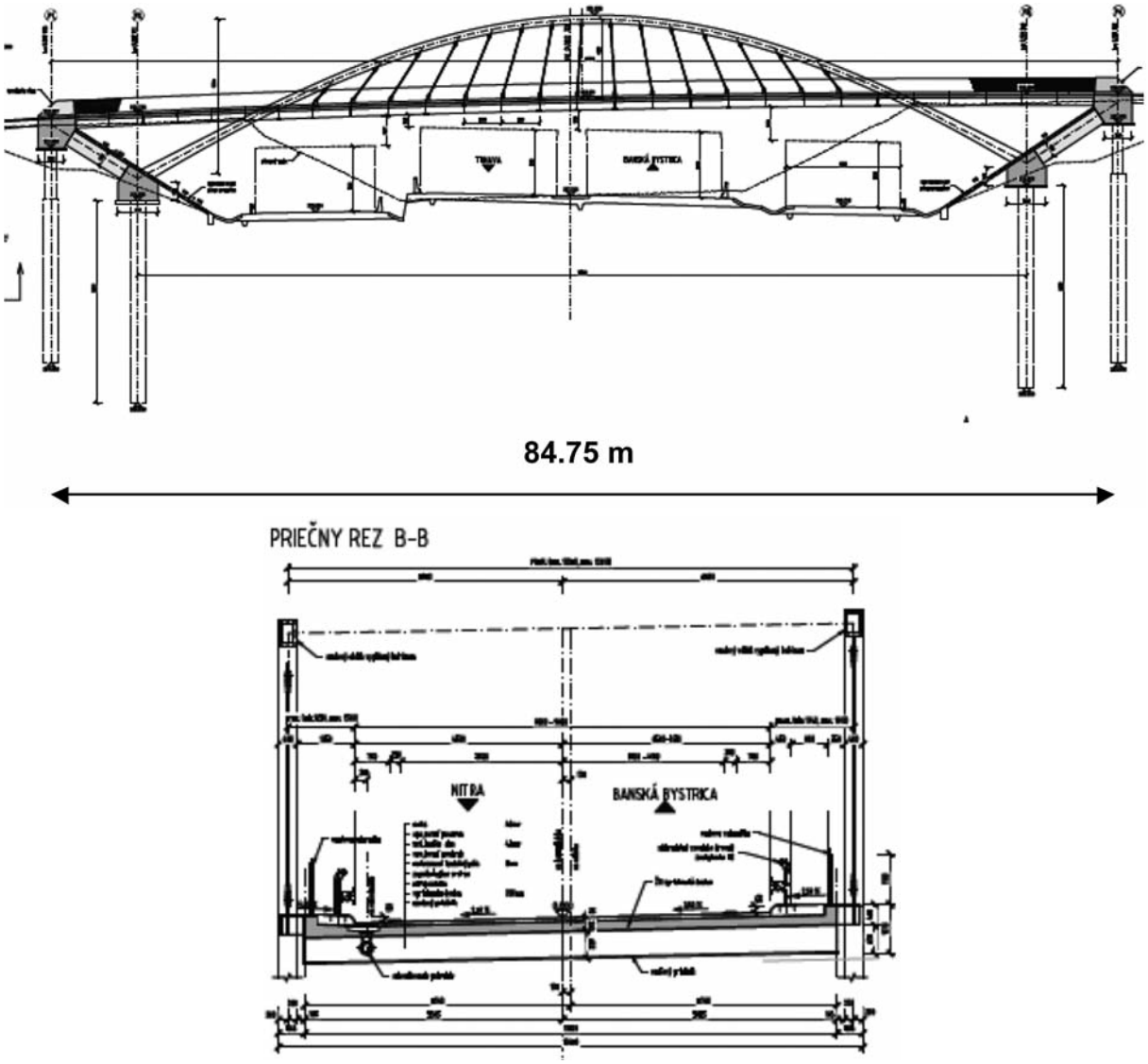

Fig. 1 The bridge model and its cross section – general arrangement.

The first ten natural vibration frequencies for the bridge loaded by the testing vehicle Tatra 815 (22,0 t) set at the middle of the bridge, [2]. Tab. 1

Analytical vibration frequencies		
Mode	Natural frekquency $f_{(i)}$ [Hz]	Shapes of vibration,characteristics of dominant forms of vibration
1	0.682	Horizontal vibration of the left arch (L.A.), the bridge deck does not vibrate.
2	0.691	Horizontal vibration of the right arch (R.A.), the bridge deck does not vibrate
3	1.850	Vibration of arches + bending vibration of the bridge deckin the 1st antisymmetric mode.
4	1,883	Vibration of arches + transverse bending vibration of the bridge deck.
5	1.927	Vibration of arches + bending vibration of the bridge deckin the 1st antisymmetric mode.
6	**2.040**	Vibration of arches + spatial bending vibration of the bridge deck.+ in the 1st antisymmetric mode.
7	**2.205**	Bending vibration of the bridge deck in the 1st symmetric mode with the max. amplitudes in the middle of the bridge deck.
8	**2.403**	Bending vibration of the bridge deck in the 1st antisymmetric mode with the max. amplitudes off the middle the bridge deck.
9	2.722	Transverse bending vibration of the bridge deck in the antisymmetric mode.
10	2.948	Bending vibration of the bridge deck with maximum amplitudes in its ends.

at the middle of the bridge. The most important theoretical natural vibration frequencies and corresponding mode shapes are presented in Fig. 2.

The theoretical natural vibration frequencies and corresponding mode shapes were calculated also for the unloaded bridge, the bridge loaded by the vehicle placed in the ½ span of the bridge deck, and the bridge loaded by the vehicle placed in the ¾ span of the bridge deck. These calculate frequencies differ only slightly and are also expected to the dynamic test of the bridge. Frequently occurred natural vibration frequencies and modes in the test are presented in Fig. 2.

4. Testing procedure

During dynamic tests different types of response in the characteristic places (x) of the bridge were measured, see Fig.3:

1. Vertical displacements measured by displacement transducers (LVDTs) of the type BOSH $R_1 \div R_2$ at the ½ range of main steel girders, and displacements $R_3 \div R_4$ at the ¾ range of main steel girders.
2. Strains measured by the strains gauges of the type KISTLER Tk1 ÷ Tk2 at the ½ range of main steel girders, and strains Tk3 ÷ Tk4 at the ¾ range of main steel girders.

- Natural frequency $f_6 = 2.040$ Hz and corresponding mode shape.

- Natural frequency $f_8 = 2.403$ Hz and corresponding mode shape.

- Natural frequency $f_7 = 2.205$ Hz and corresponding mode shape.

- Natural frequency $f_9 = 2.722$ Hz and corresponding mode shape.

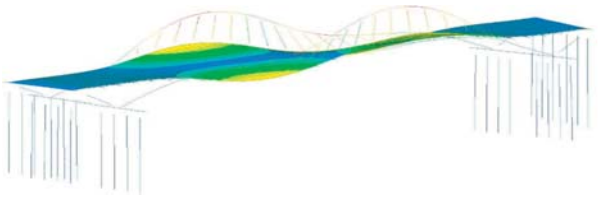

Fig. 2 Frequently occurred natural vibration frequencies $f_6 \div f_9$ in the tests and their corresponding mode shapes for vibration of the bridge deck.

3. Vertical dynamic components of the displacement A1 ÷ A2 at the ½ range of main steel girders, and components of the displacement A3 ÷ A4 at the ¾ range of main steel girders, measured by accelerometers BK 8306 of type BOSH (measured signals transformed direct on the displacements).
4. Vertical dynamic components of the displacement A5V ÷ A6V at the ½ range of arches (the top section of the arches), and the horizontal dynamic components of displacements A5H ÷ A6H at the ½ range of arches (the top section of the arches) measured by accelerometers BK 4508 of type BOSH (measured signals transformed direct on the displacement).

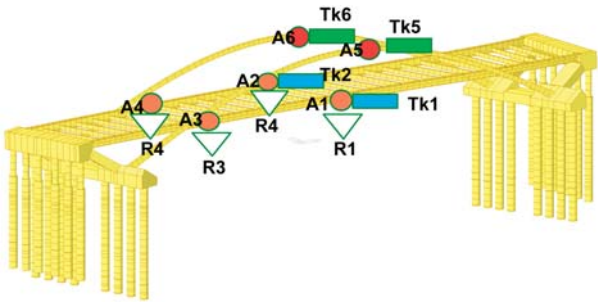

Fig. 3 Location of transducers on the bridge.

Dynamic test were carried out for passages of the testing truck Tatra 815 (the mass 22 t) at various speeds and positions on the deck:

- Passages of the testing vehicle at the centre line of the bridge:
  - symmetric passages of the testing vehicle through the centre of the bridge ("smooth crossing"),
  - symmetric passages of the testing vehicle through the centre of the bridge over the normalised (6 cm high) roughness (the normalised plank) placed on the road surface at the centre of the bridge,
  - symmetric passages of the testing vehicle through the centre of the bridge over the bridge instrumented by the normalised (6 cm high) roughness placed at the ¾ of the bridge span.
  - eccentric passages of the tested vehicle in the right line.
- Impact tests in the characteristic places ½ and ¾ of the bridge span. The impacts were applied by means of the back axes of the testing vehicle from a defined height 8 cm on the bridge deck.

The runs of the testing truck were done from the crawling speed to obtain the quasi-static loading response to the speed of 50 km/h. During the passages the dynamic response were synchronously recorded by all transducers on the computer-controlled data acquisition system DIAEM [3]. The block diagram of the measured and evaluation line is in Fig. 4.

5. Analysis of measured data

As provided in Chapter 1, dynamic tests are designed to obtain the basic characteristics of the bridge dynamic response. Obtained time measurement data were analysed in the time and the frequency range by the graphical programming environment software LabVIEW.

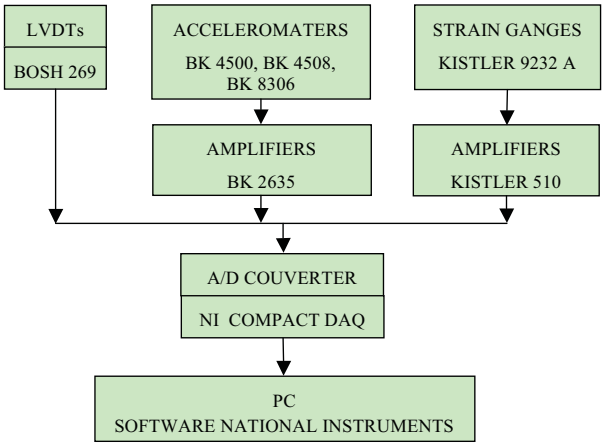

Fig. 4 The block diagram of the measured and evaluation line.

5.1 The observed dynamic coefficient (DC) $\delta_{obs}(x)$

The DC $\delta_{obs}(x)$ at a place (x) can be evaluated under controlled passage conditions – passages of the testing truck at different speeds over the bridge. The DC is defined by the relationship (1). The DC at a characteristic place (x) can be evaluated:

- directly from the vertical displacement time history $w_{dyn}(x,t)$ (transducers R1 ÷ R4) – this DC is specified as ${}^{(w)}\delta_{obs}(x)$,
- directly from the time histories of strain $\varepsilon_{dyn}(x,t)$ – the DC is specified as ${}^{(\varepsilon)}\delta_{obs}(x)$,
- combined method, using the static bridge response $w_{st}(x)$ obtained from tests or from the theoretical solution of a time history of displacement, and a dynamic increment of displacement $\Delta w_{dyn}(x,t)$ measured by accelerometers. The time history of dynamic deflection $w_{dyn}(x,t)$ at a characteristic place (x) then can be expressed:

$$w_{dyn}(x,t) = w_{st}(x) + \Delta w_{dyn}(x,t) \rightarrow {}^{(\Delta w)}\delta_{dyn}(x). \qquad (3)$$

The corresponding DC is indicated as ${}^{(\Delta w)}\delta_{obs}(x)$.

The reference value of the static quantity $S(x) \rightarrow$ the static (quasi-static) response quantity (a displacement $w_{st}(x)$, or the strain $\varepsilon(x)$) of the bridge in the place (x) was defined in the relationship (1). Examples evaluated dynamic coefficients ${}^{(w)}\delta_{obs}(x)$, ${}^{(\varepsilon)}\delta_{obs}(x)$ and ${}^{(\Delta w)}\delta_{obs}(x)$ are presented in Figs. 5÷7.

- **Dynamic coefficient ${}^{(w)}\delta_{obs}(3/4)$ – The smooth symmetric passages of the testing vehicle.**

File No. 3.6-R3: Transducer R3 placed at the ¾ span at the left main steel girder (L.G.) of the deck, Fig. 5. The vehicle speed c = 12.4 m/s = 44.6 km/h, the time of passing t_p = 7.0 s.

Dynamic coefficient:

$$^{(w)}\delta_{obs}(3/4) = \frac{w_{\max}(3/4)}{w_{st}(3/4)} = \frac{3.703}{3.423} = 1.08$$

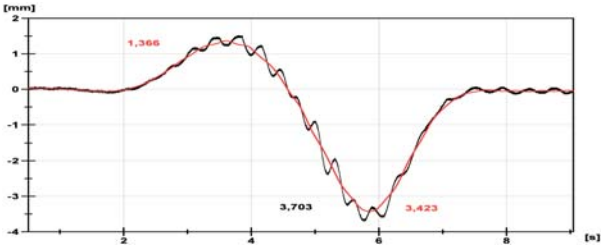

Fig. 5 Time history of the vertical displacement $w_{dyn}(4/5,t)$ and corresponding DC $^{(w)}\delta_{obs}(3/4)$ obtained directly from the vertical displacement time history $w_{dyn}(4/5,t)$.

- **Dynamic coefficient $^{(w)}\delta_{obs}{}^{*}(3/4)$ – The symmetric passage over the normalised roughness set at $x = 1/2$.**

File No. 4.6-R3: Transducer R3(3/4) placed at the ¾ span (L.G.) of the deck. The vehicle speed c = 41,7 km/h, the passage time t_p = 7,5 s Fig. 6a, b.

Dynamic coefficient:

$$\delta_{obs}{}^{*}(l = 3/4) = \frac{w_{\max}(3/4)}{w_{st}(3/4)} = \frac{5.025}{3.485} = 1.44\,.$$

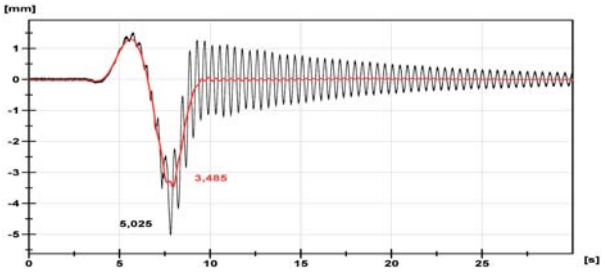

Fig. 6a Time history of the vertical displacement $w_{dyn}{}^{*}(4/5,t)$ and corresponding DC $^{(w)}\delta_{obs}(3/4)$ obtained from the passage over the normalised roughness.

- **Damping – Logarithmic decrement of damping** ϑ Logarithmic decrement of damping ϑ is evaluated from the relationship (2), Fig. 6a:

$$\vartheta = \frac{1}{20}\ln\frac{w_1}{w_{20}} = \frac{1}{20}\ln\frac{1.12}{0.50} = 0.0403$$

- **Frequency composition of the vertical displacement** $w(3/4,t)$, Fig. 6b.

Comparison of forced vertical displacements in Figs. 5 and 6 gives the comparison of the smooth symmetric passage and the passage through the normalised roughness on the dynamic coefficient $^{(w)}\delta_{obs}{}^{*}(3/4)$, and the free vertical vibration of unloaded bridge after the passage of the testing vehicle. Evaluating the logarithmic decrement of damping ϑ from Fig. 6a gives its typical small value corresponding to steel bridges.

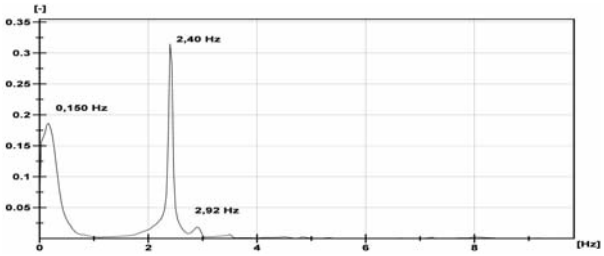

Fig. 6b Frequency composition of the forced vertical displacement $w_{dyn}{}^{*}(3/4,t)$ corresponding Fig. 6a.

The dominant frequency of the forced vertical vibration $w_{dyn}{}^{*}(3/4,t)$ for the passage of vehicle for the roughness is $\boldsymbol{f = 2.40}$*. This frequency well corresponds to the bending vibration of the bridge deck in the 1st. antisymmetric mode (the natural frequency $\boldsymbol{f_8 = 2.403}$ **Hz**) with maximum amplitudes of the vibration which correspond to the position of the testing car out of the middle of the bridge, see Fig. 6a. The other forced frequency f = 2.92 Hz corresponds to the natural frequency $\boldsymbol{f_{10} = 2.948}$ **Hz**, but this has the minority effect on the bridge vibration.

- **Dynamic coefficient – combined method $^{(\Delta w)}\delta_{obs}{}^{*}(1/2)$ – The symmetric passage over the normalised roughness in the centre of bridge.**

File No. 3.3 comb – $R2_{qst}$ /$A2$: Transducer $R2_{qst}(1/2)$ placed at the ½ span (R.G.) of the deck, accelerometer $A2(1/2)$ placed at the ½ span (R.G) of the deck. The vehicle speed c = 25.9 km/h, the passage time t_p = 12. 0 s, Fig. 7a, b.

Dynamic coefficient:

$$^{(\Delta w)}\delta_{obs}{}^{*}(1/2) = \frac{w_{\max}(1/2)}{w_{st}(1/2)} = \frac{4.795}{3.998} = 1.20\,.$$

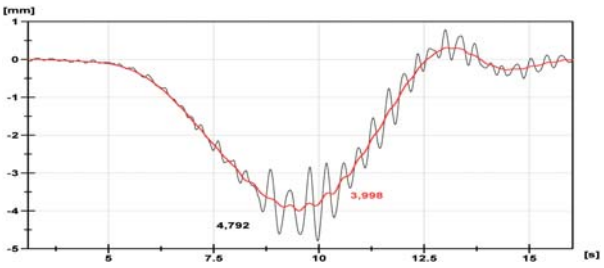

Fig. 7a Time history of the vertical displacement $w_{dyn}{}^{*}(1/2,t)$ – combined method (the transducer $R2_{qst}(1/2)$ + accelerometer $A2(1/2)$).

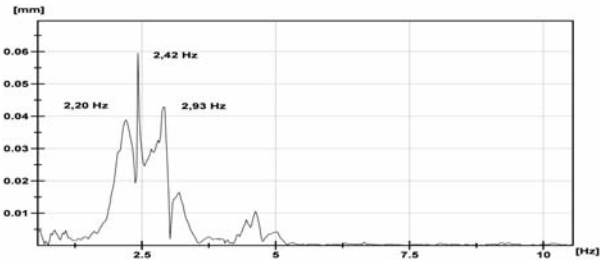

Fig. 7b Frequency composition of the forced vertical displacement $w_{dyn}^{*}(1/2,t)$ corresponding Fig. 7a.

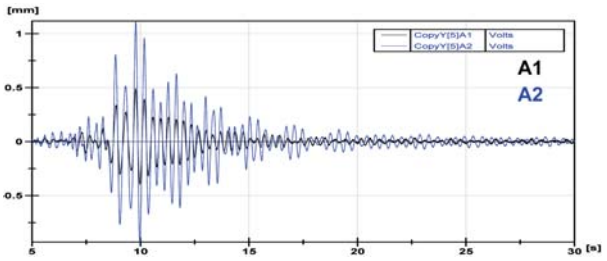

Fig. 8a Time history of the force vertical displacement $\Delta w_{dyn}(1/2,t)$ - measured by accelerometers A1(L.G. at ½), A2(R.G. at ½) on the bridge deck

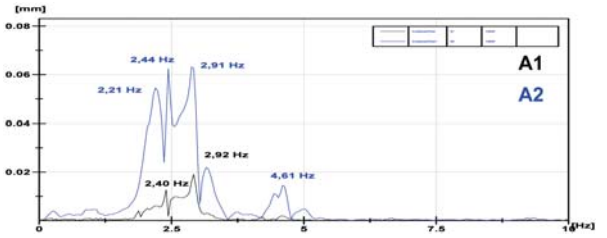

Fig. 8b Frequency composition of the forced vertical displacement - PSD $\Delta w_{dyn}(1/2,t)$ corresponding Fig. 8a.

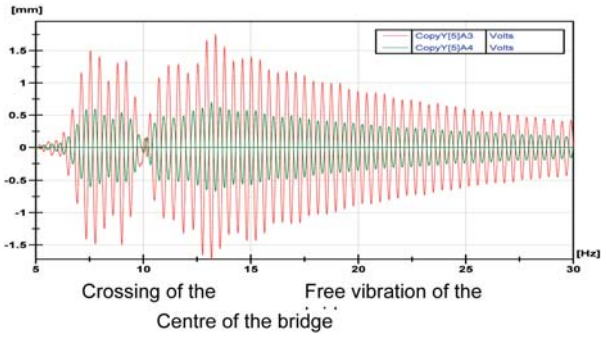

Fig. 9a. Time history of the force vertical displacement $\Delta w_{dyn}(3/4,t)$ - measured by accelerometers A3(L.G. at ¾), A4(R.G. at ¾) on the bridge deck.

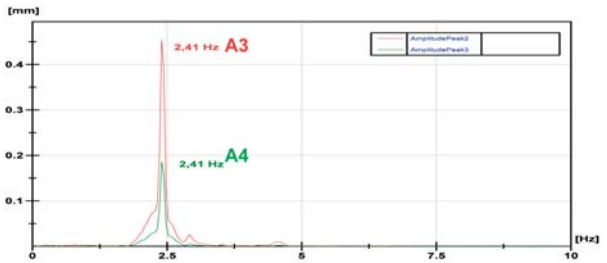

Fig. 9b Frequency composition of the forced vertical displacement - PSD $\Delta w_{dyn}(3/4,t)$ corresponding Fig. 9a.

5.2 Spectral composition of the vertical vibration of the bridge deck and arches

Vibration properties of the bridge were investigated by means of:

- A dynamic component for smooth passages $\Delta w_{dyn}^{*}(x,t)$, or passages over the normalised roughness $\Delta w_{dyn}^{*}(x,t)$ at different testing vehicle speeds.
- A dynamic component from impact tests $\Delta w_{dyn}^{**}(x,t)$ in a characteristic place (x) of the bridge – the impact generated by the back axes of the vehicle from a defined height.

The FFT were computed for each record $\Delta w_{dyn}(x,t)$. The power spectrum curves (PSD) displayed as peak amplitude values $\hat{w}(x)$ were plotted for each passage of the testing vehicle.

The time histories and power spectra of the measured response are shown in Figs. 8÷10 for the bridge deck, and in Fig. 11÷12 for the arches.

5.2.1 The bridge deck

Dynamic behaviour of the bridge deck was compared to natural frequencies and mode shapes computed using a linear elastic FEM. Analysed are records from accelerometers directly transformed on displacement $\Delta w_{dyn}(x,t)$ in the vertical direction at the positions x = A1 ÷ A4 placed at the left girder (L.G.) and the right girder (R.G.) on the bridge deck.

- **The bridge deck – Forced vibrations $\Delta w_{dyn}(1/2,t)$ generated by the smooth passage of the testing vehicle.**

File No. 3.3-A1/A2: Accelerometers A1(L.G. at ½) , A2(R.G. at ½) placed on the deck. The vehicle speed c = 25.9 km/h, the passage time t_p = 12.0 s, Figs. 8a, b.

- **The bridge deck – Forced-vibrations $\Delta w_{dyn}(1/2,t)$ generated by the smooth passage of the testing vehicle.**

File No. 3.3-A3/A4: Accelerometers A3(L.G. at ¾), A4(R.G. at ¾) placed on the deck. The vehicle speed c = 25.9 km/h, the passage time t_p = 12.0 s, Figs. 9a, b.

- **The bridge deck – Forced vibrations $\Delta w_{dyn}^{*}(1/2,t)$ generated by the passage over the normalised roughness.**

File No. 4.3-A1/A2: Accelerometers A1(L.G. at ½), A2(R.G. at ½) placed on the deck. The vehicle speed c_p = 25.9 km/h, the passage time t_p = 12.0 s, Figs. 10a, b.

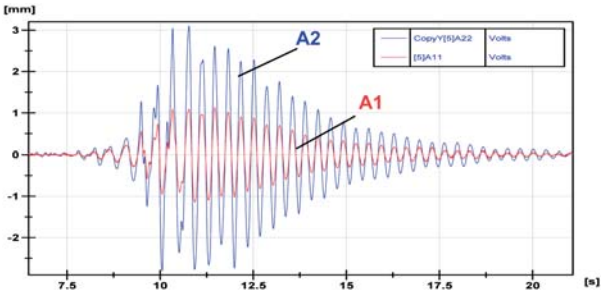

Fig. 10a Time history of the force vertical displacement $\Delta w_{dyn}^{*}(1/2,t)$ - measured by accelerometers A1(L.G. at ½), A2(R.G. at ½) on the deck.

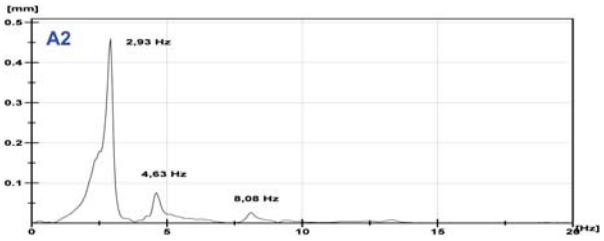

Fig. 10b Frequency composition of the forced vertical displacement - PSD $\Delta w_{dyn}^{*}(1/2,t)$ corresponding Fig. 10a.

- **The bridge deck – Forced vibrations $\Delta w_{dyn}^{**}(1/2,t)$ generated by the impact of the back vehicle axes on the bridge at ½ of the span.**

File No. 7.1-A1: Accelerometers A1(L.G. at ½) placed on the deck, Figs. 11a, b.

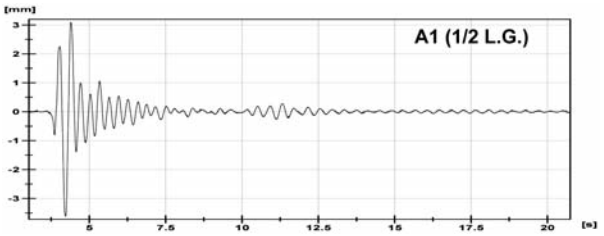

Fig.11a Time history of the force vertical displacement $\Delta w_{dyn}^{**}(1/2,t)$ generated by the impact - measured by accelerometers A1(L.G. at ½) on the deck.

The power spectra shown in Figs. 7÷10 are typical results for the measured response the bridge deck. Forced bridge vibration frequencies for all testing vehicle passages over the bridge preserved

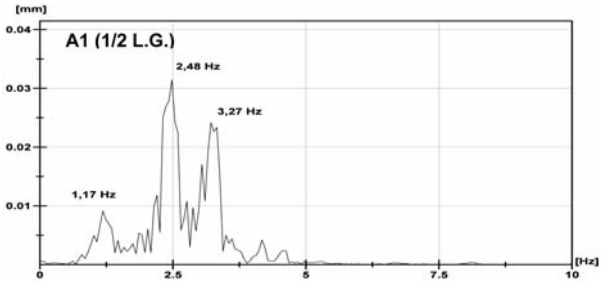

Fig. 11b Frequency composition of the forced vertical displacement - PSD $\Delta w_{dyn}^{**}(1/2,t)$ corresponding Fig. 11a.

nearly the same composition of the vertical vibration of the bridge deck.

- For the passage speeds $c_p \approx 20 \div 30$ km/h the bridge deck vibrates nearly the simple vibration shape with the bearing frequency $f^* = 2.41$ **Hz** (see Fig. 8b) which corresponds to the 8th natural frequency $f_{(8)} = 2.403$ **Hz** and the 8th shape of the bridge vibration which is loaded by the vehicle located in the centre of the bridge.
- For the speed $c_p > 20 \div 30$ km/h the bridge vibrates in a multiple shape. There are also present natural frequencies, but in the superposition with other frequency components (f_i = 2.41; 3.52; 3.21; 4.03 Hz). The frequency composition of vibration is composite and occurs in the range $f^* = 2.6 \div 5$ Hz.

5.2.2 The bridge arches

Dynamic behaviour of the bridge arches was also compared to natural frequencies and mode shapes computed using a linear elastic FEM. Analysed records from accelerometers are directly transformed on displacement in the vertical direction $^{(arch)}\Delta w_{dyn}(x,t)$ and in the horizontal direction $^{(arch)}\Delta u_{dyn}(x,t)$, at the positions x(A5, A6) placed at the top of the left arch (L.A.) and the top of the right arch (R.A.) The time histories and power spectra of the measured arch response are shown in Figs. 12÷13.

- **The arches – Forced-vibrations $^{(arch)}\Delta w_{dyn}^{*}(1/2,t)$ generated by the passage over the normalised roughness.**

File No. 4.3-A5V: The vertical accelerometer $A5_V$ (L.A. at ½) placed on the arch. The vehicle speed c = 25.9 km/h, the passage time t_p = 12.0 s, Figs. 12 a, b.

File No. 4.3-A5H: The horizontal accelerometer $A5_H$(L.A. at ½) on the arch. The vehicle speed c_p = 25.9 km/h, the passage time t_p = 12.0 s, Figs. 13 a, b.

The analyses carried out in the time and frequency domain show and confirm that the wind effect on the vibration of bridge arches was dominant in the time of the measurement of bridge and dominated over the vehicle passages effects, see Fig. 12 and

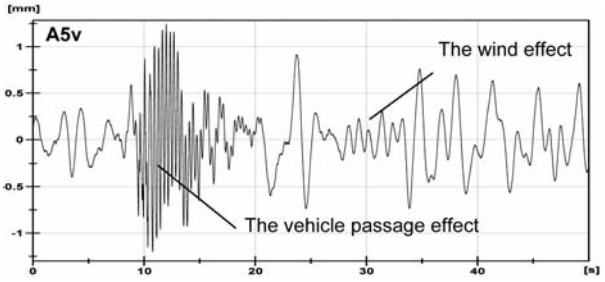

Fig. 12a Time history of the force vertical displacement $^{(arch)}\Delta w_{dyn}{}^{*}(1/2,t)$ *- measured by accelerometers* $A5_V$*(L.A. at ½) on the arch.*

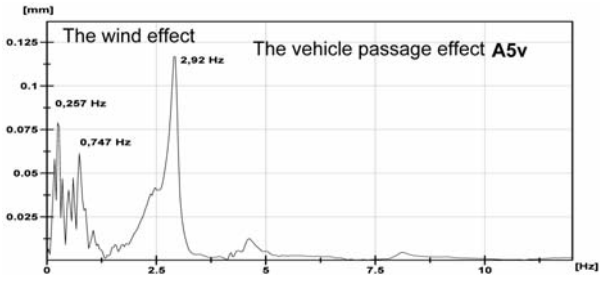

Fig. 12b Frequency composition of the forced vertical displacement - PSD $^{(arch)}\Delta w_{dyn}{}^{*}(1/2,t)$ *corresponding Fig. 12a.*

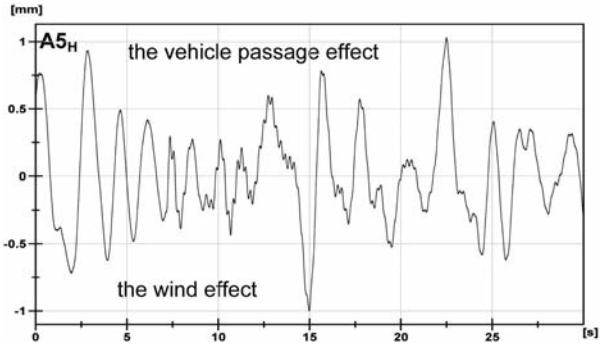

Fig. 13a Time history of the force horizontal displacement $^{(arch)}\Delta w_{dyn}{}^{*}(1/2,t)$ *- the accelerometer* $A5_H$*(L.A. at ½) on the arch.*

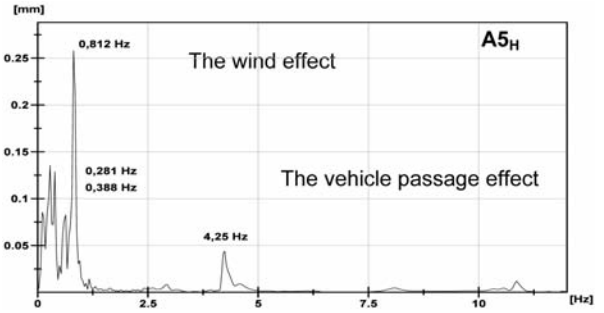

Fig. 13b Frequency composition of the forced horizontal displacement corresponding to 13a.

Fig. 13. The carrier frequencies of vertical and horizontal vibrations were different:
- The dominant frequencies for the wind effect in the vertical and the horizontal direction lie in the frequency range $f_{wind} \approx 0.8$ Hz.
- The dominant frequencies for the vehicle passage effect lie in the frequency range $f \approx 2.4 \div 4.4$ Hz

6 Conclusions

The results derived from the dynamic test of the bridge and their comparison with those theoretically predicted permit the assessment of the actual bridge stiffness. They served also to assess the actual structural behaviour in the vertical and horizontal plane. Produced loading tests:

1. Passages of a testing vehicle over the bridge at various speeds as:
   - simple smooth passages of the testing vehicle,
   - passages over the bridge instrumented by the normalised (6 cm high) roughness.
2. Impact tests on a characteristic place of the bridge – the impact generated by the back axes of the vehicle from a defined height, confirm that the bridge response parameters correspond with the expected ones of the bridge model and the theoretical results. The tests results confirm the expected values of the dynamic coefficients $^{(w)}\delta_{obs}(x)$, $^{(\varepsilon)}\delta_{obs}(x)$ and $^{(\Delta w)}\delta_{obs}(x)$:

1/ Passages of the testing vehicle Tatra 815 (22t):

- **Bridge deck**

a/ Direct measurement $\delta_{obs}(x)$:
$max\ ^{(\varepsilon)}\delta_{obs}(1/2) = 1.17$, mean $^{(\varepsilon)}\delta_{obs}(1/2) = 1.109 \div 1.16$,
$max\ ^{(w)}\delta_{obs}(3/4) = 1.108$, mean $^{(w)}\delta_{obs}(3/4) = 1.06$,

b/ Combined method $\delta_{obs}(x)$:
$^{(w)}\delta_{obs}(1/2) = 1.48$, mean $^{(w)}\delta_{obs}(3/4) = 1.17$,
$^{(w)}\delta_{obs}(3/4) = 1.08$, mean $^{(w)}\delta_{obs}(3/4) = 1.06$.

- **Bridge arches**

a/ Direct measurement $\delta_{obs}(x)$:
$max\ ^{(\varepsilon)}\delta_{obs}(1/2)^{(Obl)} = 1.12$, mean $\delta_{obs}(1/2) = 1.11$.

2/ Passages of the testing vehicle Tatra 815 (22t) over the bridge instrumented by the normalised (6 cm high) roughness:

- **Bridge deck**: Direct measurement $\delta_{obs}(x)$:
$^{(w)}\delta_{obs}(3/4) = 1.05 \div 1.44$,
$^{(\varepsilon)}\delta_{obs}(1/2) = 1.43 \div 1,69$.

- **Bridge arches:** Direct measurement $\delta_{obs}(x)$:
$^{(\varepsilon)}\delta_{obs}(1/2)^{(Arch)} = 1.12$, mean $^{(\varepsilon)}\delta_{obs} = 1.11$.

The dynamic coefficient $\delta_{obs}(x)$ in characteristic locations (x) of the bridge structure for all measured passages of the testing vehicle fulfil requirements of the Slovak National Standard STN 73 6209 "Loading tests of bridges" [1], that specifies conditions for the performance of dynamic tests for highway bridges:

$$\left(\delta_{obser} - 1\right)\eta_{dyn} \leq \delta - 1 \qquad (4)$$

where:
δ is the dynamic coefficient considered in the design, $\delta = 1.172$
η_{dyn} is the dynamic efficiency of the applied loading $\eta_{dyn} = 0.117$

All applied tests – passages of the testing vehicle and the impact tests show an elastic behaviour of the structure. Measured dynamic displacements and strains achieve values expected from the static calculation. The bridge structure behaved elastically – all measured deformations reached expected small values and no non-linear behaviour was indicated.

References

[1] STN 73 6209 Loading tests of bridges (in Slovak), 1979, in Slovak.
[2] HSP s.r.o.: Technical report (in Slovak) – Objekt 201-00: Background Papers for Loading Test, Brno 2010.
[3] National Instrument: DIAdem Guide for Storing, managing and Analyzing of Measurement Data, Digital, http://www.ni.com/manuals.nsf.

Milan Moravcik *

ANALYSIS OF VEHICLE BOGIE EFFECTS ON TRACK STRUCTURE – NON-STATIONARY ANALYSIS OF DYNAMIC RESPONSE

The present paper is concentrated on the analysis of in situ vibration measurements during operating conditions in the track structure for loading by current passenger trains at the new built up railway corridor in the section Bratislava – Trnava. Tests were carried out to determine the dynamic track behaviour and relative dynamic effects between the track components – the rails, the sleepers, and the ballast bed during the passage of characteristic passenger trains moving at the operating speeds 70 ÷ 130 km/h. Experimentally obtained signals of the dynamic response of track components – measured as vertical accelerations and displacements of the rails, sleepers, and ballast bed are analysed in detail as the nonstationary random signals corresponding passages of characteristic vehicle bogies (locomotives, coaches). Vertical dynamic response of these components were measured at two different locations of this section and the vertical dynamic behaviour of track components were investigated in the time domain and analysed in the frequency domain up to 500 Hz.

1. Introduction

Dynamic phenomena in the track structure are associated with the operating conditions and are in the direct relation with the vehicle–track dynamic interaction. Field tests were carried out to determine the dynamic behaviour and relative vertical dynamic effects between the track components – the rails, the sleepers, and the ballast bed during the passage of characteristic passenger and freight trains moving at the operating speeds. In concentrating on the track structure the dynamic effects may be divided into two groups:

1. The vibration of the track structure – the vibration of rails, sleepers, and the ballast layer and the wave propagation in the track structure.
2. The wave propagation in the surrounding of the track which can produce vibrations to adjacent structures and radiated noise.

This paper is focused on the first area of the dynamic response. The dynamic phenomena in the track structure are caused by several mechanisms which are well known:

- the quasi-static excitation due to the moving axle load of trains,
- the wheel and the rail roughness and their defects,
- the type of trains loading the track and their composition and speed,
- the excitation due to discrete supports of the rail by sleepers, etc.

When the frequencies of interest are low, we speak about "structural vibration" and for higher frequency components about "structural-borne sounds" and "air-borne sounds". Their origin of sound emission, however, is always in structural vibration of track components. One effect of the moving load is associated with the wave propagation in the rails and in the subsoil which is presented at the higher speed train. Another phenomenon is linked to the Doppler effect which forms two peaks in the frequency spectrum for any frequency component.

All these dynamic phenomena are analyzed in particular through the theoretical – simulation approaches, such as in Refs. [1, 2, 5, 6]. One simulation model developed at the Department of Structural Mechanics [5], was addressed to the study of dynamic behaviour of the track structure, especially the evaluation of the dynamic behaviour and the response of track components (rails, sleepers, the ballast bed) due to variability in the vertical stiffness of rail supports [5, 6]. In fewer cases the experimental approach is applied, especially focussed on the free field vibration measurements during the passage of train [3, 4, 7]. In addition to analytical models for the dynamic train-track interaction the experimental analyses are needed for the validation and appreciation of these vibrations. Experimental results have also important place in dynamic tuning of the moving vehicle – track. The three most common approaches to detect dynamic response of track components are based on the use of either:

(a) Deflections measurement $w_x(t)$ using the displacement transducers DR, DS imbedded in a fixed reference datum at a position x to measure the response, see Figs. 3, 4.
(b) Acceleration measurements $w''_x(t)$ using the accelerometers $x = A_R, A_S, A_B$ that are glued on the rail web or on the sleeper and which require no fixed datum to measure the response at a position x, see Figs. 3, 4.
(c) Strain measurements $\varepsilon_x(t)$ using the strain gauges T_R that are glued on the rail web (R) or on the sleeper (S) at a position X to measure the response.

* **Milan Moravcik**
Faculty of Civil Engineering, University of Zilina, Slovakia, E-mail: milan.moravcik@fstav.uniza.sk

This contribution is devoted right to experimental measurements and the detailed analyses of in situ measured signals in the frequency domain up to 500 Hz. The paper is focused on the analysis of the track response of passenger trains only. The frequency composition of the vibration is measured as vertical accelerations $w''_x(t)$ for track components X at the position x on the track: $x \rightarrow$ the rail / accelerometer A_R, sleepers / the accelerometer A_S, and the ballast bed / the accelerometer A_B. Displacement amplitudes can be calculated from measured accelerations. Displacement amplitudes $w_x(t)$ were measured also direct by displacement transducers D_R, D_S.

2. Measured track structure

The in situ measurements were made on the newly built up railway corridor in the line Bratislava – Žilina at the two locations at the straight section track Cífer – Trnava, Fig. 1. Measurements were executed in the summer 2008 and 2009. Measured track is the convectional ballasted track with UIC 60 rails supported every 0.60 m by rubber pads on the monoblock concrete sleepers of the type PB-3/Cana. The rails are continuously welded and are fixed with the Vossloh fastening system Skl 14.

The track is supported by the substructure consisting of ballast layer (gravel aggregates of the calibre 32/53 mm) of the thickness $h_1 = 0.35 \div 0.55$ m, the sub-ballast layer of the thickness h_2 – the gravel support layer $h_2 = 0.4$ m laying on the geotextile of the type Tensar SS 30 and the filtering geotextile Tatratex T200, put on the subgrade, see Fig. 2.

Fig. 1 The measured track section in the location Cífer - Trnava

3. Experimental setup

The vertical vibrations of rails (R), sleepers (S) and ballast layer (B) between the sleepers were measured as the vertical acceleration $w''_x(t)$, $x = (R, S, B)$, the vertical relative displacement $w_x(t)$, $x = (R, S)$, and the strain measurement $\varepsilon_x(t)$ at a position x

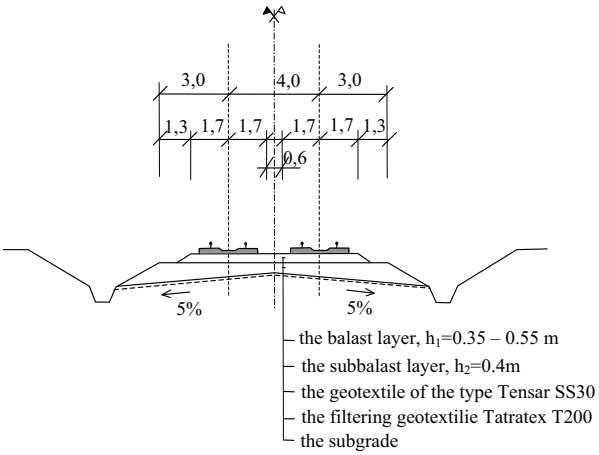

Fig. 2 The cross section of the ballasted track at the measured track section.

$= (R, S)$ on the rail or on the sleepers. The B&K piezoelectric accelerometers A_R, A_S, of the type BK 4500 were glued to the rail and the sleeper. The BK 8306 seismic accelerometer A_B was embedded into the plaster bed in ballast layer between the sleepers at the depth of placing sleepers, see Figs. 3 and 4. The vertical displacements $w_R(t)$ of the rail and the sleeper $w_S(t)$ were measured by the relative displacement transducers of the type Bosh mounted on the fixed reference datum (displacement transducers D_R, D_S). The direct dynamic strain $\varepsilon(t)$ of the rail was measured by the Kistler piezoelectric tensiometer T_R mounted on the rail flange.

Direct dynamic deflection measurements using the displacement transducers D_R, D_S provide a frequency response limited. Using accelerometers A_R, A_S, A_B gives the response in the broad frequency range and is attractive since no fix datum is required.

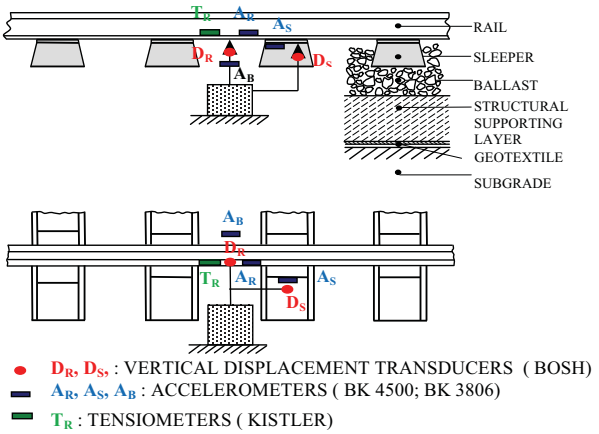

Fig. 3 Scheme of the measurement set-up and positioning transducers in the track.

Measured quantities – deflections $w_x(t)$, vertical accelerations $w''_x(t)$, and strains $\varepsilon_x(t)$ were recorded as electrical signals and

transformed by means of the analogy–digital convector of the type 32-channel NI CompactDAQ data acquisition. The A/D device records the signals with the chosen sampling frequency f_s = 1000 Hz directly into the computer memory. The NI DIAdem interactive software for managing and analysing the data was applied.

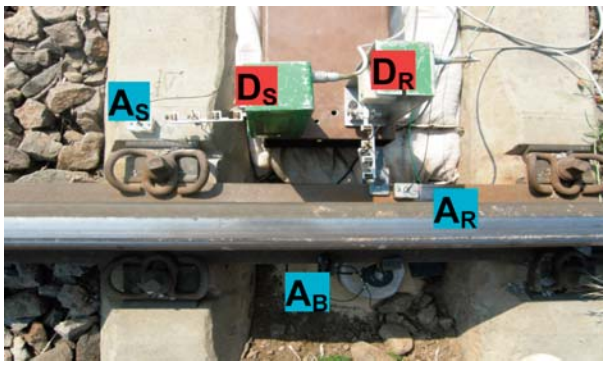

Fig. 4 Position of transducers in the track: Transducers D_R, A_R on the rail, accelerometers A_S, A_S on the sleeper, and A_B in the ballast.

4. The characteristics of the measured passenger trains

The measured track section was loaded by the passenger and freight trains running in operational conditions. As the paper is devoted to the analysis of passenger trains only, the typical configuration of a passenger train is shown in Fig. 5. They consist of a locomotive and 5÷10 carriages of a similar composition. The speed of passenger trains in the measured section varies between 90 km/h ÷ 130 km/h. The locomotives of passenger trains (types EL350, EL150, EL263) are supported by 2 bogies, equally as the coaches, see Fig. 5 and Tab. 1.

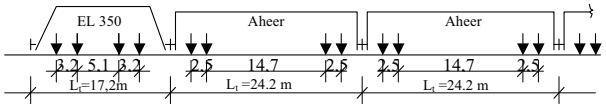

Fig. 5 A typical configuration of the measured passenger train.

The basic spatial and mass characteristics of locomotives and coaches for the passenger transport are the coach total length L_t, the distance between bogies L_b, the wheelset distance in a bogie L_a, the total vehicle mass M_t, the bogie mass m_{bog}, and the one axle mass (the unsprung mass of the one wheelset) $m_{1,uns}$. and they are summarised in Table 1. While the quasi-static contribution in the track response depends on the total mass of vehicles M_t, the dynamic load contributions depend dominantly on the unsprung mass of wheelsets m1,uns.

5. Measured time history during the passage of trains

In Fig. 6 are presented characteristic time histories of the rail deflection $w_R(t)$, the rail acceleration $w''_R(t)$, and the sleeper acceleration $w''_S(t)$ corresponding to the passage of the passenger train EL 350+8 carriages, speed c = 32.9 m/s = 119 km/h.

5.1 Time histories of the track response and their analysis – Nonstationary signals

File TN II/No.2: The passage of the passenger train EL 350+8 coaches, EL 350+8 coaches, LABWIEV, f_s = 1000 Hz, the non-filtered time records, see Fig. 6a, b, c, d:

a/ Time history of the vertical rail displacement $w_R(t)$/the transducer D_R,
b/ Time history of the vertical rail acceleration $w''_R(t)$/the accelerometer A_R,
c/ Time history of the vertical sleeper acceleration $w''_S(t)$ the accelerometer A_S,
d/ Time history of the vertical ballast bed acceleration /the accelerometer A_B.

The bogie passages of a locomotive and coaches next the locomotive form a characteristic load of the track – impulse load activated by vehicle bogies.

The obtained time histories of the vertical acceleration (measured signals) $w''_R(t)$, $w''_S(t)$ and $w''_B(t)$ represent generally random functions of time t describing the track response. In the full sense of the word they represent the generally nonstationary random

The geometrical and mass characteristics of vehicles for the coaching traffic in ŽSR — Table 1

Locomotives	Axles	The length [m]			The mass [t]		
		L_t	L_b	L_a	The total vehicle mass M_t	The bogie mass $m_{bog.}$	The axle mass $m_{1,uns.}$
EL 162, 163	4	16.80	5.10	3.20	85.0	20.520	2.466
EL350	4	17.24	5.10	3.20	87.6	20.520	2.466
EL 262, 363	4	16.80	5.10	3.20	87.0	20.520	2.466
EL 150	4	16.74	5.10	3.20	87.0	20.520	2.466
Carriages	Axles	Lt	Lb	La	Mt	mbog.	m1,uns.
Aheer, Bheer	4	24.5	14.7	2.5	43.0 ÷ 48.0	6.400	1.34
Bte	4	24.5	14.6	2.6	34.0 ÷ 42.0	6.800	1.45
Bai	4	24.5	14.7	2.6	38.0 ÷ 44.0	6.800	1.45

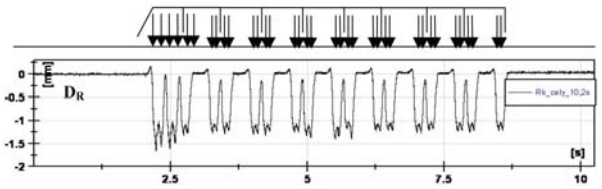

a/ Time history of the vertical rail displacement $w_R(t)$/the transducer D_R.

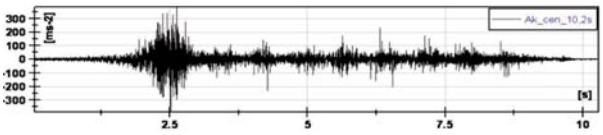

b/ Time history of the vertical rail acceleration $w''_R(t)$/ the accelerometer A_R.

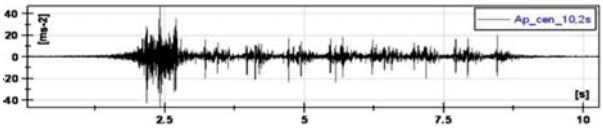

c/ Time history of the vertical sleeper acceleration $w''_S(t)$/the accelerometer A_S.

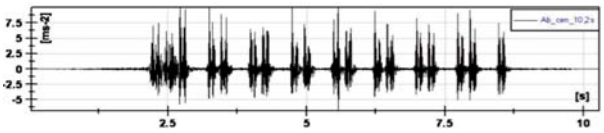

d/ Time history of the vertical ballast bed acceleration /the accelerometer A_B .

Fig. 6 Time histories of the kinematic quantities measured response $w_R(t)$, $w''_R(t)$, $w''_S(t)$, for the passenger train EL 350+8 coaches, t = 6.0 - 12.3 = 6.3 s, c = 119 km/h.

processes with the time-varying mean square value corresponding to the passage of bogies of coaches through the measured place. In the broader sense they may be considered as the stationary processes [8]. Then, the frequency analysis of obtained time signals can be applied as:

(1) The analysis of whole passage of the train – the measured signal is considered as a stationary one (the passage of the whole train over the measured site).

(2) The analysis of selected stationary parts of the signal and use the technique of window function (considering the short section as a stationary process). This is applied to the passage of locomotive bogies, characteristic coach bogies (couple of bogies), or the passage of characteristic parts of the train (the passage of characteristic coaches).

Then, the passage of the coach bogies over a measured place constitutes characteristic cyclic signals that in the long term they may be considered stationary, but in the short term they are non-stationary ones. The NI DIAdem interactive software for managing and analysing the measurement data [9] was applied for the spectral analyses of these signals.

6. Spectra of the vertical acceleration of the track components due to passenger trains

While the dominant frequency composition of the deflection $w_x(t)$ of rails and sleepers (measured by displacement transducers D_R, D_S) present a low frequency range only, the frequency content of acceleration $w''_x(t)$ of these motions gives a wide range of frequencies. At the same time we have to keep in view the relations between the displacement amplitude $\hat{w}_o(f)$ and the acceleration amplitude $\hat{w}_o''(f)$ at a given frequency component fi.

$$\hat{w}_o(f) = -\frac{\hat{w}_o''(f)}{(2\pi f)^2} \tag{1}$$

Frequency analyses performed from the time signals were focused just to the frequency content of the vertical acceleration of the track component response during the passage of trains. However, for the train speed lower than the wave speeds propagating in the ground, the measured quantities may be considered as a dynamic component of the response that strongly dominates over the quasi-static axle loads response.

In the track response measurements the sampling frequency f_s of the measured signal (the discrete sampling of a measurement time signal) plays an important role because of speedy processes (the quasi impact processes). An analysed record $\{x(t)\}$ of the total length T_r is divided into nd segments of the length T – the record length T. Then, the one-side auto-spectral density function $G_{XX}(f_k)$ for a arbitrary frequency component f_k is given [8, 9]:

$$G_{XX}(f_k) = \frac{2}{n_d T}\sum_{i=1}^{n_d}\left|X_i(f_k)\right|^2,\ k = 1, 2, 3, \ldots N/2 \tag{2}$$

where:

$$X_i(f_k) = \Delta t \cdot X_{ik} = \Delta t \sum_{n=0}^{N-1} x_{in} \cdot \exp\left[\frac{-j2\pi kn}{N}\right] \tag{3}$$

N is the sample size (the block size) → N = 128, 256, 512, 1024, 2048, 4096.

The frequency response function (FRF) $H_{X\to Y}(f)$ for an input signal $\{x(t)\}$ and output signal $\{y(t)\}$ can be displayed as the estimators:

1/ The estimator for uncorrelated output noise:

$$H_{1,X\to Y}(f) = \frac{G_{XY}(f)}{G_{XX}(f)} \tag{4a}$$

2/ The estimator for uncorrelated input noise:

$$H_{2,X\to Y}(f) = \frac{G_{YY}(f)}{G_{YX}(f)} \tag{4b}$$

where: $G_{XY}(f_k)$ is cross-spectral density function.

The important step in the frequency analysis of the time signals is the choice of a time window function. The Hanning weighting was applied in the analyses. For the applied sample frequency f_s = 1000 Hz, and a chosen sample size N the resolution frequency β is

$$\beta = \frac{1}{T} = \frac{f_s}{N} \quad (5)$$

N	128	256	512	1024	2048
β [Hz]	7.8	3.9	1.95	0.98	0.48

The Hanning weighting to "the quasi-stationary time record of the train passage" with the adequate overlapping 50% of the record length T and the averaging of these signals was applied. The spectral analyses were displayed as the Power spectrum (PWS), or the Power spectral density (PSD).

6.1 The spectral analysis of the whole train passage – analysis of a stationary signal

The passage of the train (EL 350+8 coaches) over the measurement site is considered and analysed as a stationary time record, as shown in Fig. 7. This approach does not take account of the non-stationary of signal.

- **File TN II/No. 2-AS: Passage of the train EL 350+8** coaches, t = 6.0 – 12.3 = 6.3 s, c = 32.9 m/s = 119 km/h, Analysis of the vertical sleeper acceleration $w''_S(t)$/the accelerometer A_S, f_s = 1000 Hz, Fig. 7.

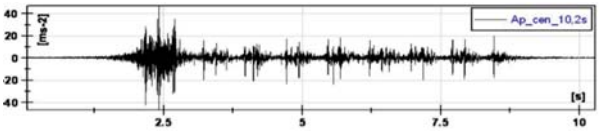

a) The time history of the vertical sleeper acceleration $w''_S(t)$/the accelerometer A_S.

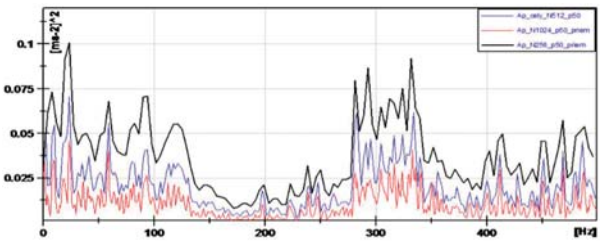

$f_{(1)}$ = 8, 23, 59, 91, 119 Hz $f_{(2)}$ = 281÷332 Hz

b) LABVIEW Analysis: The PWS of the sleeper acceleration $w''_S(t)$/ the accelerometer A_S – passage of the train EL 350+8 coaches.
The analyses for:
→ A_S: PWS, the block size N1024, overlap 50% – Mean 19 sp. PWS,
→ A_S: PWS, the block size N512, overlap 50% – Mean 39 sp. PWS,
→ A_S: PWS, the block size N256, overlap 50% – Mean 79 sp. PWS.
The non-filtering signal for frequencies f = (0 – 500 Hz).

Fig. 7 Analysis of the vertical sleeper acceleration $w''_S(t)$/the accelerometer AS for the passage of the train EL 350+7 coaches, t = 6.0 – 12.3 = 6.3 s, c = 32.9 m/s = 119 km/h.

Considering to option of the block size (N), option of the overlap (%) and averaging obtained PVS the resulting mean power spectrum (PVS) gives a gross picture of frequency composition of the response. This analysis averages the frequency composition of the response.

6.2 Spectral analysis for the locomotive EL350 passage – analysis of segmented stationary part

The passage of locomotive EL 350 bogies over the measurement site evidently differs from the coach bogies – it is considered as a non-stationary signal with the variable mean square value. This signal can be segmented into stationary parts which can be analysed as a stationary signal, as is shown in Fig. 8.

- **File TN II/No.2-A_S:** The passage of the locomotive EL 350, c = 32.9 m/s = 118 km/h, Analysis of the vertical sleeper acceleration $w''_S(t)$/the accelerometer A_S – selected stationary part of the signal for t = 2.0 – 3.05 s = 1.05 s, f_s = 1000 Hz, Fig. 8.

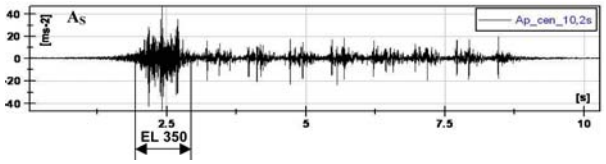

a) The time history of the vertical sleeper acceleration $w''_S(t)$/the accelerometer A_S – Passage of the locomotive EL 350, t = 2.0 – 3.05 s = 1.05 s.

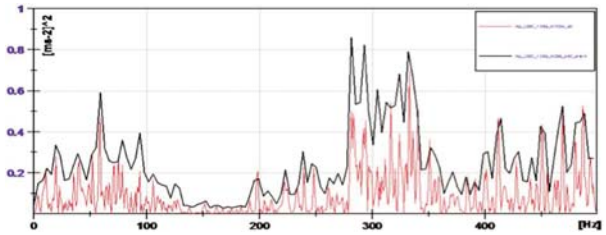

*$f_{(1)}$ = 19, **58**, 78, 93 Hz $f_{(2)}$ = 281÷332 Hz*

b) LABVIEW Analysis: The PWS of the sleeper acceleration $w''_S(t)$/the accelerometer A_S – The passage of the locomotive EL 350, t = 2.0 – 3,05 s = 1.05 s.
Analysis for: → A_S: PWS, the block size N1024, 1 sp. PWS,
→ A_S: PWS, the block size N256, overlap 50% – Mean 7 sp. PWS.
The non-filtering signal for frequencies f = (0 ÷ 500 Hz).

Fig. 8 Analysis of the vertical sleeper acceleration $w''_S(t)$/the accelerometer A_S for the passage of the locomotive EL 350 – selected stationary part of the signal for t = 2.0 – 3.05 = 1.05 s.

Comparison results of analyses in Figs. 7 and 8 show qualitative differences:
- The analysis in Fig.7 for the passage of the all train EL 350+8 coaches, t = 0 – 10.24 = 10.24 s gives different frequency com-

position at the frequency area f = 0 – 150 Hz in comparison with the analysis in Fig. 8 – the passage of the locomotive EL 350, t = 2.0 – 3.05 s = 1.05 s.
- Averaging of data for the passage of the all train EL 350+8 coaches makes smaller values as the analysis of the locomotive L350 passage.
- The general character of the frequency composition remains approximately sustained – there are two characteristic frequency areas $f_{(1)} \approx$ 0 – 150 Hz, and $f_{(2)} \approx$ 280 – 350 Hz.

6.3 Spectral analysis for the passage of coach bogies – analysis of segmented stationary part

The passage of coach bogies over the measurement site evidently differs from the passage of the locomotive as showed the time histories, Fig.9. Then the extract part of signals can be analysed as a stationary signal (cyclic signals), as is shown in Fig. 9. The Hanning weighting to the passage of coach bogies (a quasi-stationary time record) was applied.

- **File TN II/No.2-A$_S$:** The passage of coach bogies, c = 32.9 m/s = 118 km/h, t = 3.01 – 3.8 = 0.79 s, Analysis of the vertical sleeper acceleration $w''_S(t)$/the accelerometer A_S, f_s = 1000 Hz, Fig.9a, b, c.

Comparison results of analyses in Figs. 8 and 9 again show qualitative differences in the frequency composition:
- The analysis in Fig. 8 for the passage of the locomotive EL 350, t = 2.0 – 3.05 s = 1.05 s, gives different frequency composition than the analysis in Fig. 9 – the passage of coach bogies No.1-2, No. 2-3, No. 3-4, t = 3.01 – 3.8 = 0.79 s.
- Averaging of data for the passage of the whole train EL 350+8 coaches gives smaller values than for the passage of bogies of locomotive EL350.
- The general character of the frequency composition remains sustained – there are two characteristic frequency areas $f_{(1)} \approx$ $\approx$ 0 ÷ 150 Hz, and $f_{(2)} \approx$ 280 ÷ 350 Hz.

- **File TN II/No.2 -Ab:** a/ The time history of the vertical ballast bed acceleration $w''_B(t)$/the accelerometer A_B – The passage of coach bogies No.1-2, t = 0.79 s, Fig. 10 a, b.

- **File TN II/No.2 – A_S/A_B: Transfer function $H_1(A_S/A_B)$** – Transfer function "sleeper A_S" / "ballast bed A_B" for the passage of coach bogies No. 1-2, t = 3.01 – 3.8 = 0.79 s, Fig. 11.

7. Results of dynamic analyses

The measured time histories of the vertical rail acceleration $w''_R(t)$, sleeper accelerations $w''_S(t)$, and ballast bed acceleration $w''_B(t)$ and corresponding spectra PSD or PWS give the principal picture of the dynamic behaviour of the track structure for passages of the characteristic passenger trains.
- **The amplitudes of the vertical acceleration of track components** – the rail $w''_R(t)$, $w''_S(t)$, and $w''_B(t)$) are gradually damped in the

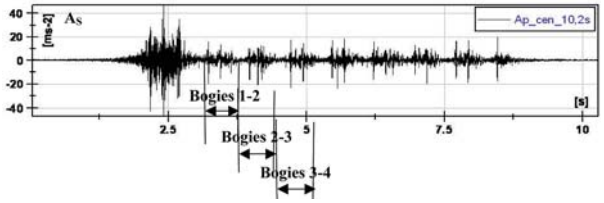

a) The time history of the vertical sleeper acceleration $w''_S(t)$/the accelerometer A_S -The passage of coach bogies No.1-2, No. 2-3, No. 3-4, t = 3.01 – 3.8 = 0.79 s.

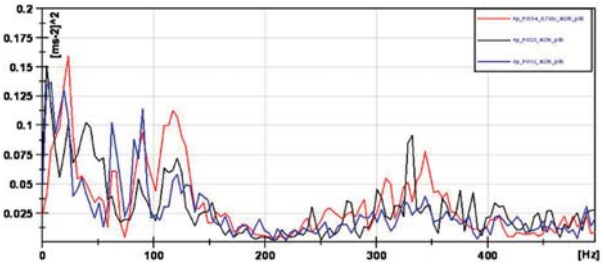

b) LABVIEW Analysis: The PWS of the sleeper acceleration $w''_S(t)$/the accelerometer A_S – The passage of coach bogies No. 1-2, No. 2-3, No. 3-4, t = 3.01 – 3.8 = 0.79 s. Analysis for bogies No.1-2, bogies No.2-3, bogies No.3-4, → the block size N256, overlap 50% – the mean of 5 PWS. The non-filtering signal for frequencies f = (0÷500 Hz).

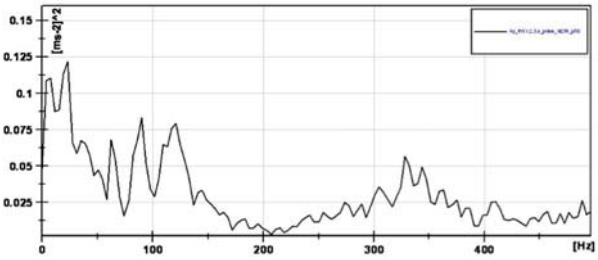

c) b) LABVIEW Analysis: The PWS of the sleeper acceleration $w''_S(t)$/ the accelerometer A_S – The passage of coach bogies No.1-2, No. 2-3, No. 3-4, t = 3.01 – 3.8 = 0.79 s. The mean of 3 PWS, for the three bogies passage: bogies No. 1-2, bogies No. 2-3, bogies No. 3-4. The non-filtering signal for frequencies f = (0 ÷ 500 Hz).

Fig. 9 Analysis of the vertical sleeper acceleration $w''_S(t)$/the accelerometer AS for the passage of coach bogies No.1-2, No. 2-3, No. 3-4, t = 3.01 – 3.8 = 0.79 s.

vertical direction. The standard acceleration rail peaks for locomotives occur up to 300 m/s^2 and for coaches up to 50 ÷ 100 m/s^2. These peaks are reduced on the sleepers up to 30 m/s^2 and on the ballast bed to 8 ÷ 10 m/s^2, as can be seen in Fig. 6.
- **Spectral analysis of segmented stationary parts of the response**

The passage of vehicle bogies generally represent nonstationary random processes with the time-varying mean square values corresponding to the locomotive bogie passages and coach bogie passages. The analysis of a selected stationary part of the signal considered as a stationary process applied on the passage of loco-

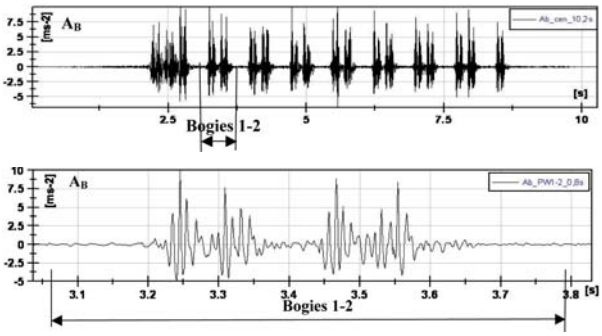

a) The time history of the vertical ballast bed acceleration $w''_B(t)$/the accelerometer A_B -The passage of coach bogies No. 1-2, t = 3.01 - 3.8 = 0.79 s.

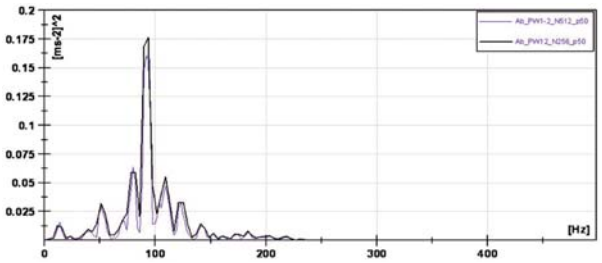

*$f_{(1)}$ = 13, 51, **92**, 123 Hz*

b) LABVIEW Analysis: The PWS of the ballast bed acceleration $w''_B(t)$/ the accelerometer A_B, the passage of coach bogies No.1-2, t = 3.01 - 3.8 = 0.79 s.

→ the block size N512, overlap 50% - The mean of 2 sp. PWS,

→ the block size N256, overlap 50% - The mean of 5 sp. PWS.

The non-filtering signal for frequencies f = (0 ÷ 500 Hz).

Fig. 10 Analysis of the vertical ballast bed acceleration $w''_B(t)$/the accelerometer A_B for the passage of coach bogies No. 1-2, t = 3.01 - 3.8 = 0.79 s.

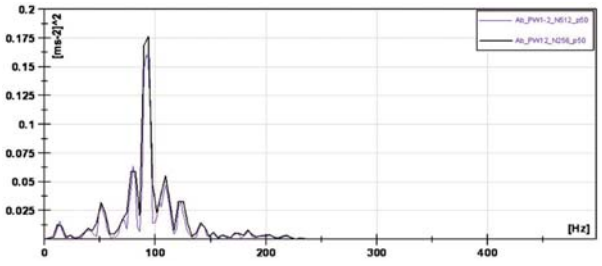

*$f_{(1)}$ = 13, 39, 55, **78, 95, 106** Hz* *$f_{(1)}$ = 171, 178, 201, 219 Hz*

Fig. 11 LABVIEW Analysis: Transfer function $\boldsymbol{H_1(A_S/A_B)}$ - The passage of coach bogies No.1-2, t = 3.01 - 3.8 = 0.79 s → the block size N512, overlap 50% - The mean of 2 sp. PWS. The non-filtering signal for frequencies f = (0 ÷ 500 Hz).

motive bogies, characteristic coach bogies (couple of bogies), or the passage of characteristic parts of the train (the passage of characteristic coaches) is analysed by the time window technique. The spectral composition corresponding to passages of bogies may be evaluated.

The frequency content of the vertical acceleration on the track components – rails, sleepers, and ballast bed differs:

- The frequency spectrum for a rail acceleration is a broadband spectrum in the frequency range f = 0–500 Hz, without any sharp spectral components. The frequency component content at the frequency area $f \approx$ (0÷150 Hz) has the dominant signification on the rail response.
- The frequency spectrum for a sleeper acceleration is a broadband spectrum too, but two marked frequency areas be detected: $f_{(1)} \approx 0 \div 100$ Hz, and $f_{(2)} \approx 280 \div 320$ Hz. They present two characteristic damped resonant areas occurring in all the measured signals:
  - a/ In the first area the frequency range $f_{(1)}$ = (55 ÷ 90 Hz) with a max. $f_{(1)} \approx 60$ Hz is dominant – the rails, sleepers, and ballast layer vibrate together and constitute dominant effect on the sleeper response.
  - b/ In the second one the frequency range $f_{(2)}$ = (280 ÷ 320 Hz) with a $max.f_{(2)} \approx 280$ Hz is dominant – the rails vibrate on sleepers.
- The frequency spectrum for ballast bed is narrow-band and always is concentrated about frequencies f = 80 ÷ 120 Hz.

The presented spectra of vertical accelerations of track components can be considered as characteristic, occurring in all the analysed passages of the passenger trains, because the dynamic loading is similar. The characteristic and important spectral components are appeared in the frequency range f = (0 ÷ 150 Hz) in all the track components when the rails, sleepers, and ballast bed vibrate together. A gradual damping of frequency components in the vertical direction is apparent in all spectral analyses in Figs. 7 ÷ 10.

- The spectra corresponding to passages of heavy freight trains are different in comparison of passenger trains, because the frequency of loading, the speed of freight trains, the mass of carriages are different from passenger trains, and a quasi-static preloaded of the track is higher.
- The comparison of the measured amplitudes of the vertical acceleration of track components (rails, sleepers and the ballast bed) indicates the proper damping and filtration of the frequency components at the transmission of dynamic loading from the rail to the substructure and to the subgrade as the consequence of the resilient rail fastening (Vossloh Skl 14), the resilient pads, and the generally proper function ballast bed and subgrade.
- A very negative impact of coaches with some defective wheels (the out-of-round wheels) to the vertical track acceleration was indicated. Peaks reached up to a double higher value of the response than the coaches with smooth wheels.

8. Conclusions

Dynamic behaviour of the track structure during the passage of passenger trains was investigated as the vertical acceleration of the track components – the rails $w''_R(t)$, the sleepers $w''_S(t)$, and the ballast layer $w''_B(t)$ at the depth of placing sleepers. The frequency analysis was made for the mid frequency range $f = (0 \div 500$ Hz). Measured signals include a large number of excitation sources – geometrical errors, or irregularity on the rails, wheel out-of-roundness, irregular track stiffness, etc. The selected stationary part of the measured signals considered as a stationary process (the passage of locomotive bogies, characteristic coach bogies or couple of bogies, the passage of characteristic coaches) were analysed by the time window technique. The spectrum changes corresponding to characteristic bogie passages were evaluated.

The presented experimental analyses for the new construction of the track structure are complementary to the other data sets – the measurement of the passage of freight trains, or the measurement of the response on other types of ballasted tracks. Frequency analyses of time histories of the vertical rail acceleration $w''_R(t)$, the sleeper accelerations $w''_S(t)$, and the ballast bed acceleration $w''_B(t)$ provide the principal picture of the dynamic behaviour of the track structure, the transmission and the damping of frequency components through the track components under the passage of the characteristic passenger trains. Although they moderately differ under the passage of different trains the main features and the character of the response is maintained.

References

[1] KNOTHE, K., GRASSIE, S.: Modelling of Railway Track and Vehicle/Track Interaction at High Frequencies. *Vehicle System Dynamic*, Nr. 22, 1993, pp. 209–262.

[2] KNOTHE, K., WU, Y.: Receptance Behaviour of Railway Track and Subgrade. *Archive of applied Mechanics,* Nr. 68, 1998, Spring Verlag, pp. 457–470.

[3] DEGRANDE, G.: Free Field Vibration Measurements During the Passage of Thalys High Speed Train. *Report BWM*-2000-06, Dept. of Civil Eng. KU Leuven.

[4] SHEN-HAW JU, HUNG-TA LIN, JENG-YUAN HUANG: Dominant Frequencies of Train-induced Vibrations, *J. of Sound and Vibration,* Nr. 319, 2009, pp. 247–259.

[5] SICAR, M.: *Vehicle-track Interaction Concentrated to the Track Response (in Slovak).* PhD Thesis, University of Zilina, p. 180, 1996.

[6] MORAVCIK, M.: *Track Mechanics – Parts 1, 2. – Theoretical Analysis and Simulation Track Mechanics Problems (in Slovak)*, EDIS, Žilina 2002. Part 1, ISBN 80-7100-983-0, 300 p., Part 2, ISBN 80-7100-984-9, p. 312.

[7] MORAVCIK, M.: Dynamic Behaviour of Railway Track – Experimental Measurements. *Communication – Scientific Letters of the University of Zilina,* Nr. 3, 2002, ISSN 1335-4205, pp. 45–62.

[8] BENDAT J., PIERSOL A.: *Random Data – Analysis and Measurement Procedures.* John Wiley and Sons, 1986, ISBN 0-471-04000-2, 566 p.

[9] DIAdem/NT Manual: Advance Course Manual, Versiom 10.0, 2006.

Jiri Huzlik – Roman Licbinsky – Daniela Durcanska *

POLYCHLORINATED DIBENZODIOXINS AND DIBENZOFURANS EMISSIONS FROM TRANSPORTATION

Measurement of Persistent Organic Pollutants (POPs) was performed in order to complement the set of known emission factors. Methodology for gasoline engines emission factors determination that uses POPs concentrations measured in exhaust gasses, limited pollutants emission factors (carbon monoxide CO, nitrogen oxides NO_x and hydrocarbons HC) and other compounds (carbon dioxide CO_2) was elaborated. Empirical value of exhaust gasses production announced by specialists of TUV SUD was used for diesel. Emission factors of four vehicle-fuel systems were determined particularly 11 congeners of Polychlorinated Dibenzodioxins (PCDDs), 34 congeners of Polychlorinated Dibenzofurans (PCDFs) and their toxic equivalents (TEQ) for each of the measured system. TEQ PCDD/F congener profile typical for POPs sources from transportation was compiled on the basis of measured data.

1. Introduction

Persistent Organic Pollutants (POPs) represent group of organic compounds with specific physico-chemical and environmental-chemical properties. The most important among them are resistance to diverse degradation processes, low solubility in water, lipophilic character. These properties results in high tendency for bioaccumulation, semi volatility enabling global atmospheric transport and significant adverse effects on human health or environment. Polychlorinated Dibenzodioxins (PCDDs) and Polychlorinated Dibenzofurans (PCDFs) belong among others to this group of compounds. They originate during communal, hospital or dangerous wastes incineration, also during coal, peat and wood combustion and can be also determined in vehicles emissions [1]. Their content in exhaust gasses is in very small concentrations and because of difficult and complicated analytical determination these compounds are measured in exhaust gasses only sporadically [2].

2. Measurements methodology

Emission factors (Ef) measurements of three vehicles using four different types of fuel were performed in two sampling campaigns in 2009 and 2010. Standard city cycle in accordance with ECE 83.04B consisting of 4 cycles ECE 15 in 195 sec. (Fig. 1) in three repetitions with previous 5 minutes engine heating up to running temperature (SDC) was chosen to simulate urban driving. Sufficient amount of exhaust gasses for PCDD/Fs and Polyaromatic Hydrocarbons (PAH) determination was sampled during these three cycles. Sampling was performed by using apparatus described in Fig. 2 connected directly to exhaust pipe. All measurements were performed in authorized station for vehicles homologation TUV SUD on dynamometer SCHENCK 364/GS56 that simulates flywheel mass and running resistance as if vehicle moves on the road.

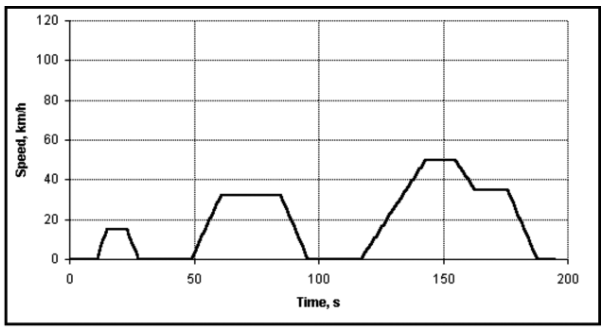

Fig. 1 Standard city cycle ECE 15

PCDD/Fs isotopic marked congeners were placed before the sampling to the sorption system to ensure control of PCDD/Fs sorption efficiency. Sampling and analyses were performed in accordance with CSN EN 1948-1-3 considering that measurements next to exhaust pipe was not possible to perform isokinetically. The same apparatus was used also for PAH sampling. Basic emission parameters such as CO_2, CO, HC, NO_2 were also measured at the same time.

Vehicle thus passed through the test in accordance with speed profile that is standard and described in ECE 83 regulation. Exhaust gasses were sampled in the whole volume using HORIBA CVS 7300 T device and were diluted to prevent condensation.

* **Jiri Huzlik[1], Roman Licbinsky[1], Daniela Durcanska[2]**
[1] Division of Transport Infrastructure and Environment, Transport Research Centre, Brno, Czech Republic, Email: jiri.huzlik@cdv.cz
[2] Faculty of Civil Engineering, University of Zilina, Slovakia

Gravimetric apparatus TESO GTE filter-condensation configuration	CSN EN 1948 - 1 CSN EN 13284
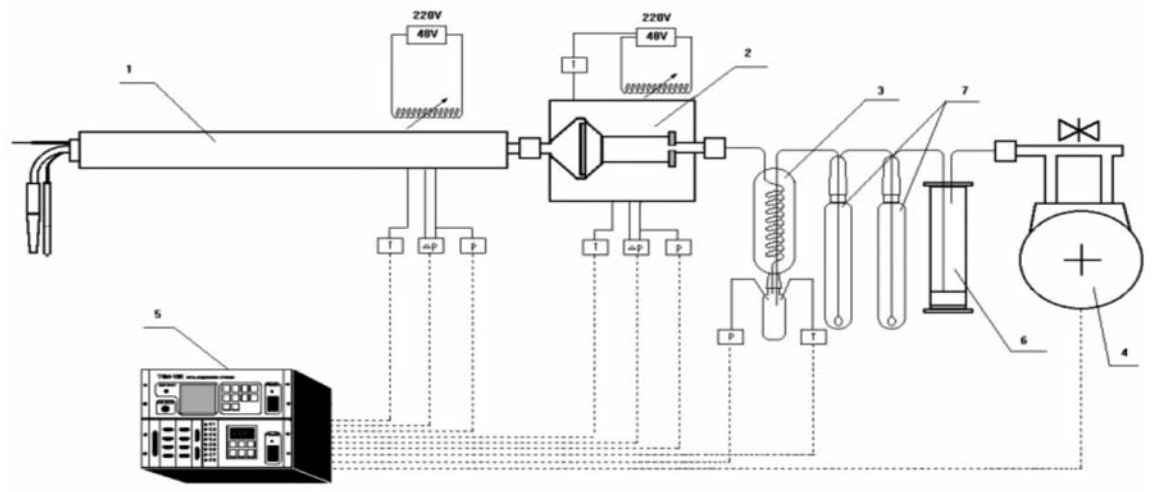	
heated sampling unit with internal filter **[1]**	
inlet jet with thermometer **[2]**	
KOMBI GTE condensation flow glass cooler **[3]** two stage absorber with ethoxy ethanole filler **[7]** drop separator – drying chamber **[6]**	
suction source – dry air pump **[4]**	
control unit **[5]**	
analytical determination	HRGC – HRMS (High resolution gas chromatography – high resolution mass spectrometry)
mean uncertainty of analysis	30%

Fig. 2 Apparatus for PCDD/F and PAH sampling

Fuels used for measurements were tanked in common petrol stations. Their average chemical composition is characterised by parameters shown in Tab. 3. Symbols n_H and n_C mean the amount of hydrogen and carbon atoms in the mean molecule of fuel, ρ_p means fuel density, BA is 95 octane gasoline and MN summer diesel fuel.

3. Ef calculation methodology

Methodology results from Ef values of CO, NO_x, CO_2 and HC measured in dry exhaust gasses on dynamometer by standard methods and from fuel consumption. Ef of pollutants are calculated from measured concentration and measured volumes of dry exhaust gasses used for chosen pollutants sampling under normal conditions (101.325 kPa, 0 °C).

Symbols marked with upper index on the right side are related to dry gasses that means to gasses without any water vapours. Amount of substances entering the combustion process are marked with capital *N* with appropriate indexes, amount of substances of

Used symbols Table 1

A_i	atomic weight of *i*-th element [g.mol-1]
a, b, c	stoichiometric coefficients for elements in mean molecule of fuel in sequence of C, H, O
c_i^s	i-th component concentration in dry exhaust gasses [g.m^{-3}]
$conc_i^s$	i-th component content in dry exhaust gasses of the sample [g.sample^{-1}]
β	ratio of hydrogen atoms versus carbon atoms in fuel
γ	ratio of oxygen atoms versus carbon atoms in fuel
Ef_m^i	i-th component emission factor [g.kg^{-1}]
Ef_1^i	i-th component emission factor [g.km^{-1}]
FC	fuel consumption [l. (100 km)$^{-1}$]
L	route passed by vehicle [km]
m_i	i-th component weight [kg]
M_i	i-th component molar weight [g.mol^{-1}]
μ_i	i-th component molar weight relative to one carbon atom in the molecule [g.mol^{-1}]

n_i	amount of substance of i-th component content in exhaust gasses [mol]
N_i	amount of substance of i-th component content in air [mol]
N_p	amount of substance of consumed fuel [mol]
N_V	amount of substance of air entering the engine during fuel combustion [mol]
π_i	i-th element percentage content in fuel [%]
V_a	gas one mol volume under standard conditions [l.mol^{-1}]
V^s	volume of dry gasses sample [m^3.sample^{-1}]
V_{exh}	volume of dry exhaust gasses originated during fuel combustion [m^3]
ρ_p	fuel density [kg.l^{-1}]

gasses in exhaust gasses are marked with *n* with appropriate indexes. Index *p* means fuel.

Physical constants used in calculations Table 2

Fuel	BA95	LPG	CNG	MN
Constant	Constant value			
M_{O_2} [mol.g^{-1}]	31.9988			
M_{H_2O} [mol.g^{-1}]	18.0015			
M_{CO} [mol.g^{-1}]	28.01055			
M_{NO} [mol.g^{-1}]	30.0061			
M_{NO_2} [mol.g^{-1}]	46.0055			
M_{CO_2} [mol.g^{-1}]	44.00995			
V_a [mol.g^{-1}]	22.414			
M_p [mol.g^{-1}]	104.07	53.53	16.014	173.64
A	7.328	3.684	1	12.36
β	1.808	2.523	4	1.913
ω	0.4389	0.6307	1	0.4739
π_O [%]	2.73	0	0	0.92
ρ_p [kg.l^{-1}]	0.748	0.538	0.000654	0.832

It is necessary to know fuel composition when calculating Ef. The meanings of factors used for calculations are described in Table 1, physical constants in Table 2. Stoichiometric coefficients are introduced for simplification of further equations and their meaning is evident from equation (4)

$$\omega = \frac{b - 2\cdot c}{4\cdot a} = \frac{\beta}{4} - \frac{\gamma}{2}. \tag{1}$$

If atomic ratio H:C (= β) and oxygen percentage content π_O are known, then

$$\omega = \frac{\beta}{4} - \frac{\pi_o\cdot(A_C + \beta\cdot A_H)}{2\cdot(100 - \pi_o)\cdot A_o}. \tag{2}$$

From the equation for fuel molecular weight relative to one carbon atom after substitution from (1) and (2), it holds

$$\mu_p = \frac{M_p}{a} = A_C + \beta\cdot A_H + \gamma\cdot A_O = \frac{100\cdot(A_C + \beta\cdot A_H)}{(100 - \pi_o)} \tag{3}$$

Emission factors of limited pollutants calculation results from equations of fuel combustion, mass balance and measured values. Fuel combustion is considered in some simplification (it is assumed that hydrocarbons contained in exhaust gasses are identical to those contained in fuel, origin of trace concentrations of PAH, N_2O, NH_3 and others are not considered):

$$\begin{aligned} &e/2\ N_2 + C_aH_bO_c + [a.(1 - z/2) + b/4 - c/2 + \\ &+ e\cdot(1 - w/2)]\ O_2 \rightarrow a\cdot(1 - z)\ CO_2 + a\cdot z\ CO + \\ &+ (b/2)\ H_2O + e\cdot(1 - w)\ NO_2 + e\cdot w\ NO. \end{aligned} \tag{4}$$

Mass balance of real fuel combustion considering presumptions characterised above can be described by following equations for separate elements:

$$\text{C:}\ \ a\cdot(N_p - n_p) = n_{CO_2} + n_{CO} \tag{5}$$

$$\text{H:}\ \ b\cdot(N_p - n_p) = 2\cdot n_{H_2O} \tag{6}$$

$$\begin{aligned} &\text{O:}\ \ (N_{O_2} - n_{O_2}) + c\cdot(N_p - n_p) = n_{H_2O} + 2\cdot n_{CO_2} + \\ &+ n_{CO} + 2\cdot n_{NO_2} + n_{NO} \end{aligned} \tag{7}$$

$$\text{N:}\ \ (N_{N_2} - n_{N_2}) = n_{NO_2} + n_{NO}. \tag{8}$$

Amount of substance of dry gasses enters combustion process

$$N_V^s = N_V - N_{H_2O} = N_{N_2} + N_{O_2} + N_{CO_2} \tag{9}$$

and for amount of substance of dry gasses getting off the exhaust pipe holds

$$\begin{aligned} &n^s = n - n_{H_2O} = n_{N_2} + n_{O_2} + n_{CO_2} + N_{CO_2} + n_{CO} + \\ &+ n_p + n_{NO_2} + n_{NO}. \end{aligned} \tag{10}$$

Symbol for i-th component concentration in entering air and in exhaust gasses formulated as molar fraction is described as

$$Y_i^s = \frac{N_i}{N_V^s},\ y_i^s = \frac{n_i}{n^s},\ y_i = \frac{n_i}{n}. \tag{11}$$

and equation solution for unknown parameters N_V^s a N_p brings formula necessary for further calculations

$$\frac{N_p}{n^s} = \frac{Y_{O_2}^s - y_{O_2}^s + (1 - Y_{O_2}^s)\cdot\frac{y_{CO}^s}{2} - \left(1 - \frac{Y_{O_2}^s}{2}\right)\cdot y_{NO_2}^s - \frac{y_{NO}^s}{2} + \left(a\cdot(1 + \omega) - (1 + \omega)\cdot Y_{O_2}^s\right)\cdot y_p^s}{a\cdot\left(1 + \omega\cdot(1 - Y_{O_2}^s)\right)}. \tag{12}$$

If pollutant concentration is expressed in mass units per volume unit, *Ef* of separate components of exhaust gasses relative to unit of consumed fuel can be described as

$$Ef_m^i = \frac{m_i}{m_p} = c_i^s \cdot \frac{V_a}{M_p} \cdot \frac{n^s}{N_p}. \quad (13)$$

Ef expressed in mass units per passed route and concentration input data in mass unit per volume unit of exhaust gasses are calculated as

$$Ef_l^i = Ef_m^i \cdot \frac{m_p}{l} = \frac{conc_i^s}{V^s} \cdot \frac{V_{exh}}{l}. \quad (14)$$

Then results from equation (14) for rates for conversion from separate pollutants concentrations in exhaust gasses (POPs in this case) to *Ef* after substitution of the molar fraction from equation (11) and after neglecting NO_2 concentration (NO predominantly originates during combustion):

$$\frac{V_{exh}}{l} = \frac{V_a}{Y_{O_2}^s} \cdot \left(a \cdot \frac{FC \cdot \rho_p}{M_p} \cdot \left(1 + \omega \cdot \left(1 - Y_{O_2}^s\right)\right) + \frac{Ef_l^{O_x}}{M_{O_2}} - \left(1 - Y_{O_2}^s\right) \cdot \frac{Ef_l^{CO}}{2 \cdot M_{CO}} - \left(1 + \omega\right) \cdot \left(a - Y_{O_2}^s\right) \cdot \frac{Ef_l^p}{M_p} + \frac{Ef_l^{NO_x}}{2 \cdot M_{NO_x}} \right) \quad (15)$$

The result from equation (14) is used for *Ef* calculation relative to passed route. After substitution of the result from equation (15) in dimensions described in Table 2 and after neglecting oxygen concentration in exhaust gasses, the formula for calculation of Ef of pollutants holds:

$$Ef_l^i = \frac{conc_l^s \cdot V_a}{1000 V^s \cdot Y_{O_2}^s} \cdot \left(a \cdot \left(1 + \omega \cdot \left(1 - Y_{O_2}^s\right)\right) \cdot \frac{10 \cdot FC \cdot \rho_p}{M_p} - \left(1 - Y_{O_2}^s\right) \cdot \frac{Ef_l^{CO}}{2 \cdot M_{CO}} - \frac{Ef_l^{NO_x}}{2 \cdot M_{NO_x}} + \left(1 + \omega\right) \cdot \left(a - Y_{O_2}^s\right) \cdot \frac{Ef_l^p}{M_p} \right). \quad (16)$$

Stoichiometric calculations without knowledge of oxygen concentration in exhaust gasses are not possible for diesel engines. Because of this fact it possible to use empirical value 1.2181 $m^3.km^{-1}$ for recalculation of POPs concentrations in exhaust gasses in accordance with recommendation of authorized station for vehicles homologation TÜV SÜD.

4. Results and discussion

Emission factors of common pollutants that were also used for POPs Ef calculations are described in Table 3. Upper index p means unburned hydrocarbons

Congener profiles for j-th measurement (17) or cumulative congener profiles (18) were compiled on the basis of measured data in accordance with following equations

$$EfTEQ_j^i = Ef_j^i \cdot TEQ_j^i \quad (17)$$

$$EfTEQ_j = \sum_i Ef_j^i \cdot TEQ_j^i, \quad (18)$$

where index i represents appropriate PCDD or PCDF congener. Cumulative Efs are counted above all PCDD and PCDF congeners. Following PCDD congeners and their toxic equivalents were considered:

2378TCDD	12378PeCDD	123478HxCDD
1	0.5	0.1
123678HxCDD	123789HxCDD	1234678HpCDD
0.1	0.1	0.01
OCDD		
0.001		

Results of limited pollutants emission factors measurements — Table 3

Date	Vehicle type	Fuel	ρ_p kg.l^{-1}	*nH*/*nC*	% O	*nC*	Tachom.	$EF_l^{CO_2}$ g.km^{-1}	EF_l^{CO} g.km^{-1}	EF_l^p g.km^{-1}	$EF_l^{NO_x}$ g.km^{-1}	$FC.10^2$ l.km^{-1}
2.12.09	SKODA Felicia 1.3/50 kW	BA 95t	0.748	1.85	2.7	6	184965	242	0.716	0.136	0.178	10.27
2.12.09	SKODA Felicia 1.3/50 kW	LPG	0.538	0.538	0	3.5	184981	193	10.49	0.91	0.223	13.05
2.12.09	SKODA Fabia 1.4/44 kW	BA 95t	0.748	1.85	2.7	6	250389	243	0.826	0.105	0.497	10.28
2.12.09	SKODA Octavia 1.9 TDI/77 kW	MNt	0.832	1.91	0.92	12.36	156295	233	0.058	0.129	0.455	8.86
22.9.10	SKODA Felicia 1.3/50 kW	BA 95t	0.748	1.85	2.7	6	188083	267	0.682	0.088	0.133	11.3
22.9.10	SKODA Felicia 1.3/50 kW	LPG	0.538	0.538	0	3.5	188091	223	12.05	0.576	0.049	15.0
22.9.10	SKODA Fabia 1.4/44 kW	BA 95t	0.748	1.85	2.7	6	266232	215	0.568	0.042	0.443	9.1
22.9.10	SKODA Octavia 1.9 TDI/77 kW	NMt	0.832	1.91	0.92	12.36	179595	218	0.086	0.054	0.465	8.2

Legend: t means tanked in petrol station (same in Table 4)

and following PCDF congeners and their toxic equivalents were considered:

2378TCDF	12378PeCDF	23478PeCDF
0.1	0.05	0.5
123478HxCDF	123678HxCDF	
0.1	0.1	
234678HxCDF	123789HxCDF	1234678HpCDF
0.1	0.1	0.01
1234789HpCDF	OCDF	
0.01	0.001	

TEQ PCDD a PCDF Ef congener profiles shown in Figs. 3 and 4 indicate higher values in 2010 but profiles for separate years of measurement can be considered as similar. TEQ 2378TCDD Ef was the highest in 2009 whereas 12378PeCDD Ef was the highest in 2010 among all PCDD congeners. 23478PeCDF Ef was the highest among all PCDF congeners in both measuring campaigns. TEQ OCDD and OCDF Ef were the lowest although TEQ 123789HxCDF Ef was once (Octavia 2010) the lowest.

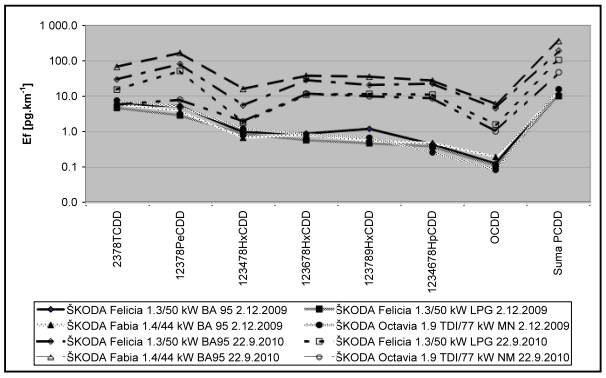

Fig. 3 TEQ-PCDD congener profiles (logarithmic scale of y axis)

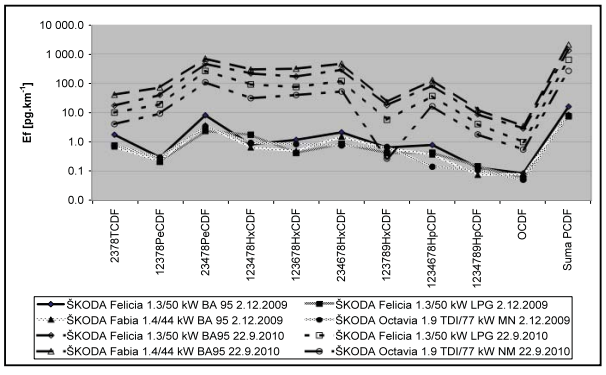

Fig. 4 TEQ-PCDF congener profiles (logarithmic scale of y axis)

Significant differences were found out among cumulative TEQ Ef in particular years. Predominant influence of Ef measured in

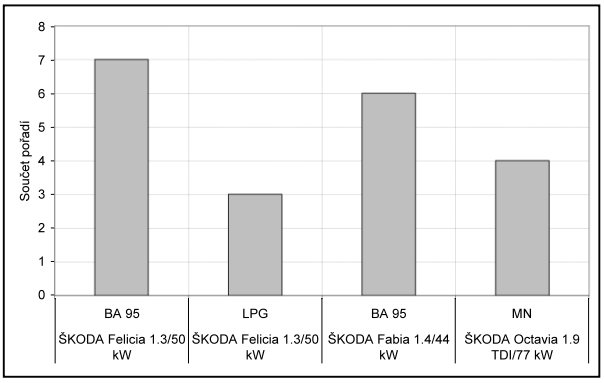

Fig. 5 Sum of rank of separate TEQ-PCDD/F emission factors of tested vehicles

2010 was demonstrated by comparison of arithmetic and geometric averages. Usage of sum of sequences of Ef measured in appropriate campaign and year according to their value is not dependent on absolute values of measured cumulative Ef (Fig. 5). In accordance with this criterion, PCDD/F Ef of Felicia with gasoline fuel had the highest toxic equivalent while PCDD/F Ef of the same vehicle using LPG fuel had the lowest toxic equivalent. Emission factors TEQ for conventional fuels (gasoline, diesel) decreased with decreasing age of vehicle. Usage of LPG in the same vehicle significantly decreased POPs emission in comparison with usage of conventional fuel. LPG had the lowest PCDD/F Ef among studied fuels.

Determined POPs Efs were compared with Efs measured by CDV for a wider selection of vehicles during 2005 – 2006 [3, 4]. Summary of measuring conditions in 2005 – 2010 is outlined in Table 4. Most of fuels were certificated. Trend of dependency of cumulative PCDD/F Ef sums for separate vehicles and fuel on measuring date for separate measuring campaign (one day or two days) is shown in Fig. 6. Efs of cold starts (CS) are also shown in this graph. Cold start represents SDC without pre heating after vehicle parking outside whole night and its movement onto the dynamometer with engine off.

Efs had similar character of their time progress. This time progress was in four campaigns similar to time progress of PAH Efs. Data variance was larger within the sampling campaigns than among campaigns. Geometric averages of Efs measured in campaigns were in the range of units up to tens of $pg.km^{-1}$ (in the frame in Fig. 6). However, PCDD/F Efs were in two campaigns in 2006 lower (tenths to units of $pg.km^{-1}$) and in the last campaign in 2010, on the contrary, hundreds to thousands of $pg.km^{-1}$.

Since differences in PAH Efs measurements in contrast to PCDD/F Efs were not relevant, entrance of different amounts of chlorine or its compounds to the measuring systems in these three campaigns than in others was considered. Probably these compounds were contained in the air entering combustion process in vehicles engines.

Cold starts Efs were higher than Efs measured under running conditions for all fuels which is probably determined by different

Summary of cumulative emission factors measuring conditions in 2005–2010 Table 4

Measurement No.	Identification	Vehicle type	Fuel	Comment	Passed km
6523	F-BA 95	SKODA Fabia 1.4/44 kW	Natural 95	Certificated	139 500
6522	F-BA 95	SKODA Fabia 1.4/44 kW	Natural 95	Certificated	139 512
6520	F-BA 95-E5	SKODA Felicia 1.3/50 kW	Natural 91 s 5 % EtOH	Certificated	139 524
6521	F-BA 5-EE15	SKODA Felicia 1.3/50 kW	Natural 91 s 15 % ETBE	Certificated	139 536
6518	OS-MN	SKODA Octavia 1.9 SDI combi	MN, summer	Certificated	82 100
6519	OS-MN-M5	SKODA Octavia 1.9 SDI combi	MN summer with 5% MERO	Certificated	82 112
10542	F-LPG	SKODA Felicia 1.3/50 kW	LPG		142 900
10544	Fa-BA 95	SKODA Fabia 1.4/44 kW	Natural 95	Certificated	179 600
10543	Fa-BA 95-E5	SKODA Fabia 1.4/44 kW	Natural 91 s 5 % EtOH	Certificated	179 612
10545	Fa-BA 95-EE15	SKODA Fabia 1.4/44 kW	Natural 91 s 15 % ETBE	Certificated	179 624
10546	OS-MN-M31	SKODA Octavia 1.9 SDI combi	MN summer with 31% MERO	Certificated	93 900
14	Fa-BA 95t-cs	SKODA Fabia 1.4/44 kW	BA95 tanked	Cold start	183 053
15	OS-MNt-cs	SKODA Octavia 1.9 SDI combi	MN tanked	Cold start	96 902
16	FF-E85	Ford Focus Flexifuel	85% EtOH		2 900
17	FF-E85-cs	Ford Focus Flexifuel	85% EtOH	Cold start	2 912
2398	FM-CNG-cs	Fiat Multipla (manufactured CNG)	CNG	Cold start	n/a
2399	FM-CNG	Fiat Multipla (manufactured CNG)	CNG		n/a
2400	FF-E85-cs	Ford Focus Flexifuel	85% EtOH	Cold start	19 888
2401	FF-E85	Ford Focus Flexifuel	85% EtOH		19 900
2402	Fa-BA 95t-cs	SKODA Fabia 1.4/44 kW	BA95 tanked	Cold start	185 914
2403	OS-MNt-cs	SKODA Octavia 1.9 SDI combi	MN tanked	Cold start	105 588
2404	OS-MN-M5	SKODA Octavia 1.9 SDI combi	MN summer with 5% MERO	Certificated	105 600
2405	OS-MN-M31	SKODA Octavia 1.9 SDI combi	MN summer with 31% MERO	Certificated	105 612
5774	Fa-BA 95t-cs	SKODA Fabia 1.4/44 kW	BA95 tanked	Certificated	192 888
5775	Fa-BA 95	SKODA Fabia 1.4/44 kW	Natural 95	Certificated	192 900
5776	Fa-95-E5	SKODA Fabia 1.4/44 kW	Natural 91 with 5 % EtOH	Certificated	192 912
5777	Fa-BA 95-EE15	SKODA Fabia 1.4/44 kW	Natural 91 with 15 % ETBE	Certificated	192 924
5778	FaP-CNG	SKODA Fabia 1,4 Combi (reconstruction to CNG)	CNG		108 200
5779	OS-N-M5	SKODA Octavia 1.9 SDI combi	MN summer with 5% MERO	Certificated	114 700
5780	OS-N-M31	SKODA Octavia 1.9 SDI combi	MN summer with 31% MERO	Certificated	114 712
61700	F-BA 95t	SKODA Felicia 1.3/50 kW	BA95 tanked		185 000
61701	F-LPG	SKODA Felicia 1.3/50 kW	LPG		185 012
61702	Fa-BA 95t	SKODA Fabia 1.4/44 kW	BA95 tanked		250 400
61703	OT-MNt	SKODA Octavia 1.9 TDI/77 kW	MN, summer, tanked		156 300
68843	F-BA 95t	SKODA Felicia 1.3/50 kW	BA95 tanked		188 083
68844	F-LPG	SKODA Felicia 1.3/50 kW	LPG		188 091
68842	Fa-BA 95t	SKODA Fabia 1.4/44 kW	BA95 tanked		266 232
68845	OT-MNt	SKODA Octavia 1.9 TDI/77 kW	MN, summer, tanked		179 595

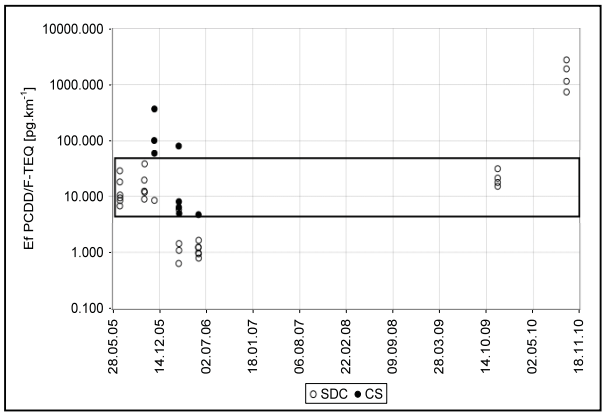

Fig. 6 Summary of cumulative PCDD/F emission factors measured by CDV (logarithmic scale)

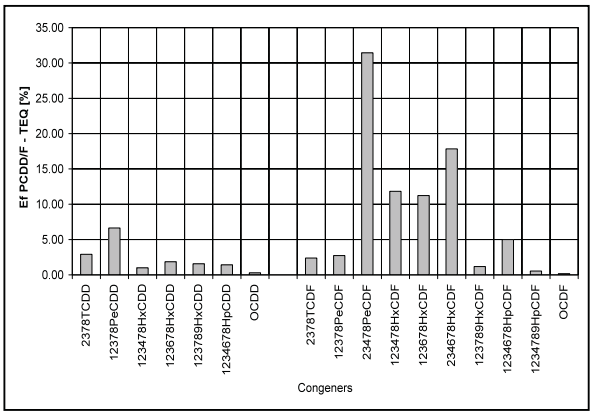

Fig. 7 Congener profile of TEQ PCDD/F emission factors mean values of all tested Vehicles

conditions of combustion (lower temperatures, incomplete combustion)

Cumulative TEQ emission factors for all the measuring campaigns, all the tested vehicles and fuels shown in Fig. 7 in percentage were calculated in accordance with equation (19)

$$EfTEQ^{i} = \frac{\sum_{j} Ef_j \cdot TEQ_j^{i}}{\sum_{j}\sum_{i} Ef_j \cdot TEQ_j^{i}} \cdot 100\,. \qquad (19)$$

Congener profile calculated in accordance with equation (19) represents congener profile estimation of sources from individual passenger road transport.

Acknowledgement

This study was supported by the Czech Ministry of Transport within R&D project “POPs emissions from transport” No. CG912-081-520.

References:

[1] HOLOUBEK I., KOCAN A., HOLOUBKOVA, I., KOHOUTEK J.: Persistent Organic Pollutants (in Czech), *Edice Planeta,* Vol. 9, No. 2, 2001, p. 13, ISSN: 1213-3396

[2] SEBOR G., KOZAK P., POSPISIL M., BLAZEK J.: Gasoline Properties and their Influence on Environment (in Czech), *Chemicke listy* 89, pp. 233–244, 1995

[3] JEDLICKA, J., ADAMEC, V., CHOLAVA, R., DUFEK, J., HUZLIK, J., OCELKA, J., GRABIC, R., CHMELOVA, M., VASUTOVA, L.: *Nonlimited Pollutants Measurements and Emission Factors Calculations of Mixed Biofuels in Dependence on their Composition and Operating Mode (in Czech)*, Final report VaV 1F54G/104/520, CDV Brno, p. 32, 2007

[4] DUFEK, J., HUZLIK, J., DURCANSKA, D., SLANINKA, S.: *Vehicles Emission Factors Corporate Database (in Slovak),* Final report of a bilateral project Czech Republic – Slovak Republic, CDV Brno - Zilinska univerzita, 2006.

Marcela Malindzakova *

SIGNIFICANCE EVALUATION OF ENVIRONMENTAL ASPECTS

The identification of environmental aspects is an essential premise for implementation of EMS in a production company, but not a sufficient one. In order to effectively reduce negative environmental impacts, first it is necessary to undertake a thorough examination of given environmental aspects. For this purpose, several methods can be used. In this article, 3 such methods are described in detail, namely the method of Total pair comparison, the Rank method and the Saaty method. A properly prepared classification of all involved environmental aspects, evaluated by their importance can be considered a first step for successful environmental pollution reduction or elimination. In order to determine and quantify which environmental aspects have the highest priority, the Pareto analysis and Lorenz curve method can be used.

1. Introduction

To establish a functional and successful environmental system in a company, the first key step is to identify all aspects with potentially negative impact on the environment, including a significance analysis, with the goal to determine which aspects are the most harmful for the environment. The most harmful aspects are then called significant environmental aspects. These aspects can be controlled directly, modifying the main production process, or indirectly through supporting processes, such as the distribution, packaging, transport, design, etc. The approach the company takes to manage their environmental system, depends on company's economic situation, market share and competition ability. Those companies that inflict significant impacts on environment are required to create a system for better identification, monitoring and evaluation of significant environmental aspects.

2. Environmental aspects identification and monitoring

It is important to mention that environmental aspects identification does not require meticulous investigation of product life cycle, only the production processes. Aspects that were identified as important, must be monitored, managed and analyzed, to prevent, or at least minimize the scope of potential environmental damage. For this reason it is important to systematically and continually measure and monitor significant environment damaging aspects during EMS implementation. To identify environmental aspects, it is important to focus on:

- Specific significance of each environmental aspect, considering the state legislation and environmental norms requirements,
- The frequency of performed activities, or provided services, frequency of goods and services purchase related to identified environmental aspects,
- The probability of environmental aspect occurrences,
- Significance and potential impact of given environmental aspect.

In the example below, a given company identified 7 groups of environmental aspects (Table 1). To determine their influence on environment, following three methods were applied, namely:

- The method of total pair comparison,
- The rank number method,
- Analytic Hierarchy Process – AHP method also called Saaty method[3].

The above mentioned methods indicate the sequence rank number of the most significant aspects, which deserve more attention. Electro energy consumption causes depletion of available natural resources and at the same time represents high production costs. Excessive electro energy consumption is caused mainly by high performance engines of wood processing facilities. As the wood processing industry relies heavily on high performance machines with considerable electro energy consumption, the old obsolete wood processing facilities should be gradually replaced by new energy efficient models.

Alternatively, the company might consider investing into electro energy generators based on ecological systems and clean ecological technologies. Water energy can be used to produce electricity in small water energy power plants. Water energy belongs among renewable energy sources. For renewable energy projects the most considerable cost item is the initial investment. After the company paid for the renewable energy technology, the most significant factor affecting the product price are operational costs. These however are relatively low for renewable energy technologies.

Overall evaluation H_i of each aspect can be calculated by multiplication of all values for given row, expressed as $H_i = \prod_i a_{ij}$.

* **Marcela Malindzakova**
Process Control and Geotechnology, Institute of Control and Informatization of Production Processes, Faculty of Mining, Ecology, TU Kosice, Slovakia, E-mail: marcela.malindzakova@tuke.sk

Comparing aspect groups utilizing method of total pair comparison

Table 1

Aspect groups											
1	2		3		4		5		6		7
Sawdust	Electro energy consump-tion	Electro energy consump-tion	Wood	Wood	Bark	Bark	Cutting discs attrition	Cutting discs attrition	Tools attrition	Tools attrition	Chemicals consump-tion
Sawdust	Wood	Electro energy consump-tion	Bark	Wood	Bark	Bark	Tools attrition	Cutting discs attrition	Chemicals consump-tion		
Sawdust	Bark	Electro energy consump-tion	Cutting discs attrition	Wood	Bark	Bark	Chemicals consump-tion				
Sawdust	Cutting discs attrition	Electro energy consump-tion	Tools attrition	Wood	Chemicals consump-tion						
Sawdust	Tools attrition	Electro energy consump-tion	Chemicals consump-tion								
Sawdust	Chemicals consump-tion										

Environmental aspect identification

Table 2

Aspect group	Impact	Evaluation	Significance [%]	Weight w_i
Sawdust	Waste production	1	5%	0.05
Electro energy consumption	Natural resources consumption	4	19%	0.19
Wood	Natural resources consumption	3	14%	0.14
Bark	Pollution production	0	0%	0.00
Cutting discs attrition	Pollution production	6	28%	0.28
Tools attrition	Pollution production	5	24%	0.24
Chemicals consumption	Dangerous waste production	2	10%	0.10
Total		21	100 %	1.00

Saaty matrix

Table 3

	Sawdust	Electro energy con-sumption	Wood	Bark	Cutting discs attrition	Tools attrition	Chemicals consumptio n	H_i	R_i	Weights w_i
Sawdust	1	1/7	1/6	1/2	1/5	1/9	1/3	0.000	0.263	0.030
Electro energy consumption	7	1	2	1/3	4	5	5	466.667	2.406	0.272
Wood	6	1/2	1	1/4	3	1/2	1/3	0.375	0.869	0.098
Bark	2	3	4	1	1/6	1/5	1/3	0.267	0.828	0.094
Cutting discs attrition	5	1/4	1/3	6	1	1/7	3	1.071	1.010	0.114
Tools attrition	9	1/5	2	5	7	1	7	882.000	2.635	0.298
Chemicals consumption	3	1/5	3	3	1/3	1/7	1	0.257	0.824	0.093
									8.835	1.000

From that we get $R_i = H_i^{1/n}$ (or $\left(\prod_i a_{ij}\right)^{\frac{1}{n}}$). Sum on all R_i, expressed as $\sum_i R_i = R$ serves for weight calculation $w_i = \frac{R_i}{R}$.

The weights are then used to determine the rank for each environmental aspect.

The rank numbers and weights calculated using different methods are shown in Table 4. The final rank numbers of all monitored environmental aspects are based on their weight values. After displaying the rank numbers using polygons chart (Fig. 1), different position numbers of individual environmental aspects indicate their significance. In this specific example, the most significant difference can be observed for chemicals consumption, which indicates that further inquiry for this environmental aspect is needed. In cases like this the Spearman's rank correlation coefficient can be used.

$$R = 1 - \frac{6 \cdot \sum d_i^2}{n \cdot (n^2 - 1)},$$

where:

d_i – is the difference in environmental aspect rank number for each used methods,

$n = 7$ is the number of identified and evaluated environmental aspects.

The results of the correlation methods are shown in Table 5. It is apparent that between the method of total pair comparison and the Saaty method there is a strong correlation $R = 0.79$. Between the method of total pair comparison and the rank method, the relation is insignificant. It is also advisable to calculate "average" of all three methods as indicated by correlation coefficients for each method and the "average" ($R = 0.82; 0.75; 0.89$).

After retrieving "representative" rank numbers based on significance of individual environmental aspect, it is apparent that the first 3 environmental aspects in the overall evaluation show a 63% influence. As shown in Pareto analysis and Lorenz curve results (Fig. 2), these 3 environmental aspects are the ones where the attention should be focused first. [1]

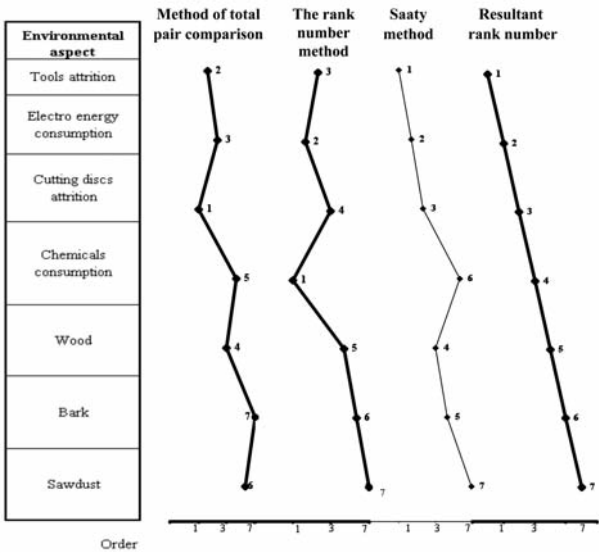

Fig. 1 Polygons of environmental aspect rank number for all applied methods

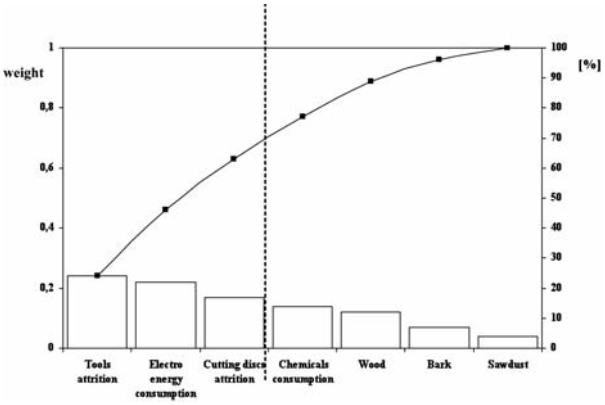

Fig. 2 Pareto analysis and Lorenz curve of environmental aspect evaluation

Evaluation of environmental aspects significance — Table 4

Method						Environmental aspect			Final sequence
Of total pair comparison		The rank number		Saaty					
R.n.	weight	R.n.	weight	R.n.	weight		R.n.	weight	
1	0.28	4	0.12	3	0.19	Cutting discs attrition	2.7	0.20	3
2	0.24	3	0.19	1	0.30	Tools attrition	2.0	0.24	1
3	0.19	2	0.19	2	0.27	Electro energy consumption	2.3	0.22	2
4	0.14	5	0.11	4	0.10	Wood	4.3	0.12	5
5	0.10	1	0.23	6	0.09	Chemicals consumption	4.0	0.14	4
6	0.05	7	0.05	7	0.03	Sawdust	6.7	0.04	7
7	0.00	6	0.11	5	0.09	Bark	6.0	0.07	6
	1.00		1.00		1.00			1.00	

Second power of rank numbers subtract for each two methods Table 5

	d_i^2-					
Environmental aspect	TPC /RN	TPC/SAAT	RN/SAAT	TPC/AVE	RN/AVE	SAAT/AVE
Cutting discs attrition	9	4	1	4	1	0
Tools attrition	1	1	4	1	4	0
Electro energy consumption	1	1	0	1	0	0
Wood	1	0	1	1	0	1
Chemicals consumption	16	1	25	1	9	4
Sawdust	1	1	0	1	0	0
Bark	1	4	1	1	0	1
Σd_i^2	30	12	32	10	14	6
R	0.46	**0.79**	0.43	**0.82**	**0.75**	**0.89**

3. Conclusion

Regular and long-term monitoring of environmental aspects can help providing a proper company evaluation, in regard to adhering to state environmental legislation and fulfilling legislation limit for given country. Such monitoring also indicates the areas of environmental protection where the company must dedicate more effort and more financial investment.

A sudden change in one of the environmental aspects might indicate an incident in company operation. This information is vital for the management, for company's employees as well as for other organizations, especially considering social and civic responsibilities of the company. The implementation of new environmental and renewable sources technologies, can provide an increased yield of natural resources and might reduce the risk of negative impacts on environment. Therefore, such technologies are of increasing importance, especially to companies with positive attitude towards environmental and social issues. The recent increase in the number of projects focused on electrical energy production from renewable sources shows the importance and support of this research within the European Union.

Acknowledgements

This work was partially supported by grant VEGA 1/0571/10 from the Slovak Grant Agency for Science.

Reference

[1] BENKOVA, M., FLOREKOVA, L., BOGDANOVSKA, G.: *Systems of Quality Management (in Slovak),* Elfa, s.r.o., Kosice, 2007, p. 220, ISBN 978-80-8086-066-0.

[2] STN EN ISO 14001 : 2005 *Systems of Environmental Management (in Slovak).* Poziadavky s pokynmi na pouzitie.

[3] MAJERNIK, M., HUSKOVA, V., BOSAK, M., CHOVANCOVA, J.: *Appraisal Methodology of Impact to Environment (in Slovak),* Strojnicka fakulta, TU Kosice, 2008, p. 212, ISBN 978-80-8073-947-8.

Jozef Komacka *

CHANGE OF BEARING CAPACITY CHARACTERISTICS OF ASPHALT PAVEMENT

Time succession of data for monitored variable parameter of pavement state is the first step in development of degradation models and determination of degradation functions. Procedure used for characteristics of bearing capacity is described in the paper.

Data from long time monitored (since 1995) test section on road network were used. First of all homogeneity of subgrade was tested. The deflections at distance of 1500 mm from load centre were used for this purpose. Data that met criteria of homogeneity were corrected taking into account influence of temperature. Two characteristics of bearing capacity (central deflection and surface curvature index) were evaluated in relation to number of heavy vehicles that had passed test section.

Results showed that investigated characteristics of pavement bearing capacity changed in time. It was stated that tendency of development was not very clear because values oscillated in the narrow range. Generally saying the bearing capacity of tested pavement has not changed since 1995 significantly.

1. Introduction

Prognosis of change for variable parameters of pavements is a very important element of Pavement Management Systems (PMS). Degradation models and functions have to be determined for this purpose. Development of degradation models and determination of degradation functions requires in the first step time succession of data for monitored variable parameter of pavement. Deflections of pavement are the most used characteristics in the case of bearing capacity of pavement but other characteristics calculated from deflections (modulus, indices etc.) can be used too. Changes of deflections or other parameters at determined test points are usually related to traffic intensity that is obviously expressed in number of heavy vehicles or in equivalent standard axle loads (ESAL).

Long time repeated measurements on real pavements or accelerated testing on testing tracks have to be done for development of degradation model. The first possibility was chosen in Slovakia. 23 test sections (each of them with length of 1 km) on road network were chosen and measurements have been repeated since 1995 twice a year. The pavement structure of twelve sections is flexible and eleven sections have semi-rigid pavement structure. Aim of the paper is presentation of time succession of data for one of the test sections with flexible pavement. Deflections at centre of load and surface curvature indexes were evaluated and related to number of heavy vehicles that passed through the section.

2. Checking and selection of data

Deflections were regularly measured in spring and autumn but temperature conditions and moisture of subgrade were different during the measurements. Moreover, load force varied in the range of $\pm$ 5 kN about 50 kN. Therefore, corrections of measured deflection were necessary.

All central deflections were recalculated to equivalent load force of 50 kN (one half of equivalent standard axle load of 100 kN) according to [1] in the first step.

Second stage was related to evaluation of subgrade and its homogeneity. Deflections at distance of 1500 mm from load centre were used. An aim was to discard measurements that were carried out during conditions in subgrade that markedly differed from most of the measurements (frozen or very wet subgrade). Values at all tested points were checked and examples for values at some points are in Fig. 1.

It is evident from Fig. 1 that values of deflections at distance of 1500 mm from load centre are variable in time, time behaviour is different at individual points and there are values that are very different in comparison to other values for the same test point. Coefficient of variation was used for homogeneity test and value of 0.1 was used as criterion. When the criterion was not met outliers were identified. The value that was out of range of

* **Jozef Komacka**
Faculty of Civil Engineering, University of Zilina, Slovakia, E-mail: komacka@fstav.utc.sk

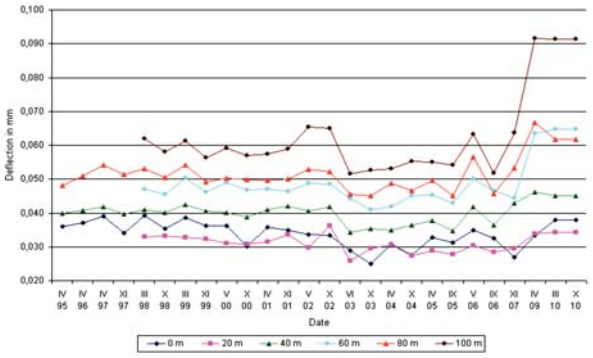

Fig. 1 Time succession of deflections at distance of 1500 mm from load centre for beginning of the test section

$$\bar{w} \pm \sigma \qquad (1)$$

where:
$\bar{w}$ is an average deflection
σ – standard deviation

was considered as an outlier. These values were discarded and average deflection at distance of 1500 mm from load centre was calculated for each test point. Visual display (Fig. 2) indicated homogeneity of subgrade for the whole test section. As can be seen subgrade on test section is not homogenous because spread of average deflections is very large. It was confirmed by statistical evaluation using coefficient of variation (value 0.235). Moreover, modulus of subgrade calculated according to equation published in [2] varied from 90 MPa to 400 MPa. Therefore, values of deflections were distributed into groups. The range of values in each of the groups was not higher than 40 MPa. Median of data was used as initial value for determination of these groups. Only two groups (range of deflections 0.05 mm – 0.059 mm and 0.060 mm – 0.069 mm respectively) were chosen for next evaluation taking into account number of values in individual groups (Fig. 3). Positions of test points (chainage) for chosen groups are in Tab. 1.

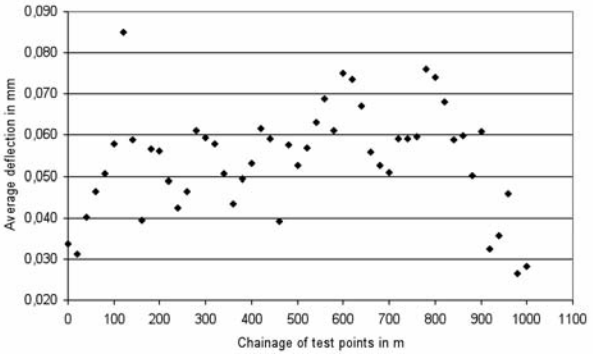

Fig. 2 Average values of deflections at distance of 1500 mm from load centre

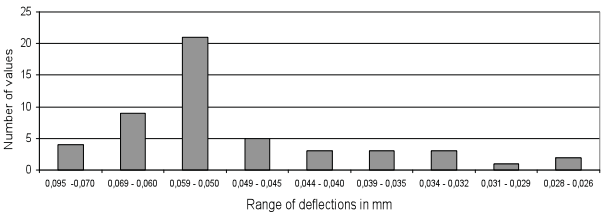

Fig. 3 Number of values in individual groups of deflections

Test points chosen from homogeneity of subgrade point of view — Tab. 1

Range of deflections	Chainage of test points
0.05 mm – 0.059 mm	80, 100, 140, 180, 200, 220, 300, 320, 340, 380, 400, 440, 480, 500, 520, 660, 680, 700, 720, 740, 840, 860, 880
0.060 mm – 0.069 mm	280, 420, 540, 560, 580, 640, 760, 820, 900

3. Corrections of data

Moisture of subgrade and temperature of asphalt layers are two main factors that have to be taken into account when long time measured data are used for determination of a degradation model.

Of course, moisture of subgrade varies during long period. Higher moisture of subgrade leads to lower stiffness of subgrade, thereby to lower bearing capacity of pavement expressed by higher value of deflections. It is known that deflection recorded by the farthest sensor of FWD could be used for evaluation of bearing capacity of subgrade. In this case it is a sensor at distance of 1500 mm. Variability of deflections at this distance is evident from Fig. 1 and necessity to recalculate deflections to average moisture content (or average stiffness) of subgrade is clear. Correction of deflections was carried out according to the conclusions in [3]. There was stated that stiffness of subgrade changes the numeric value of deflections but does not change the shape of a deflection bowl. It only shifts a bowl in a parallel way in vertical direction. Corrections were calculated from equation

$$w_{i,50,v} = w_{i,50} + (w_{1500,50,avg} - w_{1500,50}) \qquad (2)$$

where:
$w_{i,50,v}$ – deflection at distance of "i" from load centre recalculated to load of 50 kN and average moisture content [mm];
$w_{i,50}$ – deflection at distance of "i" from load centre recalculated to load of 50 kN [mm];
$w_{1500,50,avg}$ – average deflection at distance of 1500 mm from load centre recalculated to load of 50 kN [mm];
$w_{1500,50}$ – deflection at distance of 1500 mm from load centre recalculated to load of 50 kN [mm].

Temperature of asphalt layers influences their stiffness (higher temperature leads to lower stiffness) and consequently values of

deflections (higher temperature leads to higher deflections). As repeated measurements of deflections were carried out at different temperatures it is very important to make temperature corrections, that means, to recalculate deflection to equivalent temperature of asphalt layers. The value of + 20 °C is used in Slovakia. The procedure determined in [1] was used. The average temperature of asphalt layers was determined using temperature gradients in asphalt layers of pavements presented in [4] according to equation

$$T_{osf} = T_p + \Delta T, \tag{3}$$

where:

T_p – temperature of pavement surface during measurement of deflection [°C];

ΔT – temperature difference between temperature of pavement surface and average temperature of asphalt layers according to [1] [°C].

Consequently, recalculation of deflections to equivalent temperature of + 20 °C was carried out using the formula

$$w_{T\,20} = w_T + k_{T(R)} \cdot (20 - T_{asf}), \tag{4}$$

where:

$w_{T\,20}$ – deflection recalculated to equivalent temperature of 20°C [mm];

w_T – deflection measured at temperature T [mm];

T_{asf} – average temperature of asphalt layers [°C];

$k_{T(R)}$ – correction coefficient for sensor at distance R.

Values of correction coefficients were determined for each sensor at all evaluated test points using relationships between average temperature of asphalt layers and deflection (see Fig. 4).

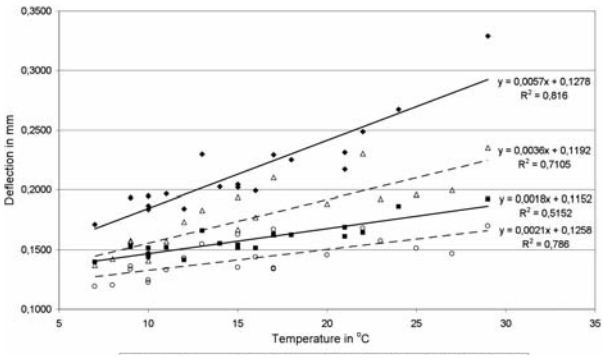

Fig. 4 Correlation between average temperature of asphalt layers and deflection

4. Change of deflections

As time succession of recalculated deflections did not express the influence of traffic intensity it was necessary to determine the number of heavy vehicles that had passed through the test section between individual measurements. Outputs of statewide traffic censuses from 1995, 2000 and 2005 were used. When central deflections were plotted against number of heavy vehicles it was stated that the change of central deflections was similar (Fig. 5) and it was possible to use average of all chosen test points for evaluation of change in central deflection.

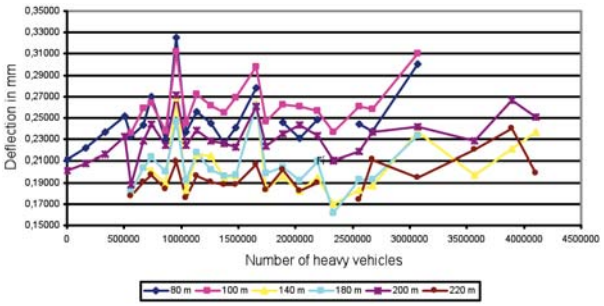

Fig. 5 Deflection versus traffic intensity

Final outputs showed in Fig. 6 document that there is not clear development of central deflection in this case. Moreover, relationship between change of central deflection and number of heavy vehicles is not very strong (value of correlation coefficient is relatively low). One of reasons of these findings could be the fact that central deflection reflects reaction of whole pavement. Therefore, surface curvature index (SCI) was chosen for investigation in the next stage because it reflects only stiffness of asphalt layers of pavement.

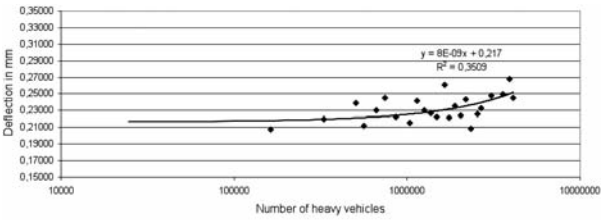

Fig. 6 Change of central deflection against traffic intensity

The values of recalculated deflections were used for calculation of SCI according to following equation

$$SCI_{300} = w_{0,50,T\,20} - w_{300,50,T\,20} \tag{5}$$

where:

$w_{0,50,T\,20}$ – deflection at load centre recalculated to load of 50 kN and equivalent temperature of 20 °C [mm];

$w_{300,50,T\,20}$ – deflection at distance of 300 mm from load centre recalculated to load of 50 kN and equivalent temperature of 20 °C [mm].

The values of SCI_{300} were plotted against the number of heavy vehicles that had passed through test section (Fig. 7). As in the

case of central deflection it was possible to state that the change of SCI_{300} at all chosen test points was similar and average values could be used.

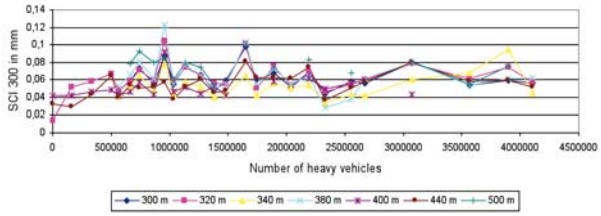

Fig. 7 Surface curvature index versus traffic intensity

Results given in Fig. 8 are similar to the outputs for central deflection. It means the conclusions are the same as in the previous case – not clear development of SCI and not very strong relationship between SCI development and increase of traffic intensity.

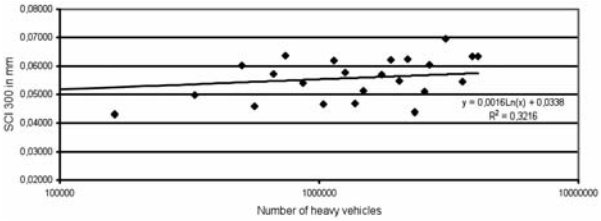

Fig. 8 Change of surface curvature index in relation to traffic intensity

5. Conclusions

Results of long term measurements at the test section show that characteristics of pavement bearing capacity change in time. Moisture content of subgrade and temperature of asphalt layers influence these changes.

After corrections of deflections with respect to the mentioned factors it was stated that tendency of development was not very clear because values oscillated in the narrow range. It is valid for central deflection and surface curvature index too. Generally saying the bearing capacity of tested pavement has not changed since 1995 significantly. As for relationship between characteristics of bearing capacity and number of heavy vehicles it was found that this dependence is not very strong. These findings are not quite in conformity with theoretical assumptions that suppose increase of deflections with traffic intensity. May be the number of heavy vehicles that had passed through the test section was too small to influence markedly characteristics of bearing capacity.

Anyway, performed measurements enlarge database of data that can be used for determination of degradation model of bearing capacity of asphalt pavements. It would be necessary to carry out the diagnostics of pavement bearing capacity for all test sections during next years according to the same methodology. New data could be used for a modification of the theoretical degradation model that is used for prediction of performance of asphalt pavements.

References

[1] TP 01/2009 Measuring and Evaluation of Bearing Capacity of Asphalt Pavements Using FWD KUAB (in Slovak), MDPaT SR, Bratislava, 2009.

[2] KOMACKA, J.: Diagnostics of Subgrade of Asphalt Pavements Using FWD Device and Obtained Results (in Slovak), *Silnicni obzor,* No. 9, 2000, p. 197–201.

[3] KOMACKA, J.: *Diagnostics and Evaluation of Bearing Capacity of Pavement from Road Database Point of View (in Slovak),* PhD thesis, Zilina : VSDS Zilina, 1996, p. 142.

[4] KOMACKA, J., KORENKO, M., PIALA, J.: Relation of Temperature Changes in Asphalt Pavements to Pavement Bearing Capacity Evaluation, *Communications – Scientific Letters of the University of Zilina,* Vol. 9, No. 3, 2007, pp. 33–36, ISSN 1335-4205.

Jan Celko – Matus Kovac – Martin Decky *

ANALYSIS OF SELECTED PAVEMENT SERVICEABILITY PARAMETERS

The parameters of pavement serviceability have the notable effect to the road life time and to the conditions of safe and comfortable driving. The serviceability of flexible pavements is defined by three parameters: skid resistance, unevenness and pavement distress. The Slovak Road Administration observes 24 specific road sections on which the parameters have been measured two times per year since 1998. The obtained data should be used for determination of the degradation models that describe the qualitative decreasing of the parameters depending on time and traffic load. The functions are very important for definition of the optimal road maintenance and rehabilitation. The degradation models describing the parameters changes over time are the substantial research problem in dependence on many affecting factors.

The results of pavement serviceability parameters evaluation are presented in the paper. The basic functions are described and discussed.

1. Introduction

The pavement serviceability is defined as a complex of parameters affecting the drive of vehicles. The parameters have the notable effect to the road life time and to the conditions of safe and comfortable driving. The serviceability is defined by three parameters: skid resistance, unevenness and pavement distress. The skid resistance includes characteristics of microtexture and macrotexture and often is named like roughness. The unevenness includes two parameters – longitudinal unevenness and ruts as the transverse unevenness. The pavement distress describes the surface failures that decrease a quality of wearing course.

The Slovak Road Administration observed 24 specific road sections on which the parameters have been measured two times per year since 1998. The technical conditions are defined for measuring and evaluation of data. The observance of measured rules is not a simple process but it is very important for quality of results performance. The obtained data are used for determination of the degradation models that describe the qualitative decreasing of the parameters depending on time or traffic load. The functions are very important for definition of the optimal and effective road maintenance and rehabilitation. They also notably affect cost analysis of the pavement management system.

2. Pavement serviceability

The pavement serviceability is based on measurement and assessment of pavement surface characteristics. It quantifies overall performance of a pavement and is further used to manage a road network, called a Pavement Management System (PMS). The Slovak Pavement Management System (PMS) [8] is a tool for effective dividing of budget for the management of road rehabilitation. The system includes processes for effective maintenance, repairs and renewal of road surfaces and structures. The processes are based on the diagnostics of the pavement surface parameters (serviceability level of the road) and bearing capacity [1]. The pavement serviceability parameters are skid resistance, longitudinal unevenness, ruts, and surface distress. Pavement surface characteristics and their changes over time that are discussed in this article are the skid resistance, and longitudinal unevenness.

2.1. Friction, Skid resistance

Friction, in the context of tyres and roads, represents the grip developed by a particular tyre on a particular road surface at a particular time. The coefficient of friction is a measure of this, defined as the ratio of the load (the force applied in the vertical direction) to the traction (the force resisting movement in the horizontal direction). Friction is influenced by a large number of parameters relating to the road and the tyre but it is also affected by other influences that may not be directly attributable to them, such as the vehicle suspension, ambient conditions, speed and the presence of localised contaminants (including water) [2]. The mechanisms of tyre/road friction are not fully understood, but it is widely recognized that there are two main mechanisms involved: molecular adhesion and hysteresis losses, ideas proposed by Kummer in a unified theory of tyre/road friction in the 1960s [3], [4], and developed further by Moore a decade later [5]. The overall friction between tyre and road surface is the sum of these two components according to the following formula.

$$f_p = \frac{A \cdot S}{A_n \cdot p} + \frac{Q \cdot D}{A_n \cdot b \cdot p}. \qquad (1)$$

* **Jan Celko, Matus Kovac, Martin Decky**
Faculty of Civil Engineering, University of Zilina, Slovakia, E-mail: jan.celko@fstav.uniza.sk

Where:
f_p – coefficient of friction
A – sum of contact areas of each element – actual contact area, m^2
A_n – overall contact area, m^2
S – shear stress in the interface, MPa
p – tyre load, MPa
Q – deformed rubber bulk, m^3
D – energy losses due to damping in the rubber bulk, $M.J.m^{-3}$
b - slip distance, m

Skid resistance describes the contribution that the road makes to tyre/road friction. Essentially, it is a measurement of friction obtained under specified, standardised conditions, generally chosen to fix the values of many of the potential variable factors so that the contribution that the road provides to tyre/road friction can be isolated. Unless indicated otherwise, the term skid resistance applies to wet roads and measurements are made on a wetted surface [2].

Skiddometer BV-11 is a skid-resistance measurement unit that is used for observation by The Slovak Road Administration. It measures skid resistance using the longitudinal principle in one of wheel path. Measurements are done with wetting at about 17 % slip ratio. Vertical load is 1000 N, and a Trelleborg T 49 tyre with a size of 4.00-8 inflated at 120 kPa is used. The water film thickness is 1 mm [10, 11, 13].

There are many different devices throughout whole Europe for skid resistance measuring, and there is a new general effort to introduce a harmonised index with a complex process for calibrating the different measuring devices used in Europe, as well. This harmonisation process combines macrotexture measurement with measurement of pavement surface friction, which leads to determination of Skid Resistance index (SRI) computed by means of the following equations [19]:

$$SRI = B * F * e^{(S - S_R)/S_0} \quad (2)$$

where
B – parameter specific to the friction measuring device
F – measured friction coefficient at slip speed S, for Skiddometer BV11 it is Mu value
S – slip speed derived from the operating speed according to test principle
S_R – reference slip speed
S_0 – speed parameter, defined by equation:

$$S_0 = a \cdot MPD^b \quad (3)$$

where
a, b – parameter specific to the texture measuring device/method
MPD – mean profile depth obtained by processing the profiles recorded with a mobile profilometer.

The key to the harmonization process is the adequacy of the mathematical models used to represent the influence of road surface texture and slip speed or slip ratio on the measured values in combination with empirically-derived coefficients. It is clear that current models do not fully describe the behavior of all types of device across their practical operating ranges: in particular, some influence of speed remains even after harmonized values have been calculated [2]. There is a substantial influence of reference slip speed (SR) value, as well. The reference value was earlier set to 60 kph, and now it is 30 kph. The comparability influences of results related to test speed are illustrated in Figs. 1–3.

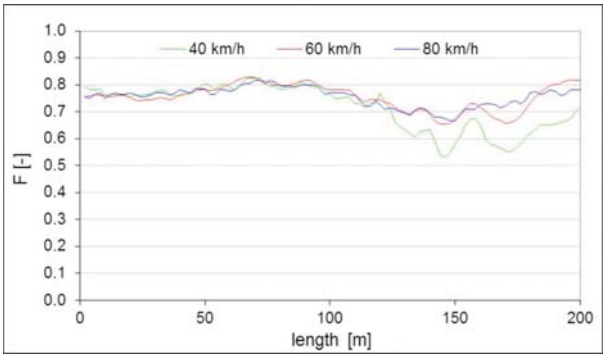

Fig. 1 Measured friction coefficient at different test speeds

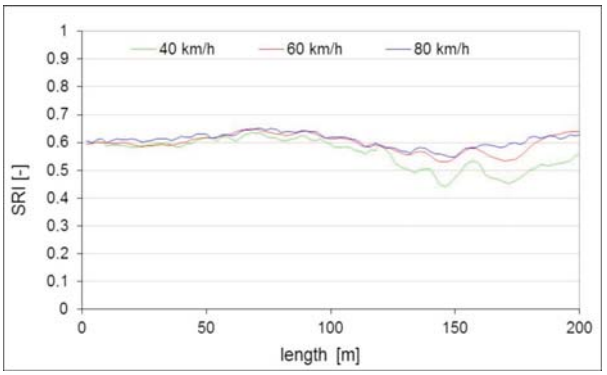

Fig. 2 SRI values for all test speeds computed for reference slip speed S_R = 30kph

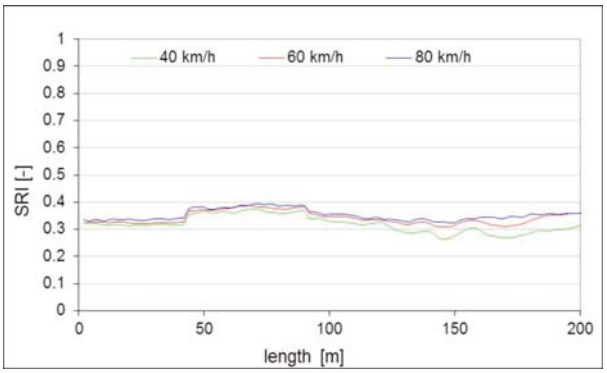

Fig. 3 SRI values for all test speeds computed for reference slip speeds S_R = 60kph

As shown in Figs. 2 and 3 a reference slip speed needs to be taken into account when the skid resistance measurement is harmonized. The reference slip speed S_R = 60 kph, by computing SRI, considers test speeds much better than if the value is set to S_R = 30 kph. For evaluation of skid resistance changes over time the reference slip speed S_R = 60 kph was used.

The skid resistance can alter for the first year or two as a result of traffic action before settling to an equilibrium value around which the skid resistance will fluctuate slightly. Once equilibrium has been reached, the skid resistance at any time may vary as a result of seasonal variation and a significant change in traffic level may alter the equilibrium level [2]. Because of seasonal variation changes of friction only spring measurements values were taken into account.

2.2. Unevenness

The road evenness is one of the basic factors of the pavement quality. It represents the characteristic of the road serviceability, and also road safety and comfort.

a) Longitudinal unevenness

The longitudinal elevation profile of a highway pavement refers to both grade and evenness in the vertical plane parallel to traffic flow. As a pavement develops distresses over time, its longitudinal profile can become altered by those distresses, leading to decreased smoothness and subsequently decreased wheel-pavement interaction, and increased noise, among other things. Longitudinal unevenness is described by International Roughness Index (IRI), which is obtained using the Reference Quarter Car Simulation (RQCS) according to [6, 11]. The ride comfort is described by vertical acceleration of sprung mass of testing vehicle (a_z), and the safety is described by vertical dynamic strength (F_z) at the contact of the wheel with pavement surface. How longitudinal unevenness influences ride comfort (and safety) is shown in Figs. 4 and 5.

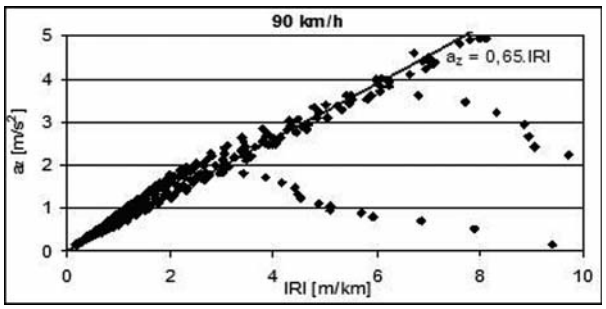

Fig. 4 Relationship between longitudinal unevenness (IRI) and ride comfort (a_z) at 90 kph

The relation tendency shows a mainstream of points that delimited an area of maximal discomfort by minimal IRI values. The line by basic points group was interleaved for determination of the relation between IRI and a_z. The other points lying below tendency are irrelevant from point of view of a comfort evaluation, because the bigger values of IRI respond the lower values of the response. Points lying out of mainstream confirm that one value of IRI can describe different unevenness with different car responses. These points have identical amplitude but different wavelength, which leads only to lower value of acceleration for even higher IRI. This fact is determined by overestimation of the short wavelengths and underestimation of the longer wavelengths by reference quarter car model.

The important characteristic of ride safety from point of view of longitudinal unevenness is the vertical strength Fz at the contact between vehicle and surface. The moment of minimal value was observed. The determined relation is presented in Fig. 5.

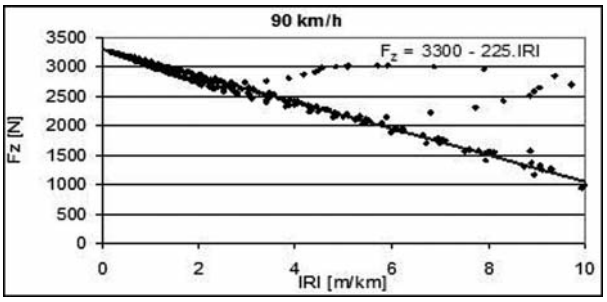

Fig. 5 Relationship between longitudinal unevenness (IRI) and ride safety (F_z) at 90 kph

The strength F_z has decreasing tendency with increasing IRI values. The different values of F_z for identical IRI value are possible to achieve alike for acceleration. The loss of contact does not occur by simulation with harmonic unevenness at speed 60 kph. On the other hand, at speed 90 kph and 130 kph the F_z achieved the zero value yet for low IRI values. The danger is not only a loss of contact but a low intensity of F_z, as well. An intensity of the vertical strength has influence on the stability of a car in horizontal curve and on the breaking distance, too. The differences are determined by characteristics of the reference model. In this case, the generally valid relation is not possible to establish because each vehicle has different weight so also different press strength of axle to the road surface.

3. The degradation functions

The methodology of the degradation functions creating includes two steps:

a. To create a degradation model that describes decreasing in the parameter quality.
b. To define the correlation function that describes a forecast of the parameter changes over time, and its value in particular time.

The model creation uses three research approaches:

1. The principles of the mechanics that use the regularity of structure degradation.
2. The empirical principles by using specific functions.
3. The combination of the mechanical and empiric approaches.

The degradation progress registers the basic tendencies of development, periodical changes based on climatic characteristics and traffic load, and non-regular changes affected by casual influences.

In practice, we evaluate the road degradation by two basic influences – time or traffic load. The mathematical formula of degradation model has an exponential shape (4) [18], (5) [20]

$$P(t) = 1 - \left(\frac{t}{T}\right)^{a}, \text{ or} \tag{4}$$

$$P(x,t) = 1 - A \times \left(\frac{n}{N}\right)^{B} \tag{5}$$

Where

$P(t)$ is the relative performance as a function of time
$P(x,t)$ is the value of a parameter "x" in time "t"
t – time of exploitation
n – number of traffic load (esal) during exploitation
T – time in which the parameter will be exhausted (the value will be 0)
N – overall traffic load (esal) till the parameter will be exhausted
a,A,B – shape parameters which value depend on the kind of effects that are considered.

The parameters A and B are dependent on materials of the road structure. The specific shape of the degradation model is shown in Fig. 6.

For determination of selected parameters changes over time the data measured between years 1998 and 2006 were processed. From all of measured sections were as an example chosen two of them – Poprad – Ganovce and Brodno – Zilina.

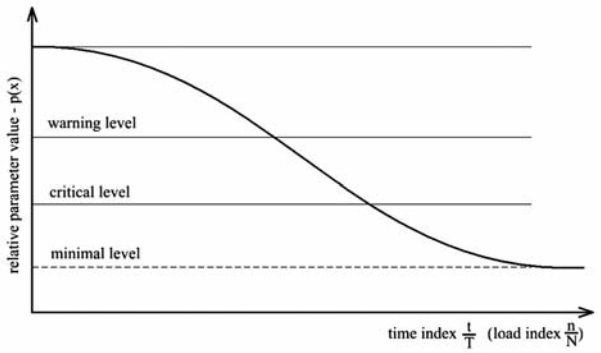

Fig. 6 The specific shape of the degradation model

3.1. Skid resistance

An evaluation of the skid resistance development over time is presented in Fig. 7. Depending on seasonal changes of friction only spring measurements values were taken into account.

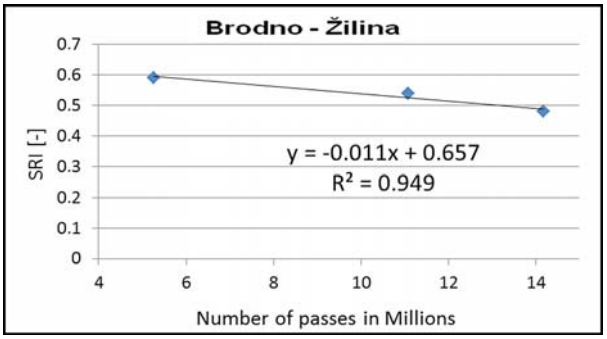

Fig. 8 Friction coefficient versus number of equivalent standard axle load passes

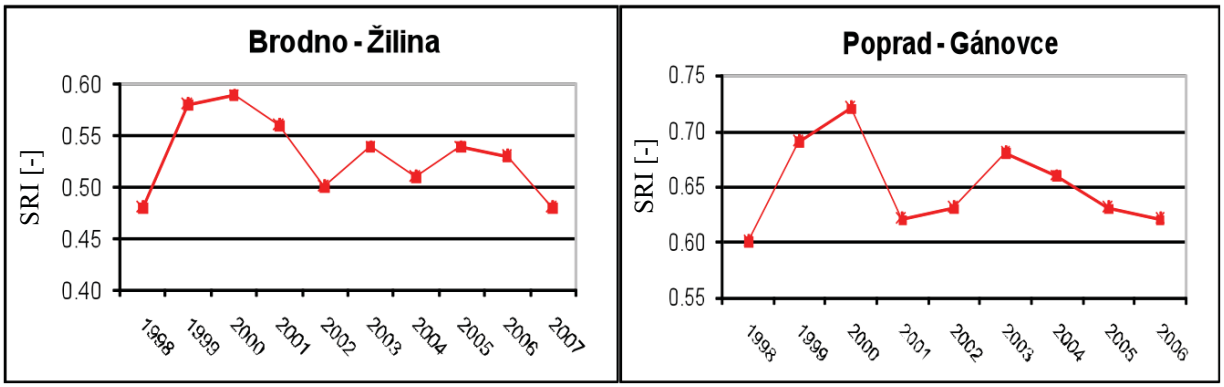

Fig. 7 Changes of SRI values over time

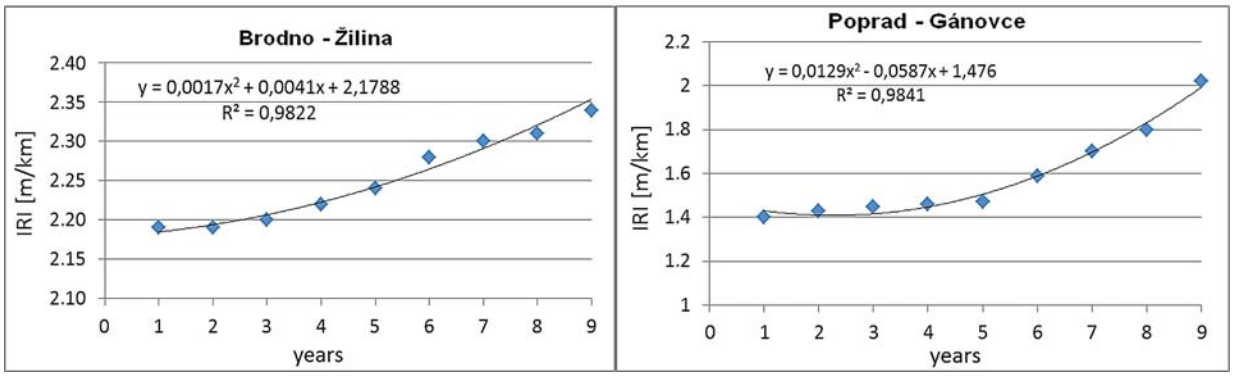

Fig. 9 Changes of longitudinal unevenness over time

Fig. 7 illustrates that there isn't any stable decrease of SRI values over years when friction was monitored. The same chaotic behavior appeared with the other sections. It may be caused by different test conditions every year, such as pavement surface temperature, test speed, measuring device calibration and keeping the same wheel path. Relationship between Skid Resistance Index and number of equivalent standard axle load passes is shown in Fig. 8.

3.2. Longitudinal evenness

An evaluation of the longitudinal evenness development over time is presented in Fig. 9.

As Fig. 9 shows, there is a clear evidence of IRI values increase during pavement usage over years. Increasing tendency is evident by all of the observed sections. All tendencies can be described by a quadratic regression line. Coefficients of the regression line may vary depending on number of passes, pavement construction and climatic conditions. Coefficients scale is very small because of weak unevenness changes over time, so it is possible to describe the tendency by linear equation as well. However, the question of describing life-cycle pavement surface characteristics changes should result from physical fundamentals, such as materials fatigue etc. Exact shape of tendency line is necessary to determine and verify after long-lasting observation on sections with different traffic load and pavement construction by unconditional considering its locality. Fig. 10 shows relationship between longitudinal unevenness and number of equivalent standard axle load passes.

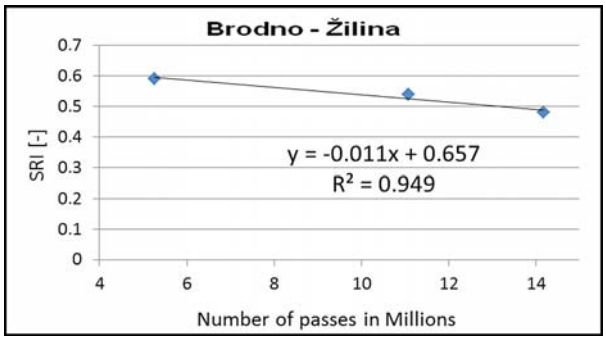

Fig. 10 Relation between longitudinal unevenness and count of equivalent standard axle load passes

4. Longitudinal unevenness and skid resistance interdependency

Can longitudinal unevenness influence the pavement skid resistance? Longitudinal unevenness induces a vehicle vibrating and subsequently vertical force (axle load) increase. On the assumption of increased tread pressure after passing unevenness and subsequently surface wearing and polishing, there were all sections observed from point of view of interdependency of longitudinal unevenness and skid resistance. A course of two mentioned parameters on selected sections (selected from road sections Zilina – STK and Rovensko – Senica) is shown in Fig. 11.

As is illustrated in Fig. 11 on some rough sections (described by higher IRI values) were measured lower skid resistance values, and on the contrary on smooth sections (described by lower IRI values) were measured higher skid resistance values. The assumption was confirmed on few sections but if the general relation of longitudinal unevenness to skid resistance was made, the correlation turned out as very weak. The speculation that the correlation is so weak because of generally low IRI values on observed sections (very smooth pavement surface from point of view of vibrating and tread pressure increasing) was contradicted by research published in [9].

5. Conclusions

There have been done a lot of research work in the field of flexible pavement parameters degradation. However, the question of accurate measuring and evaluating of the observed parameters is still open and the further research is needed. It has been found out that the reference slip speed S_R = 60 kph, by computing SRI, considers test speeds much better than S_R = 30 kph. In term of consideration of longitudinal unevenness influence to ride safety

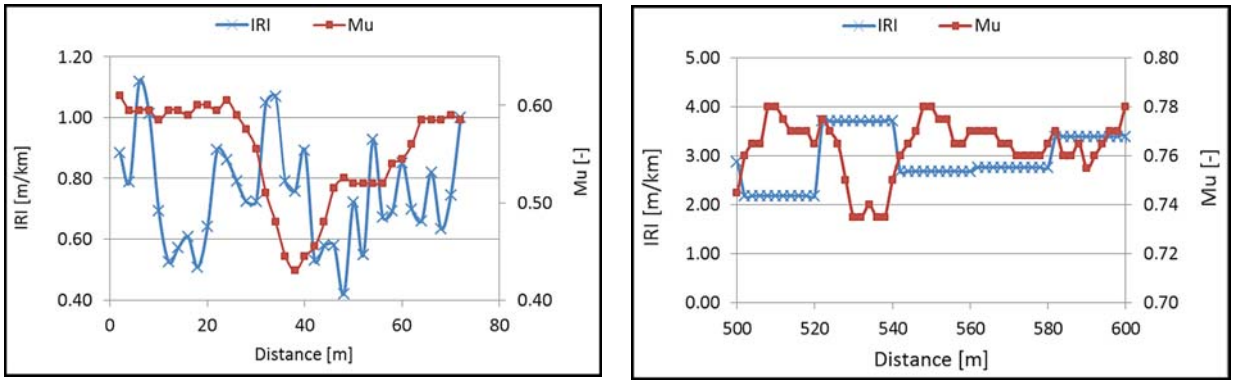

Fig. 11 Comparison of parameters by mutual dependency on 100m long section

(comfort) it is necessary to take into account the overestimation of the short wavelengths and underestimation of the longer wavelengths by reference quarter car model.

The analysis of serviceability parameters and their time and load development is very important part of PMS. It is not possible to choose an optimal time and technology of the road maintenance and repairing without the knowledge of the surface parameters development forecast. In addition, a determination of degradation functions is inevitable for specification of relationships between parameters as an important factor of the road safety increasing.

On the other hand, the analysis of degradation processes is very demanding to the exact observance of the same test conditions. The different climatic conditions and different driving traces are the basic sources of the measuring inconsistency. It is necessary to be aware of long time observation of the parameters for determination of developed functions, which can mean some decades.

References

[1] CELKO J., DECKY, M., KOMACKA, J., KOVAC, M.: Pavement Diagnosis as Integrant of the Pavement System, *Communications – Scientific Letters of the University of Zilina,* Vol. 10, No. 2, 2008. ISSN 1335-4205.
[2] TYRO SAFE - Tyre and Road Surface Optimisation for Skid Resistance and Further Effects, European Community's Seventh Framework Programme (FP7/2007-2013) under grant agreement n°217920.
[3] KUMMER, H. W.: Unified Theory of Rubber and Tire Friction, *Engineering Research Bulletin B-94,* Pennsylvania State University College of Engineering, Pennsylvania, 1966.
[4] KUMMER, H. W., Meyer, W. E.: Unified Theory of Rubber Friction Reveals Adhesion Component's Role in the Tire-road Surface Coupling, *SAE Journal,* Vol. 75, No. 8, 1967.
[5] MOORE, D. F.: Principles and Applications of Tribology, Perg. Inter. Libr., Vol. 14, P-388, 1975.
[6] SAYERS, M. W. et al: The International Road Roughness Experiment (IRRE): Establishing Correlation and Calibration Standard for Measurements, World Bank, Techn. Paper, No. 45.
[7] SJOGREN, L., HENDEBY, G.: Aquaplaning – Development of a Risk Pond Model from Road Surface Measurements, *Linkoping 2003*, ISRN LITH-ISY-EX-3409-2003.
[8] TP 10/2006 Pavement Management System. *Technical regulation.* MTPT SR, 2006.
[9] FUENTES, L., GUNARATNE, M., HESS, D.: Evaluation of the Effect of Pavement Roughness on Skid Resistance. *J. of Transportation Eng.,* Vol. 136, No. 7, 2010. ©ASCE, ISSN 0733-947X/2010/7-640–653.
[10] TP MDPT SR 14/2006 Measuring and evaluation of the pavement skid resistance by measurements SKIDDOMETER BV 11 and PROFILOGRAPH GE. In Slovak. (Meranie a hodnotenie drsnosti vozoviek pomocou zariadení SKIDDOMETER BV11 a PROFILOGRAPH GE).
[11] DECKY, M.: Comparison of Dynamic Methods of Road Pavement Evenness Evaluation, *Communications – Scientific Letters of the University of Zilina,* No. 2, 1999. ISSN 1335-420.
[12] CELKO, J., KOVAC, M.: Evaluation of Pavement Friction According to European Standards, *Communications – Scientific Letters of the University of Zilina,* No. 3, 2004. ISSN 1335-4205.
[13] HUSZAROVA, K.: Measuring and Evaluation of the Skid Resistance of Selected Road Covers (in Slovak), Diploma work, University of Zilina, Department of Highway Engineering, 2008.
[14] CELKO, J., DURCANSKA, D., KOMACKA, J.: Diagnostics and Evaluation of Road Pavements, Scientific Letters of the University of Zilina, No. 3, 2003, ISSN 1335-4205.

[15] COREJ, J., DECKY, M.: Pavements from the Point of View of Future Requirement of Road Transport, *Communications – Scientific Letters of the University of Zilina,* No.1, 1999, ISSN 1335-4205.
[16] FEHRL Report 2006/01, Harmonization of European Routine and research Measuring Equipment for Skid Resistance, © FEHRL 2006, ISSN 1362-6019
[17] CELKO, J. et al: Surface properties of the pavements (in Slovak), Scientific monograph. EDIS Zilina, 2000, ISBN 80-7100-774-9.
[18] Koning, P.C., Molenaar, A.A.A.: Pavement management system for municipalities with emphasis on planning and cost models. Proc. 6th Int. Conf. Struct. Design of Asphalt Pavement. Vol. I, pp. 1041-1049, Ann Arbor - 1987.
[19] CEN/TS 13036-2: Road and airfield surface characteristics - Test methods - Part 2: Assessment of the skid resistance of a road pavement surface by the use of dynamic measuring systems.
[20] STU Bratislava, Stavebna fakulta, KDS: Pavement diagnostics. Degradation models. Report of research project 04-95-97, Bratislava 1997 (In Slovak).

This contribution is the result of the project implementation: “Centre of Excellence in Transport Engineering” (ITMS: 26220120027) supported by the Research & Development Operational Programme funded by the ERDF.

Libor Izvolt – Jan Kardos *

INFLUENCE OF PARAMETERS OF RAILWAY TRACK CONSTRUCTION ON VERTICAL DYNAMIC INTERACTION VEHICLE/TRACK

By analysing the dynamic interaction between the railway vehicle and the track we are able to explain complex interactive phenomena that are particularly important in the case of higher and high speed of a moving rail vehicle on railway track.The paper focuses on the solution of the above mentioned problem with the help of numerical computer simulations. The important step on the way to create a respective simulation model is setting objective entry parameters of railway track as well as taking its imperfections into consideration. These imperfections significantly influence the results of dynamic interaction. Out of the considered track imperfections, we particularly solve deformation resistance inhomogeneity of track grid subgrade and vertical irregularities of rail belt.

1. Introduction

The railway infrastructure presents a strategical component of Slovak transport infrastructure from the point of view of securing continuous national and transit transport within the European Union.The most important transit rail tracks crossing the Slovak Republic are defined according to international conventions *AGC* (1985) and *AGTC* (1993). These rail tracks have to fulfill Technical Interoperability Specifications (TSI). From the point of view of rail track construction, for the chosen track corridors it means that there has to be enabled reaching the operating speed 160 kmh-1 at the maximal axle weight 22.5 tons (loading capacity class *D4UIC*) in the whole longest possible rail localities. The rail track, as it is a significantly inhomogeneous construction, is a subject to influence of operation and climatic factors. Together with the passing time they result in geometric and material deformities by wearing of all the components of track grid and particularly construction layers of sleeper subgrade. By the influence of load increase on modernised rail localities, these geometrical and material degradations are more obvious as a consequence of higher force effects. Recognition and subsequent development prediction of these degradations are conditioned by perfect recognition of acting force effects of rail vehicles. Particularly in the case of high and higher speed, the dynamic interaction force effects are significantly noticeable. They influence the durability and reliability of rail construction in a crucial way and therefore they ought to be expressly considered in the process of construction design and dimensioning.

Lately, the computer simulation of dynamic interaction of complex mechanical system vehicle/ track has had significant influence on the knowledge of structure of interactive wheel forces. In the ties of a mechanical system defined in such a way, dynamic interactive forces are produced whose character and size are necessary to be precisely specified. In this paper we focus not only on the determination of a suitable model for simulation of dynamic interaction vehicle/track, but also on setting objective track parameters that will form a basis for wide application in various application simulations. There is also reference to the present deficiencies in the process of design of rail track construction and there are implied solution possibilities in the form of new approaches to rail track construction dimensioning. They are a result of theoretical simulation analyses that we suppose to verify by experimental measurements in near future in the new laboratory of Faculty of Civil Engineering in Veľký Diel campus. In this laboratory there will also be located a dynamic pulsator for cyclical loading tests.

2. Basic Model Characteristics of Track and Rail vehicle in the SR

The theoretical solution of mechanical problems of rail tracks is carried out on a certain physical model that should sufficiently characterize the basic properties of a mechanical system being solved. These basic properties should also be determinant for the correct interpretation of behaviour of the construction in the given model and they should keep the geometrical similarity with the real construction.The parameters that characterize the construction should at the same time correlate with the parameters that could be determined by standard or other simple diagnostic methods.

* **Libor Izvolt, Jan Kardos**
Faculty of Civil Engineering, University of Zilina, E-mail: libor.izvolt@fstav.uniza.sk

2.1 Rail Vehicle

To make a suitable physical model of a train unit it is necessary to use a model of such train unit that is determinant from the point of view of size of effective dynamic forces and the most sensitive from the point of view of feedback e.g. in the form of comfort by travelling. In the conditions of *ŽSR*, these are mainly passenger train units *EPJ 671* that were purchased in 2010 for the operation in corridor tracks with maximum speed up to 160 kmh^{-1}. The mentioned train unit consists of electrical double decker rail car *EPV 671*, double decker trailer car *PVV 071* and double decker managing car *PRV 971*. From the point of view of possible activity of dynamic force effects on the rail track, the car *EPV 671* is determinant. Its weight according to Tab. 1 is 87.5 tons, which presents static wheel loading 107.3 kN for the four-axle symetrical bogie.

To evaluate the dynamic effects of rail vehicles on the construction of rail track, the symetry of vehicle/track system is used. This task is practically always solved as a plane problem i.e. applied load of one rail belt and the respective plane interactive model of vehicle/track system are considered (analyzed in detail in *chapter 4*). In the process of transformation of solution of a given system from three-dimensional to plane one, it is desirable to take several factors into account. They influence the results of solution and are often neglected in plane interactive tasks. The basic factors influencing the force symetry of rail car system are particularly real irregular crosswise mass distribution in the rail cars, influence of centrifugal force in arc with unbalanced crosswise acceleration, change of rail nivelity, transition to superelevation, etc. In Tab. 2 there is a summary of maximum effects of increase of wheel force for the car *EPV 671*.

We have to be aware of the fact that the maximum loading capacity of a train unit is not always utilised and the occurence of increase of wheel force from Tab. 2 even in the case of reaching high values is only in specific short track localities, possibly in the case of specific climatic influences. Therefore the synergic coaction of these effects is rare and for the objective analysis of dynamic interaction vehicle/track it is enough to consider the standard wheel

Basic parameters of unit EPJ 671 Tab. 1

Parameter	EPJ 671		
	EPV 671	PVV 071	PRV 971
Maximum operational speed	$V = 160\ km.h^{-1} = 44.45\ m.s^{-1}$		
Length of car along the buffer plane	3 × 26,400 mm		
Height of car from the rail surface	4,635 mm		
Width of car	2,820 mm		
Arrangement of bogies	*Bo′Bo′*	2′2′	2′2′
Gauge	1,435 mm		
Wheel base of bogie	L_W = 2,600 mm	L_W = 2,400 mm	L_W = 2,400 mm
Distance of centre of bogies´ rotation	L_B = 19,000 mm	L_B = 19,000 mm	L_B = 19,000 mm
Distance of external bogies	21,600 mm	21,600 mm	21,600 mm
Number of sitting/standing passengers	61/67	134/134	106/134
Weight of empty car	74 t	45.3 t	47.3 t
Maximum car weight at full loading capacity	87.5 t	69.5 t	69.5 t
Maximum bogie weight	22 t	18 t	18 t

Growth of maximum possible increases of wheel force for EPV 671 Tab. 2

Effect of increase of wheel force as a result of...	Increase of wheel force ΔP_k at maximum loading EPV 671	Maximum size of wheel force P_k with increase ΔP_k
transition to the superelevation of maximum inclination 1:1,600 and 1:1,280 according to STN 73 6360 [1] for RP4	0.3 kN/0.5 kN	107.6 kN/107.8 kN
maximum side wind according to III. and IV. wind area in accordance with STN 73 0035 at average centre height according to STN P ENV 13803-1 [2]	12.0 kN/15.5 kN	119.3 kN/122.8 kN
centrifugal force in arc with maximum irregular acceleration 0.65 ms^{-2} and 0.85 ms^{-2} according to STN 73 6360 [1]	9.5 kN/12.0 kN	117.1 kN/119.3 kN
change of the rail nivelity (taper to the elevation arc) with vertical acceleration 0.22 ms^{-2} and 0.31 ms^{-2} according to STN P ENV 13803-1 [2]	2.5 kN/3.5 kN	109.8 kN/112.3 kN
irregular mass distribution in the rail car at the heigth of 5 % and 7 % (estimated)	5.5 kN/7.7 kN	112.8 kN/115.0 kN

force P_k = 112.5 kN. This force is 5 % bigger compared with maximum wheel force of the considered car EPV 671. This difference will sufficiently cover wheel force fluctuations concerning possible effects of wheel force increase and their probable occurence. In this case there should not be considered static wheel force but quasi-static wheel force that takes the motion of the vehicle and the wind influence into account but does not cause crosswise system vibration (2D model).

2.2 Rail Track Construction

The rail superstructure on already modernised corridor tracks of ZSR is formed by the system that consists of rails *60 E1* on concrete sleepers with inclination of upper areas 1:40 (classic superstructure), non-plate flexible rail fastening system *VOSSLOH Skl14*, with sleeper spacing of type *UIC* (600mm). With the rail of shape *60 El* there is most often used typal ferroconcrete sleeper *BP3* or *B91S/1*. A certificate has been issued for using this type in *ZSR*. Between the rail and sleeper there is placed an elastic rubber pad, most frequently *WU7* or *WS7*. The concrete sleepers are embedded in railway ballast of gravel of fraction 31.5/63 mm, while the width of railway ballast under the lower area of sleepers is 350 mm. The subbase has an unstable width depending on the initial deformation resistance of subgrade. According to *TNZ 73 6312* [3] there is required an equivalent value of static deformation module on the level of subgrade surface 30 MPa and on the level of surface of railway substructure 50 MPa. By calculating in accordance with dimensioning methodology *SOJUZDORNII* it is possible to determine the static deformation module on the level of lower area of sleepers to 95 MPa. Reaching the normative values depends on season, technology of construction manufacturing, and on the state of compaction of construction layers by operation [4]. The summary of basic parameters of a modernised track (state of new building) is given in Tab. 3.

The size of pad stiffness coefficient K_p and attenuation C_p, (parameters stated according to *STN EN 13146-3* and *STN 13146-9*), depend on the type of pad material (HDPE, rubber, rubbercork), width, environment temperature, its age (i.e. entire amount and size of loading cycles applied to the pad), as well as contact force of rail fastening. Because of this, values of these parameters are given in wide application interval in various studies ($K_P = 60\times10^3$ to 1000×10^3 kNm^{-1} and $C_P = 40$ to 120 kNsm^{-1}). However, for dynamic evaluation of rail track construction in the model there should be used values of the pad stiffness set by dynamic measurement. According to *STN EN 13481-2*, in case of using concrete sleepers in the main track they should reach values 100 to 200 MNm^{-1}. In *Tab. 3* there are used the average parameter values for the pad leading from comparison of several studies.

The biggest deficiencies in determining parameters given in *Tab. 3* are in stating the values of the module elasticity, stiffness, and attentuation of construction layers of sleeper subgrade. The equivalent modules of elasticity of a given construction layer of subgrade defined in *Tab. 3* were determined from minimum required values of deformation modules, on the basis of analogy of determination of equivalent elasticity modules with the static loading test according to *STN 73 6190 [5]* (the relation leads from the definition of Bousinesque's elastic half-space). The elastic deformations for the calculation of elasticity modules were considered from the second lightening branch, in the interval of tension according to anticipated tension range in a given construction layer (geostatic tension to the addition of geostatic and incremental tension). This approach to determination of equivalent elasticity modules takes into account the theoretical principles of Hook's law (the dependence of tension and deformation in a small interval is linear and this interval is also the interval of real operation of tension in a given construction layer). The indicative elasticity intervals are on the level of lower area of sleeper in the interval <0.01 to 0.30 MPa>, on the level of surface of rail substructure for the width of railway ballast 0.35 m in the interval <0.02 to 0.30 MPa> and on the level of subgrade surface for the width of subbase 0.30 m in the interval <0.03 to 0.05 MPa>. The problem of using loading diagrams from the static loading test according to regulation *ŽSR S4 [6]* is the fact that the most frequently used tension interval under loading board <0 to 0.20 MPa> on the level of subgrade surface with the deformation module 30 MPa is significantly overestimated concerning the interval of operation tension in this depth. Because of this, in Tab. 3 there are used entire tension intervals from the average static loading test for the required level of deformation module 30 MPa, 50 MPa and 95 MPa to calculate elasticity modules. From an elasticity module deduced in such a way it is possible to determine the static stiffness of subbase (elastic constante) from the following theoretical relation [7]:

$$K_i = \frac{E_i}{\left(1 - v_i^2\right)} \cdot 2r \quad (\mathrm{kNm}^{-1}) \tag{1}$$

where:

E_i – is elasticity module in strain of i-th construction layer material,

r_i – is radius of loading board (0.15 m),

v_i – is Poisson´s constant of i-th construction layer material.

The theoretical relation does not count with the fact that the elasticity module, used in the relation, is determined from the second lightening branch according to *STN 73 6190 [5]*, while the coefficient of compressibility (elastic constant) defines the dependence of loading and deformation from steady hysteresis curve (n-th load branch) without permanent deformations (linear elastic constant).The compressibility coefficients should also be determined in the interval of assumed tension state for the given construction layer. The required increase of value of elastic constant from relation (1) as a result of elimination of plastic transformation is approx. 20 % and the elastic constant parameters stated in *Tab. 3* are also changed according to this value.

In the construction layers of sleeper subgrade, damping takes place as a result of internal friction of particles (dissipation).The diagnostics of attenuation characteristics of sleeper subgrade construction has not been stated yet, while these parameters are vital for creation of a respective simulation model for determining the dynamic response vehicle/track. For damping of oscillation of mechanical system we introduce a supposition that the resistance

Summary of basic track parameters for modeling vertical dynamic interaction Tab.3

Parameter description			Parameter value
Railway superstructure		Young´s model of elasticity in strain of rail 60 E1	$E = E_R = 2.07\times10^{11}$ Nm^{-2}
		Cross-sectional moment of inertia of rail 60 E1	$I_y = I_R = 3.055\times10^{-5}$ m^4
		Flexural stiffness of rail in the vertical direction 60 E1	$EI_y = 6.3239\times10^3$ kNm^3
		Longitudinal weight of rail 60 E1	$M_R = 60.34$ kgm^{-1}
		Hertz´s contact stiffness wheel/rail (better to consider a nonlinear one in the calculation)	$K_H = 2{,}4.105$ kNm^{-1}
		Cross-sectional rail area 60 E1	$A_y = A_R = 76.86\times10^{-4}$ m^2
		Poisson´s constant of rail material 60 E1	$v_R = 0.27$
		Volume weight of rail 60 E1	$\rho_R = 7{,}850$ kgm^{-3}
		Weight of half-sleeper BP 91/S1	$M_S = 304/2$ kg = 152 kg
		Pad stiffness coefficient WU 7	$K_P = 120\times10^3$ kNm^{-1}
		Pad attenuation coefficient WU 7	$C_P = 50$ kNsm^{-1}
Railway substructure	Subgrade surface	Minimum equivalent deformation module according to TNŽ 73 6312 [3]	$E_{ekv,1} = 30$ MPa
		Equivalent elasticity module according to STN 73 6390	$E_1 = 35$ MPa
		Poisson´s constant for soil S1 to S5 with reachable $E_{ekv,1} = 30$ MPa	$v_1 = 0.35$
		Typical value of volume weight at standard rate of compaction	$\rho_1 = 1{,}850$ kgm^{-3}
		Equivalent co-oscillating mass for plane model	$M_1 = 430$ kg
		Coeff. of subbase stiffness determined from the curve of static load test according to (1)	$K_1 = 15\times10^3$ kNm^{-1}
		Coefficient of subbase attenuation determined according to relation (2)	$C_1 = 85$ kNsm^{-1}
	Surface of railway substructure	Minimum equivalent deformation module according to TNŽ 73 6312 [3]	$E_{def,2} = 50$ MPa
		Equivalent elasticity module according to STN 73 6390	$E_2 = EF = 60$ MPa
		Poisson´s constant for crushed stone S1 to S5 with reachable $E_{ekv,2} = 50$ MPa	$v_2 = v_F = 0.25$
		Typical value of volume weight at standard rate of compaction	$\rho_2 = 2{,}050$ kgm^{-3}
		Equivalent co-oscillating mass for plane model	$M_2 = M_F = 480$ kg
		Coeff. of subbase stiffness determined from the curve of static loading test according to (1)	$K_2 = K_F = 23\times10^3$ kNm^{-1}
		Coefficient of subbase attenuation determined according to relation (2)	$C_2 = C_F = 110$ kNsm^{-1}
	Lower area of sleeper	Calculated equivalent deformation module according to TNŽ 73 6312 [3]	$E_{def,3} = 95$ MPa
		Equivalent elasticity module according to STN 73 6390	$E_3 = E_B = 110$ MPa
		Poisson´s constant for crushed stone (fr. 31,5/63 mm) with reachable $E_{ekv,3} = 95$ MPa	$v_3 = v_B = 0.25$
		Typical value of volume weight at standard rate of compaction	$\rho3 = 2{,}400$ kgm^{-3}
		Equivalent co-oscillating mass for a plane model	$M_3 = M_B = 750$ kg
		Coeff. of subbase stiffness determined from the curve of static load test according to (1)	$K_3 = K_B = 42\times10^3$ kNm^{-1}
		Subbase attenuation coefficient determined according to relation (2)	$C_3 = C_B = 170$ kNsm^{-1}
		Coefficient of subbase stiffness in slide	$K_{3h} = K_W = 40\times10^3$ kNm^{-1}
		Coefficient of subbase attenuation in slide	$C_{3h} = C_W = 80$ kNsm^{-1}

of system movement is proportional to the speed of movement (linear possibly viscous attenuation). According to [8] it is possible to use the following theoretical relation to calculate the coefficient of attenuation:

$$C_i = \sqrt{\frac{E_i \cdot \rho_i}{1 - v_i^2}} \quad (\text{kNsm}^{-1}) \qquad (2)$$

where:

E_i – is elasticity module in strain of i-th construction layer material,

ρ_i – is volume weight of i-th construction layer material,

v_i – is Poisson´s constant of i-th construction layer material.

All the values of elasticity and deformation modules, Poisson's constants, coefficients of stiffness and damping given in Tab.3 are stated by static loading. The dynamic characteristics of soil of sleeper subgrade are necessary to be found out by experimental measurements e.g. via cyclic loading tests with different frequency composition and deviation (dynamic pulsator). The analysis of dynamic soil characteristics is carried out e.g. in [9]. From this one we can conclude that all the dynamic quantities have higher values as a result of shorter and cyclically active force and in this way smaller deformation (at frequency 5 to 10 Hz dynamic elasticity modules and Poisson's constants are bigger in 10 to 35 % when compared to static ones). By assembling a model for simulation of dynamic

interaction vehicle/track with consideration of dynamic characteristics of entry parameters, there is obvious higher model stiffness of train construction and in this way also possibly higher values of dynamic interactive forces. There is a recent plan to observe the dynamic characteristics of common materials constituting sleeper subgrade in accordance with valid norms and regulations with the help of newly-built dynamic pulsator of the University of Žilina. These results will significantly help specify the entry parameters in order to create a relevant dynamic interactive track model.

3. Mathematical Model of Vertical Dynamic Interaction Vehicle/Track

The method of mathematical modeling of the vehicle and rail track is used for understanding the complicated dynamic interactions between vehicle and track. The solution of dynamic response of construction of rail and vehicle as a plane task gives in the case of correct formulation and setting entry parameters almost the same results as solutions of complex three-dimensional tasks. To observe the vertical dynamic interactions of wheel and rail track it is thus enough to use the plane calculation model of vehicle and track.

3.1 Calculation Model of Rail Vehicle

The calculation model of rail vehicle is usually considered as a 2-level plane model with sprung bogies and car body. In the design of the mathematical model that serves to study dynamic behaviour of vehicles, it is usually supposed that the system components are solid, and the elastic deformations and vibrations are ignored. All the relations between wheel and bogie and bogie and car body (viscous dampers, spring elements) are considered linear. A plane vehicle model, made in this way, enables to model the influence of vertical movement of sprung mass (heavy effect) and the influence of swinging of sprung mass in longitudinal direction (pitch effect). The influence of inclination of sprung mass in crosswise direction (roll effect) on the formation of kinematic quantities of the model is not taken into consideration. However, it is included in quasi-static speculation of wheel force as in *part 2.1.* The contact of wheel and rail takes into account contact deformation on the basis of Hertz' theory, considering the contact stiffness K_H. The Hertz's theory assumes elastic deformations on the contact of wheel and rail depending on vertical interactive force and the way of contact of rail surface and wheel rim [10]. As a consequence, in the model it is necessary to consider the Hertz' contact stiffness as a function of vertical interactive force that has inconstant value (non-linear Hertz contact spring).To solve the equations of entire system with non-linear Hertz theory, it is suitable to use the iteration method to calculate K_H. in each time step. The example of interactive model of system vehicle/track that is sufficient to analyse the standard characteristics of dynamic interaction of rail car *EPV 671* is demonstrated in *Fig. 1*. The vehicle model has 10 degrees of freedom. The bogie frame is connected to the wheels of unsprung mass through the primary springs of suspension and connected to the car body through secondary springs of suspension. The designed discreet calculation model has to respect geometrical and physical parameters of vehicle and track as well as the most important imperfections influencing dynamic interaction vehicle/track (*Tab. 1* and *Tab. 3*).

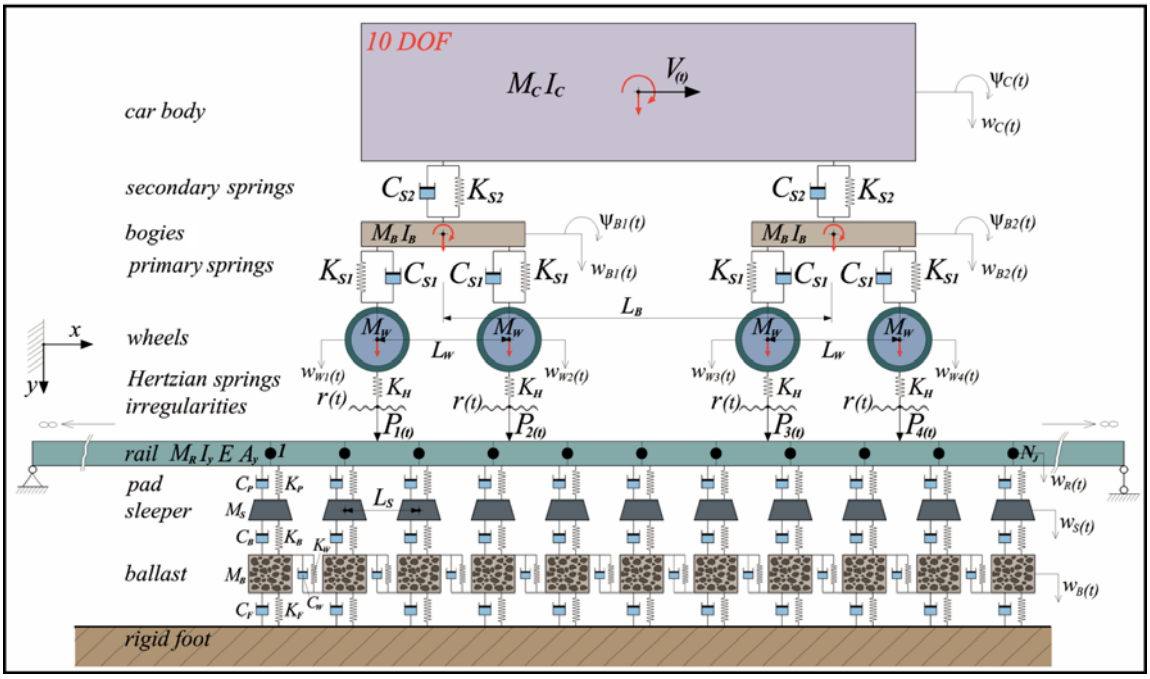

Fig. 1 Example of interactive model of system vehicle/track

3.2 Calculation Model of Track Construction

The calculation model of rail track is considered as a plane model of one rail belt that is modelled by simple beam component (rail), solid support component (sleepers), connecting and damping components.The connecting components (ties)- rail/pad, pad/sleeper, and sleeper/subgrade layers are double-nodal spring- damping components.The characteristics of these components could be set as either linear or non-linear characteristics, although in practical calculations they are solved as linear ones. The parameter values of these components should unequivocally be set in dynamic loading mode (see *part 2.2*) The rail is assumed as a homogenous beam with N_J nodes and N_E components. Each beam mode (rail structure) has two degrees of freedom. In the model we consider the effect of half-sleeper on viscous-elastic basis. The number of sleepers in model N_S depends on the way of analysing the dynamic interaction. In the case of considering stochastic stiffness of beam and imperfection of rail geometry, it is more advantageous to consider a higher number of sleepers in the model (50 to100 sleepers). To model the subgrade unhomogeneity, it is better to use a multi-layer model consisting of railway ballast, subbase, possibly soil of subgrade surface. The model of sleeper subgrade contains additional gravel mass under each sleeper. The sleepers are connected through the spring and damper in skid (K_W and C_W). According to several well-known studies, with this type of model there could be gained better correlations between the calculated and measured responses. The model is usually limited in vertical direction on the level of subgrade surface (solid plane). To this there are connected spring-damping components with parameters of subbase K_F, C_F (surface of railway substructure) according to *Tab. 3*. The main movement equations for discreet system with several degrees of freedom (dynamic balance equations) are composed according to a following relation [11]:

$$[M]\{\ddot{w}\} + [C_b]\{\dot{w}\} + [K]\{w\} = \{P\} \qquad (3)$$

where:

$\{w(x,t)\}$ – is a vector of generalised shifts in nodal points of final components,
$[M]$ – is a global matrix of system weight,
$[C_b]$ – is a global matrix of system damping,
$[K]$ – is a global matrix of system stiffness,
$\{P\}$ – is external node load.

The components of shift vector$\{w(x,t)\}$ undoubtedly determine the deformation state of track in any place of construction x and in any time t. The shift vectors are primarily composed by unknown quantities, that serve to calculate the internal forces of construction and reactions within the system ties. The global matrices of weight, damping and stiffness of the system are generated from component matrices (connecting components and masses). The numerical time integration is applied to differential equations of dynamic balance. As a result, the movement of rail vehicle on the track is discretized and the equations of dynamic balance are fullfilled only in the final number of time moments. The length of integration step Δt is usually chosen between 0.025 to 0.200 ms [11]. The actual interactive analysis of the vehicle moving on the track is based on the use of so-called topical position of the vehicle in a movable coordinate system. This involves automatic leaving out the sleeper and its ties on one side and addition of sleepers with ties on the second one. After the sleeper shift from the end to the beginning of the examined area, the update takes place – new system parameters are introduced to the matrix of stiffness and attenuation (in the case of stochastic model).This means that the dynamic calculation model works inversely.

4. Software Systems for Solution of Dynamic Interaction Vehicle/Track

The computer simulation of vertical dynamic interaction rail vehicle/track helps clarify complex interaction phemomena and at the same time evaluate the influence of chosen parameters on the quantities of dynamic response of rail track. The task formulated in such way cannot be effectively solved using conventional business numeric programe systems (*FEAT, NEXIS, SCIA, ANSYS, ABAQUS, LUSAS, DIANA, ATENA, SOFISTIK, NASTRAN, ADINA, PLAXIS, COSMOS* etc.), but has to use special calculation programmes that are individually programmed prevailingly for the purposes of calculation, most frequently in the programming languages *C++, FORTRAN, VISUAL BASIC* or *MATLAB*. On this purpose several programmes were created, short overview of these is listed in *Tab. 4*. Most of them enables to take all the requirements defined in this paper into account.

5. Conclusion

The experimental measurements of dynamic interaction vehicle/track realized in situ present the only way of verification of numeric results and also the only way of revealing objective reality. At the same time it is necessary to emphasize that carrying out of such experimental measurements in the rail track under operation is often limited by the possibility of sensor installation in one measured place only. In the case of placing the measuring devices on the car bogies we cannot reliably describe the rail track parameters that cause the given dynamic reaction [17]. Because of this, the computer simulations of dynamic interaction vehicle/track are really important.They enable us to analyse specific problems of dynamic interaction. From the parametric analysis of several programmes of dynamic interaction vehicle/track as well as from several studies carried out in this area we could conclude that the programmes in use are sensitive to the values of entry parameters of subgrade of rail track. The authors of several studies deal freely with the subgrade parameters as with variable quantity and they subsequently use these parameters to match them with simulation results so they would correlate with the results of experimental measurements or other simulations. The entry characteristics of rail track should be expressly defined on the basis of carried out diagnostic methods realized in real rail track construction possibly from limit standard values that are tolerable in operational conditions. The diagnostic methods of construction layers of sleeper subgrade should also consider dynamic mode of construction loading in the range of frequency and tension that will be active in the given construction

Overview of programmes for direct solution of dynamic interaction vehicle/track Tab. 4

Name of programme	Responsible author	Institution where programme was developed
DIFF [12]	Dr. Jens Nielsen	centre of excellence in Railway Mechanics at Chalmers University of Technology, Sweden
NUCARS [12]	Dr. Nick Wilson	American Association of Railroads (AAR), Transportation Technology Centre Inc. (TTCI)
3DWTSD [12]	Dr. Yan Quan Sun	Central Queensland University, Australia
TRACK [12]	Dr. Stuart Grassie	Stuart Grassie Engineering Solutions, Cambridge University, United Kingdom
DTRACK [13]	Dr. Zhengi Cai	DynTrack Systems, USA and Queen´s University, Canada
DARTS [14]	Prof. Coenraad Esveld	Esveld Consulting Services, Delft University of Technology, Netherlands
SUBTTI [12]	Dr. Ulf Gerstberger	Technical University Berlin, Germany
VICT [12]	Prof. Wanhimng Zhai	Southwest Jiaotong University, China
RAIL [14]	Dr. Valéri Markine	Delft University, Netherlands
DATI [15]	Dr. Jabbar Ali Zakeri	University of Science and Technology, Iran and Beijing Jiaotong University, China
IIT [12]	Dr. G. Kumuran	Indian Institute of Technology, India
VIA [13]	Dr. Buch A. Roda	University of Valencia, Spain
RTRI [12]	Dr. Makoto Ishida	Railway Technical Research Institute, Japan
TRADYS [15]	Dr. Miwa Masahiro	Central Japan Railway Company and Tokyo University of Technology
DIASTARS [16]	Dr. Makoto Tanabe	Kanagawa Institute of Technology and Railway Technical Research Institute, Japan
C32/Interakcia [11]	Prof. Milan Moravcik	University of Zilina, Slovakia

layer during operation. To determine the dynamic parameters in the given construction layer, the simulation of dynamic interaction vehicle/track is notably applicable. By advancing iteration of values of operational frequencies and tensions determined from computer simulations, and values of dynamic characteristics of materials in individual construction layers determined e.g. by experimental measurements with dynamic pulsator, it will be possible to design a mathematical model with entry parameters in accordance with real operational conditions.From the simulation results, it will be subsequently possible to verify the criteria for geometrical position and rail arrangement in synergy with criteria for deformation resistance of subgrade. It can also be assumed that it will be necessary to define the requirements of reaching a certain homogeneity level of deformation resistance of subgrade, possibly to set such technological methods of manufacturing the construction layers of subgrade (e.g. by intelligent compaction cylinders [18]) that will secure the required and verifiable level of subgrade homogeneity. The important part of considering these and defining new criteria is applying stochastic parameters of track and vehicle in models. These could be stiffness of rail fastening, sleeper spacing, stiffness and attenuation of subgrade, regular and irregular imperfection of rail geometry, wheel imperfection, floating sleepers, unstable speed of rail vehicle etc. The dynamic analysis with stochastic rail parameters (created by Monte Carlo method or by sampling from the real track) will enable to identify the critical states of dynamic interaction in a more actual way. Their result is exceeding the level of safety, comfort or critical degradation of components of rail track and vehicle.

This contribution paper is the result of the project implementation: “Centre of Excellence in Transport Engineering“ (ITMS 26220120027) supported by the Research & Development Operational Programme funded by the ERDF.

References

[1] *STN 73 6360 – Geometrical Position and Arrangement of 1435 mm Gauge Railways (in Slovak),* SUTN, Bratislava 09/1999, 84 p.

[2] *STN P ENV 13803-1 – Railway Applications – Track – Track Alignment Design Parameters – Track Gauges 1435 mm and Wider - Part 1: Plain line (in Slovak)*, SUTN, Bratislava 08/2004, 82 p.

[3] *TNZ 73 6312 – Designing of Railway Substructure Layers, Railway of Slovak Republic (in Slovak)*, Bratislava 09/2005, 58 p.

[4] IZVOLT, L.: *Railway Substrucutre. Straining, Diagnostics, Designing and Realization of Construction Layers of Railway Subgrade (in Slovak)*, Zilinská univerzita, Zilina 2008, 324 p., ISBN 978-80-8070-802-3

[5] *STN 73 6190 – Static Plate Load Test of Subgrade and Construction Layers of Roadway (in Slovak).* SUTN, Bratislava 9/1980, 14 p.

[6] *Predpis ZSR S4 – Railway Subgrade (in Czech),* Nakladatelství dopravy a spojů, Praha 1988

[7] MORAVCIK, Mi., MORAVCIK, Ma.: *Mechanics of Railway Tracks 1. Theoretical Analysis and Simulation of Railway Tracks' Mechanics (in Slovak),* Zilinska univerzita, 2002, 300 p., ISBN 80-7100-983-0

[8] CHOUDHURY, D., BHARTI, K. R., CHAUHAN, S., INDRARATNA, B.: Response of Multilayer Foundation System beneath Railway Track under Cyclic Loading, *J. of Geotechnical and Geoenviromental Eng.,* ASCE, pp. 1558–1563, http://dspace.library.iitb.ac.in/jspui/bitstream/10054/ 1616/1/ASCE5.pdf

[9] SCHUGERL, R.: *Dynamic Parameters of Rocks and Processes of their Detection (in Slovak),* Acta Geologica Slovaca, Vol. 1, No. 1/2009, pp. 15–26, http://geopaleo.fns.uniba.sk/ageos/archive/ 2009_01/ schugerl_ 2009.pdf

[10] GERLICI, J., LACK T.: *Railway Wheels and Track Interaction (in Slovak),* Zilinská univerzita, Zilina 2004, p. 200, ISBN 80-8070-317-5

[11] MORAVCIK, Mi., MORAVCIK, Ma.: Mechanics of Railway Tracks 2. Theoretical Analysis and Simulation of Railway Tracks´ Mechanics (in Slovak), Zilinska univerzita, 2002, 312 p. ISBN 80-7100-984-9

[12] STEFFENS, D. B.: *Identification and Development of a Model of Railway Track Dynamic Behaviour,* A Thesis Submitted for the Degree of Master of Engineering, Queenland University of Technology, Queenland 2005, 317 p., http://eprints.qut.edu.au/16029/ 1/David_Steffens_Thesis.pdf

[13] LEONG, J.: *Development of Limit State Design Methodology for Railway Track,* A Thesis Submitted for the Degree of Master of Engineering, Queenland University of Technology, Queenland 2007, 228 p., http://eprints.qut.edu.au/16565/1/ Jeffrey_Leong_Thesis.pdf

[14] ESVELD, C.: *Modern Railway Track – Second Edition,* Delft University of Technology, Delft 2001, 654 p. ISBN 90-8004-324-3-3

[15] ZAKERI, A. J., XIA, H., FAN, J. J.: Dynamic Responses of Train-track System to Single Rail Irregularity, *Latin American J. of Solids and Structures,* Vol. 6, No. 2/2009, pp. 89-104, ISSN 1679-7817, http://www.lajss.org/index.php/LAJSS/article/view/ 208/170

[16] TANABE, M., WAKUI, H., MATUMOTO, N.: *DIASTARS – Dynamic Interaction Analysis for Shinkansen Train And Railway Structure,* http://www.rtri.or.jp/infoce/wcrr97/B595/B595.html

[17] MORAVCIK, Mi., MORAVCIK, Ma.: *Mechanics of Railway Tracks 3. Experimental Analysis of Straining and Deformation of Railway Components (in Slovak).* Experimentalna analyza namahania a pretvorenia komponentov trate, Zilinska univerzita, Zilina 2002, 220 p. ISBN 80-7100-985-7

[18] IVOLT, L., KARDOS, J., MECAR, M.: Reinforces Subbases and Application of other Chosen Parameters in Sleeper Subgrade Dimensioning. *Communications – Scientific Letters of the University of Zilina,* No. 3/2007, pp. 21–27, ISSN 1335-4205

[19] IZVOLT, L., KARDOS, J.: Intelligent Compaction Technique as a Tool of Objective and Effective Application of Geosynthetics, *Communications – Scientific Letters of the University of Zilina* No. 3A/2010, pp. 104–111, 2010, ISBN 80-8070-193-8

[20] MORAVCIK, M.: Dynamics Behavior of Railway Track-experimental Measurements. *Communications – Scientific Letters of the University of Zilina*, No. 3/2002, pp. 10–16, ISSN 1335-4205

[21] MORAVCIK, M.: Vertical Track Stiffness Effect on Dynamics Behavior of Track Structure. *Communications – Scientific Letters of the University of Zilina,* No. 3/2004, pp. 45–62, ISSN 1335-4205.

Djordje N. Dihovicni *

ANALYSIS OF PRACTICAL STABILITY FOR TIME DELAY AND DISTRIBUTED PARAMETER SYSTEMS

This paper points to sufficient conditions for practical stability of linear systems with time delay in state. Particularly, in control system engineering practice, despite the contribution to the contemporary control theory and system thinking, the problems of practical stability are not developed in details. Taking into account that the system can be stable in a classic way, but it can also possess inappropriate quality of dynamic behavior, and because of that, it is not applicable. For engineers it is crucial to take the system into consideration in relation to permitted states in phase space which are defined for such a problem, Dihovicni et al. (2006). Although, there are some papers covering practical stability problems, the lack of exploring it by using fundamental matrix and matrix measure was observed. Our main idea is to present definitions and conditions for practical stability, applying matrix measure approach. From a practical view point, it is crucial to find intervals on which the system is stable, and to know the function of initial state, the "prehistory" of system motion. The practical stability for a class of a distributed parameter system is also presented. The system is described in state space and a unique theory for such a problem is developed where a fundamental matrix of system and matrix measure is used. Using an efficient approach based on matrix measure and system fundamental matrix, the theorems for practical stability of distributed parameter systems are developed, and superiority of our results is illustrated with a numerical example.

Keywords: distributed parameter systems, time delay, practical stability.

1. Introduction

During the process of analysis and synthesis of control systems, the fundamental problem is stability, Wang (1992). From strictly engineering point of view it is very important to know the boundaries where a system trajectory comes during the motion in state space. The most often case for consideration of control systems, is behaving on an infinite interval which in real cases is only of academic importance in spite of practical stability which has significance in real life, Nedic *et al.* (2006). The linear systems might have delay in state, in control, or in both of them, but the most frequent occurring delay is in state, Debeljkovic (1994). Considering engineering practice needs, it is important to explore the time intervals where the system is stable. Thus, the development of efficient theory is essential for necessary and sufficient conditions for practical stability, Nedic *et al.* (2006). In Tissir *et al.* (1996) are given conditions for practical stability, making relation between the matrix and its maximal and minimal singular values. Most authors focus on solving practical stability for modified Ljapunov concepts, according to Dihovicni *et al.* (2006). This paper contradicts the majority of theories dealing with this topic by developing a unique theory in state space using a fundamental matrix and matrix measure approach combined with conditions of singular values of matrix A_0 and A_1.

2. General Consideration

Consider the time delay system described by:

$$\dot{\underline{x}} = A_0 \cdot \underline{x}(t) + A_1 \cdot \underline{x}(t-\tau) \tag{1}$$

with an appropriate function of initial state:

$$x(t) = \underline{\psi}_x(t) - \tau \le t \le 0 \tag{2}$$

where the system described by equation (1) is presented in a free working state, $\underline{x}(t)$ is the state vector, and A_0 and A_1 are constants of the system matrix of appropriate dimension, and τ is time delay.

The system behavior described by equation (1) is defined on time interval, $J = [t_0, t_0 + T]$, Nenadic *et al.* (1997), and T can be a positive real number.

3. Main Result

Theorem 1: Time delay system (1) with a function of initial state (2), is stable on a finite time interval in relation with [α, β, τ, T] if the following conditions are satisfied :

* **Djordje N. Dihovicni**
Technical College, New Belgrade, Serbia, E-mail: ddihovic@ Eunet.yu

a) $$\|A_1\| < \frac{\sigma_{\max}(Q^{1/2})}{\sigma_{\max}(Q^{-1/2}P)} \quad (3)$$

where P is a solution of matrix equation:

$$A_0^T \cdot P + P \cdot A_0 = -2 \cdot Q \quad (4)$$

and $\sigma_{\max}(A_0)$ and $\sigma_{\min}(A_0)$, are maximal and minimal singular values of matrix A_0, and holds:

$$\|A_1\| < \frac{\sigma_{\max}(Q^{1/2})}{\sigma_{\max}(Q^{-1/2}P)} \quad (5)$$

b) $$e^{\mu(A_0)t} < \frac{\sqrt{\beta/\alpha}}{1+\tau\|A_1\|}, \forall t \in [0,T] \quad (6)$$

Proof of conditions a): Consider the functional, presented in Tissir *et al.* (1996):

$$v = \underline{x}^T(t) \cdot P \cdot \underline{x}(t) + \int_{t-\tau}^{t} \underline{x}^T(s) \cdot Q \cdot \underline{x}(s) \cdot ds \quad (7)$$

$$\begin{aligned} \dot{v}(t) &= \underline{x}^T(t) \cdot (A_0^T \cdot P + P \cdot A_0 + Q) \cdot \underline{x}(t) + 2 \cdot \underline{x}^T(t) \cdot \\ &\cdot P \cdot A_1 \cdot \underline{x}(t-\tau) - \underline{x}^T(t-\tau) \cdot Q \cdot \underline{x}(t-\tau) \\ &= \underline{x}^T(t) \cdot (A_0^T \cdot P + P \cdot A_0 + 2 \cdot Q) \cdot \underline{x}(t) \cdot Q \cdot \underline{x}(t) + \quad (8) \\ &+ 2 \cdot \underline{x}^T(t) \cdot P \cdot A_1 \cdot \underline{x}(t-\tau) - \underline{x}^T(t-\tau) \cdot \\ &\cdot Q \cdot \underline{x}(t-\tau) \end{aligned}$$

From equation (4) and the inequality:

$$\begin{aligned} &2 \cdot \underline{x}^T(t) \cdot P \cdot A_1 \cdot \underline{x}(t-\tau) = \\ &= 2 \cdot \underline{x}^T(t) \cdot P \cdot A_1 \cdot Q^{-1/2} \cdot Q^{1/2} \cdot \underline{x}(t-\tau) \quad (9) \\ &\le \underline{x}^T(t) \cdot P \cdot A_1 \cdot Q^{-1} \cdot A_1^T \cdot P \cdot \underline{x}^T(t) + \underline{x}^T(t-\tau) \cdot Q \cdot \underline{x}(t-\tau) \end{aligned}$$

it is obtained:

$$\begin{aligned} \dot{v} &= -\underline{x}^T(t) \cdot Q \cdot \underline{x}(t) + 2 \cdot \underline{x}^T \cdot P \cdot A_1 \cdot \underline{x}(t-\tau) - \underline{x}^T(t-\tau) \cdot Q \cdot \underline{x}(t-\tau) \\ &\le -\underline{x}^T(t) \cdot Q \cdot \underline{x}(t) + \underline{x}^T(t) \cdot P \cdot A_1 \cdot Q^{-1} \cdot A_1^T \cdot P \cdot \underline{x}(t) \quad (10) \\ &\le -\underline{x}^T(t) \cdot Q^{1/2} \cdot (t - Q^{-1/2} \cdot P \cdot A_1 \cdot Q^{-1} \cdot A_1^T \cdot P \cdot Q^{-1/2}) \cdot Q^{-1/2} \cdot \underline{x}(t) \end{aligned}$$

where $\dot{v}(t)$ is negative definite if the following equation holds:

$$1 - \lambda_{\max}(Q^{-1/2} \cdot P \cdot A_1 \cdot Q^{-1} \cdot A_1^T \cdot P \cdot Q^{-1/2}) > 0 \quad (11)$$

which is satisfied if the following equation holds:

$$1 - \sigma_{\max}^2(Q^{-1/2} \cdot P \cdot A_1 \cdot Q^{-1/2}) > 0 \quad (12)$$

Using the properties, Amir-Moez (1956), condition (10) holds if:

$$1 - \sigma_{\max}^2(Q^{-1/2} \cdot P) \cdot \sigma_{\max}^2(A_1 \cdot Q^{-1/2}) > 0 \quad (13)$$

which is satisfied if:

$$1 - \frac{\|A_1\|^2 \cdot \sigma_{\max}^2(Q^{-1/2} \cdot P)}{\sigma_{\min}^2(Q^{1/2})} > 0 \quad (14)$$

and the proof is complete.

Using a similar approach, Nenadic *et al.* (1997):

$$\left| \int_a^b \varphi(x) dx \right| \le \int_a^b |\varphi(x)| \cdot dx \quad (15)$$

it is obtained:

$$\begin{aligned} \underline{a}^T(t)\underline{c}(t) &\le \left| \underline{\psi}_x^T(0) \Phi^T \int_{-\tau}^{0} \underline{b}(t,\theta) d\theta \right| \le \left\| \underline{\psi}_x^T(0) \Phi^T(t) \right\| \left\| \int_{-\tau}^{0} \underline{b}(t,\theta) d\theta \right| \\ &\le \left\| \underline{\psi}_x^T(0) \right\| \left\| \Phi^T(t) \right\| \left\| \int_{-\tau}^{0} \underline{b}(t,\theta) \right\| d\theta \end{aligned} \quad (16)$$

and equation (16) can be written as:

$$\begin{aligned} \underline{x}^T(t)\underline{x}(t) &= \underline{\psi}_x^T(0) \cdot \Phi^T(t) \cdot \Phi(t) \cdot \underline{\psi}_x(0) + 2 \cdot \left\| \underline{\psi}_x^T(0) \right\| \cdot \left\| \Phi^T(t) \right\| \cdot \\ &\cdot \int_{-\tau}^{0} \left\| \Phi(t-\theta-\tau) \right\| \left\| A_1 \right\| \left\| \underline{\psi}_x(\theta) \right\| \cdot d\theta + \left\| \int_{-\tau}^{0} \underline{b}(t,\theta) d\theta \right| \end{aligned} \quad (17)$$

or:

$$\begin{aligned} \underline{x}^T(t)\underline{x}(t) &= \underline{\psi}_x^T(0) \cdot \Phi^T(t) \cdot \Phi(t) \cdot \underline{\psi}_x(0) + 2 \cdot \left\| \underline{\psi}_x^T(0) \right\| \cdot \left\| \Phi^T(t) \right\| \cdot \\ &\cdot \int_{-\tau}^{0} \left\| \Phi(t-\theta-\tau) \right\| \left\| A_1 \right\| \left\| \underline{\psi}_x(\theta) \right\| \cdot d\theta + \left[\int_{-\tau}^{0} \left\| \Phi(t-\theta-\tau) \right\| \left\| A_1 \right\| \left\| \underline{\psi}_x(\theta) \right\| \cdot d\theta \right]^2 \end{aligned} \quad (18)$$

If we use the well known relation:

$$m(t) \le \left\| \Phi(t-\theta-\tau) \right\| \cdot \left\| \underline{\psi}_x(\theta) \right\| \le M(t), \forall \theta \in [-\tau, 0] \quad (19)$$

then it yields:

$$m(t) \cdot \tau \le \left\| \Phi(t-\theta-\tau) \right\| \cdot \left\| \underline{\psi}_x(\theta) \right\| \le M(t) \cdot \tau \quad (20)$$

It is possible to show that it yields:

$$\left\| \Phi(t-\theta-\tau) \right\|_{\theta \in [-\tau,0]} \le \left\| \Phi(t) \right\|, \left\| \underline{\psi}_x(\theta) \right\|_{\theta \in [-\tau,0]} < \sqrt{\alpha} \quad (21)$$

and:

$$\left\| \underline{\psi}_x(0) \right\| < \sqrt{\alpha}, \left\| \Phi^T(t) \right\| = \left\| \Phi(t) \right\| \quad (22)$$

so the equation (18) can be shown as:

$$\begin{aligned} \underline{x}^T(t) \cdot \underline{x}(t) &\le \left\| \Phi(t) \right\|^2 \underline{\psi}_x^T(0) \underline{\psi}_x(0) + 2 \cdot \left\| \underline{\psi}_x^T(0) \right\| \cdot \left\| \Phi^T(t) \right\| \cdot \left\| A_1 \right\| \cdot \tau \cdot \sqrt{\alpha} \\ &+ \left\| \Phi^T(t) \right\|^2 \cdot \left\| A_1 \right\|^2 \cdot \tau^2 \cdot \alpha \end{aligned} \quad (23)$$

and if we use the well-known inequality, it is given:

$$\left\| \Phi(t) \right\| = \left\| \exp\left[A_0(t) \right] \right\| \le \exp\left\{ \mu(A_0) \cdot t \right\} \quad (24)$$

where μ is defined as:

$$\mu(A_0) = \frac{1}{2} \cdot \lambda_{\max}(A^T + A) \tag{25}$$

and if we use the following inequality:

$$\underline{\psi}_x^T(0) \cdot \underline{\psi}_x(0) < \alpha\left(\left\|\underline{\psi}_x^T(0)\right\| = \left\|\underline{\psi}_x(0)\right\| < \sqrt{\alpha}\right) \tag{26}$$

then it yields:

$$\begin{aligned}\underline{x}^T(t) \cdot \underline{x}(t) \le e^{2\mu(A_0)\cdot t} \cdot \alpha + 2 \cdot e^{2\mu(A_0)\cdot t}\left\|A_1\right\| \cdot \tau \cdot \alpha \\ + 2 \cdot e^{2\mu(A_0)\cdot t}\left\|A_1\right\|^2 \cdot \tau^2 \cdot \alpha = e^{2\mu(A_0)\cdot t}\alpha\left(1 + \tau\left\|A_1\right\|\right)^2\end{aligned} \tag{27}$$

If we apply the theorem basic condition given by equation (5) to the previous inequality, then it is obtained:

$$\underline{x}^T(t) \cdot \underline{x}(t) < \left(\frac{\sqrt{\beta/\alpha}}{1 + \tau \cdot \left\|A_1\right\|}\right) \cdot \alpha\left(1 + \tau \cdot \left\|A_1\right\|\right)^2 < \beta \tag{28}$$

and thus the proof is complete.

Theorem 2: Time delay system (1) with the function of initial state (2) is stable on finite time interval in relation with [α,β, τ, *T*, $\mu_2(A_0) \neq 0$], if the following conditions are satisfied:

$$\text{a)}\ \ \mathrm{Re}\left[\lambda_i(A + A_1 \cdot e^{-s\cdot\tau})\right] < 0 \ \ i = 1, \text{É}\ , n \tag{29}$$

$$\text{B)}\ \ e^{\mu_2(A_0)\cdot t} < \frac{\beta/\alpha}{1 + \mu_2^{-1}(A_0) \cdot \left\|A_1\right\|_2 \cdot \left(1 - e^{-\mu_2(A_0)\cdot\tau}\right)}, \forall t \in [0, T] \tag{30}$$

In Tissir *et al.* (1996) the proof of condition a is given.

Theorem 3: Time delay system (1) with the function of initial state (2), is stable on finite time interval in relation with [α, β, τ, *T*], if condition a) of theorem 2 is satisfied, and if the following condition is satisfied:

$$1 + t \cdot \left\|A_1\right\|_2 < \beta/\alpha, \ \ \forall t \in [0, \tau] \tag{31}$$

Proof: It yields from theorem 2 when $\mu_2(A_0) = 0$.

4. Definitions and Conditions of Practical Stability

Let us consider the first order hyperbolic distributed parameter system which is decribed by the following state-space equation:

$$\frac{\partial \underline{x}(t,z)}{\partial t} = A_0 \cdot \underline{x}(t,z) + A_1 \frac{\partial \underline{x}}{\partial z} \tag{32}$$

with an appropriate function of initial state:

$$\begin{aligned}&\underline{x}_0(t,z) = \underline{\psi}_x(t,z) \\ &0 \le t \le \tau,\ 0 \le t \le \zeta\end{aligned} \tag{33}$$

where $\underline{x}(t,z)$ is n-component real vector of system state, A is the matrix appropriate dimension, t is time and z is the space coordinate.

Definition 1: The distributed parameter system described by equation (32) that satisfies the initial condition (33) is stable on finite time interval in relation to [ξ(*t,z*), β, *T*, *Z*] if and only if:

$$\begin{aligned}&\underline{\psi}_x^T(t,z) \cdot \underline{\psi}_x(t,z) < \xi(t,z) \\ &\forall t \in [0,\tau],\ \forall z \in [0,\varsigma]\end{aligned} \tag{34}$$

then it follows:

$$\begin{aligned}&\underline{x}^T(t,z)\big) \cdot \underline{x}(t,z) < \beta \\ &\forall t \in [0,T],\ \forall z \in [0,Z]\end{aligned} \tag{35}$$

where ξ(*t,z*) is the scalar function with feature $0 < \xi(t,z) \le \alpha$, $0 \le t \le \tau$, $0 \le z \le \zeta$ where α is a real number, $\beta \in R$ and $\beta > \alpha$.

Let us calculate the fundamental matrix for this class of system:

$$\frac{d\Phi(s,\sigma)}{d\sigma} = A_1 \cdot (sI - A) \cdot \Phi(s,\sigma) \tag{36}$$

where after double Laplace transformation and necessary approximation it yields:

$$\Phi(t,z) = \exp(A \cdot t \cdot z) \tag{37}$$

where $A = \dfrac{I - A_0 \cdot A_1}{A_1}$.

Theorem4: The distributed parameter system described by equation (32) that satisfies the internal condition (33) is stable on finite time interval in relation to [ξ(*t,z*), β, *T*, *Z*] if and only if the following condition is satisfied:

$$e^{2\mu(A)\cdot t\cdot z} < \frac{\beta}{\alpha} \tag{38}$$

Proof: The solution of equation (32) with the initial condition (33) can be described as:

$$\underline{x}(t,z) = \Phi(t,z) \cdot \underline{\psi}(0,0) \tag{39}$$

Using the above equation it follows:

$$\begin{aligned}\underline{x}^T(t,z) \cdot \underline{x}^T(t,z) = \left[\underline{\psi}_x^T(0,0) \cdot \Phi(t,z)\right] \cdot \\ \left[\underline{\psi}_x^T(0,0) \cdot \Phi(t,z)\right]\end{aligned} \tag{40}$$

Using the well-known ineqality:

$$\left\|\Phi(t,z)\right\| = \left\|\exp[A \cdot t \cdot z]\right\| \le \exp\left\{\mu(A) \cdot t \cdot z\right\} \tag{41}$$

and taking into account that:

$$\begin{aligned}&\underline{\psi}_x^T(0,0) \cdot \underline{\psi}_x(0,0) < \alpha \\ &\left(\left\|\underline{\psi}_x^T(0,0)\right\| = \left\|\underline{\psi}_x^T(0,0)\right\| < \alpha\right)\end{aligned} \tag{42}$$

then it follows:

$$\underline{x}^T(t,z)\cdot\underline{x}(t,z)\le e^{2\mu(A\cdot t\cdot z)}\cdot\alpha \tag{43}$$

Applying the basic condition of theorem 1 by using equation (38) to further inequality the following is obtained, Dihovicni *et al.* [4]:

$$\underline{x}^T(t,z)\cdot\underline{x}(t,z)<\left(\frac{\beta}{\alpha}\right)\cdot\alpha<\beta \tag{44}$$

Theorem 5: The distributed parameter system described by equation (32) that satisfied the initial condition (33) is stable on finite time interval in relation to [$\xi(t,z)$, β, T, Z] if the following condition is satisfied:

$$e^{\mu(A)\cdot t\cdot z}<\frac{\sqrt{\beta/\alpha}}{1+\tau\cdot\zeta\|A\|}$$
$$\forall t\in[0,\tau],\ \forall z\in[0,\varsigma] \tag{45}$$

The proof of this theorem is given in Dihovicni *et al.* [3].

Let $|\underline{x}|_{(\cdot)}$ be any vector norm and any matrix norm $\|\cdot\|_2$ which originated from this vector. Following expresions are used:

$$|\underline{x}|_2=(\underline{x}^T\cdot\underline{x})^{1/2}\ \text{ and }\ \|\cdot\|_2=\lambda_{\max}{}^{1/2}(A^*\cdot A)$$

where * and T are transpose-conjugate and transport matrixes.

It is important to define the matrix measure as:

$$\mu(A)=\lim_{\varepsilon\to 0}\frac{\|1+\varepsilon\cdot A\|-1}{\varepsilon} \tag{46}$$

$$\mu_1(A)=\max\left(\mathrm{Re}(a_{kk})+\sum_{i=1,i\neq k}^{n}|a_{ik}|\right)$$
$$\mu_2(A)=\frac{1}{2}\max\lambda_i(A^T+A) \tag{47}$$
$$\mu_\infty(A)=\max\left(\mathrm{Re}(a_{ii})+\sum_{k=1}^{n}|a_{ki}|\right)$$

Definition 2: The distributed parameter system described by equation (32) that satisfies the initial condition (33) is stable on finite time interval in relation to [$\xi(t,z)$, β, T, Z] if and only if, Dihovicni *et al.* [3]:

$$|\underline{\psi}_x(t,z)|<\xi(t,z) \tag{48}$$

then it follows:

$$|\underline{x}(t)|_2<\beta \tag{49}$$

where $\xi(t,z)$ is scalar function with feature $0<\xi(t,z)\le\alpha$, $0\le t\le\tau$, $0\le z\le\zeta$) α is real number, $\beta\in R$ and $\beta>\alpha$.

Theorem 6: The distributed parameter system described by equation (32) that satisfies the initial condition (33) is stable on finite time interval in relation to [α, β, T, Z] if and only if the following condition is satisfied:

$$e^{\mu_2(A)\cdot t\cdot z}<\frac{\sqrt{\beta/\alpha}}{1+\mu^{-1}{}_2(A)}$$
$$\forall t\in[0,T],\ \forall z\in[0,Z] \tag{50}$$

Proof: The solution of equation (1) with the initial condition (2) can be described by the fundamental matrix as:

$$\underline{x}(t,z)=\Phi(t,z)\cdot\underline{\psi}_x(0,0) \tag{51}$$

Using the norms of the left and right side of the equation (51) it follows:

$$\underline{x}^T(t,z)\cdot\underline{x}(t,z)\le e^{2\mu(A\cdot t\cdot z)}\cdot\alpha \tag{52}$$

and using the well-known inequality:

$$\|\exp(A\cdot t\cdot z)\|_2\le\exp\{\mu(A\cdot t\cdot z)\} \tag{53}$$
$$t\ge 0,\ \ z\ge 0$$

it follows:

$$|\underline{x}(t,z)|_2\le e^{\mu_2(A)\cdot t\cdot z}|\underline{\psi}_x(0,0)|_2 \tag{54}$$

and using equation (49) the following is obtained:

$$|\underline{x}(t,z)|_2\le\alpha\cdot e^{\mu_2(A)\cdot t\cdot z} \tag{55}$$

so finally the following is obtained:

$$|\underline{x}(t,z)|_2\le\alpha\cdot e^{\mu_2(A)\cdot t\cdot z}\{1+\mu_2{}^{-1}(a)\} \tag{56}$$

Applying the basic condition of theorem 3 by using equation (50) the following is obtained:

$$|\underline{x}(t)|_2<\beta \tag{57}$$

$$\forall t\in[0,T],\ \forall z\in[0,Z] \tag{58}$$

Theorem 7: The distributed parameter system described by equation (32) that satisfies the initial condition (33) is stable on finite time interval in relation to [α, β, T, Z], if and only if the following condition is satisfied, Dihovicni *et al.* [3]:

$$e^{\mu(A\cdot t\cdot z)}<\frac{\beta}{\alpha}$$
$$\forall t\in[0,T],\ \forall z\in[0,Z] \tag{59}$$

Theorem 8: The distributed parameter system described by equation (1) that satisfies the initial condition (2) is stable on finite time interval in relation to [t_0, J, α, β, Z], if and only if the following condition is satisfied:

$$\left[1+(t-t_0)\cdot\sigma_{\max}\right]^2\cdot e^{2(t-t_0)\cdot z\cdot\sigma_{\max}}<\frac{\beta}{\alpha},\quad \forall t\in[0,J],\ \forall z\in[0,Z] \tag{60}$$

where σ_{max} represents the maximum singular value of matrix. The proof of this theorem is given in Dihovicni et al. [4].

5. Example

Consider the distributed parameter system:

$$\frac{\partial \underline{x}(t,z)}{\partial t}=\begin{bmatrix}2 & 1\\ -2 & 4\end{bmatrix}\frac{\partial \underline{x}}{\partial z}+\begin{bmatrix}1 & 0\\ 2 & -1\end{bmatrix}\underline{x}(t,z) \tag{61}$$

where

$$A_0=\begin{bmatrix}1 & 0\\ 2 & -1\end{bmatrix},\ A_1=\begin{bmatrix}2 & 1\\ -2 & 4\end{bmatrix} \tag{62}$$

and according to equation (47) it is obtained:

$$A=\begin{bmatrix}0.548 & 0.904\\ 0.1653 & 3.320\end{bmatrix} \tag{63}$$

with the initial condition:

$$\underline{x}_0(t,z)=\underline{\psi}_x(t)=\begin{bmatrix}0 & 1\end{bmatrix}^T \tag{64}$$

Let us assume the following values:

$$\alpha=2.0;\ \beta=60.22;\ \kappa_{est}=0.7s \tag{65}$$

where $\kappa = t\cdot z$, and by using initial condition

$$\left\|\underline{\psi}_x\right\|^2=1<2.01 \tag{66}$$

Let us calculate the matrix measure μ and the norm:

$$\mu(A)=3.37,\quad \|A\|=3.45 \tag{67}$$

Combining this values into equation (7), it yields:

$$e^{2\cdot t\cdot z}<29.96,\quad \forall t\in[0,T],\ z\in[0,1] \tag{68}$$

with solution:

$$\kappa_{est}=1.69s \tag{69}$$

Upon theorem 5 it yields:

$$e^{t\cdot s}<1.23,\quad \forall t\in[0,T],\ z\in[0,1] \tag{70}$$

with solution:

$$\kappa_{est}=0.207s \tag{71}$$

Using theorem 6 it follows:

$$e^{t\cdot s}<23.31 \tag{72}$$

whose solution is:

$$\kappa_{est}=3.14s \tag{73}$$

Upon theorem 7 it yields:

$$e^{t\cdot s}<29.96 \tag{74}$$

and solution is:

$$\kappa_{est}=3.39s \tag{75}$$

If we use theorem 5 then it is obtained:

$$\left[1+3.45t\right]^2\cdot e^{2\cdot 3.45\cdot t\cdot z}<29.96 \tag{76}$$

with solution:

$$\kappa_{est}=0.06s \tag{77}$$

Analysing the values for estimation it is obvious that the best result is obtained using theorem 5.

6. Conclusion

During the analyse the process systems from safety and optimal cost perspective, it is important to recognize which systems are not stable in real conditions. From engineering point of view we are interested in such systems which are stable in finite periods of time. Therefore, our first concern should be to maintain stable and safe systems.

Taking into account the principle of practical stability, the following conditions must be satisfied:

- determine the set $S_{\beta-}$ find the borders for the system motion;
- determine the set $S_{\varepsilon-}$ find maximum amplitudes of possible disturbance;
- determine the set S_{α} of all initial state values.

In case that these conditions are regularly determined it is possible to analyse the system stability from a practical stability view point.

The main conclusion from the result for distributed parameter systems is that the estimated interval which is determined by previously explained theorems and which represents the product of tz for this class of distributed parameter systems is very near to the real value. Therefore, the theory is applicable and has a widespread use in determination where the system is stable.

References

[1] TOKASHIKI, L.R, FUJITA, T., KAGAWA, T., PAN, W.: *Dynamic Characteristics of Pneumatic Cylinders Including Pipes,* 9th Bath Int'lFluid Power Workshop, 1996, pp 1-14.

[2] DIHOVICNI, N. DJ., NEDIC, N.: *Stability of Distributed Parameter Systems on Finite Space Interval,* 32end Yupiter Conference, Zlatibor, 2006, pp 306-312.

[3] DIHOVICNI, N.DJ., NEDIC, N.: *Stability of Distributed Parameter Systems on Finite Space Interval described by cubic equations,* 32-end Yupiter Conference, Zlatibor, 2006, pp 321-325.

[4] DIHOVICNI, N.DJ., NEDIC, N.: Practical Stability of Linear Systems with Delay in State, *AMSE*, Association for the Advancement of Modelling & Simulation Techniques in Enterprises, Tassin La-Demi-Lune, France, Vol. 62, No. 2, 2007, pp 98–104.

[5] NOVAKOVIC, B.: Control Methods of Technical System, *Skolska knjiga,* Zagreb 1989.

[6] ERNAT, J., GILLES, D.: *A Systeme mit Verteilten Parametern, (Book style),* Wien 1973.

[7] BROWN, F.T.: The Transient Response of Fluid Lines, *J. of Basic Engineering,* Trans of ASME, Series D, 84-4, 547/553, 1962.

[8] KAGAWA, T., FUJITA, T., TAKEUCHI, M.: *Dynamic Response and Simulation Model of Pneumatic Pipe Systems,* Proc. of 7th Bath International Fluid Power Workshop, 1994.

Vladislav Krivda *

VIDEO-ANALYSIS OF CONFLICT SITUATIONS ON SELECTED ROUNDABOUTS IN THE CZECH REPUBLIC

The paper deals with video-analysis of conflict situations in road traffic and presents results of researches which were performed on selected roundabouts in the Czech Republic. This article refers to suitability of usage video-recording to analysis of behavior of participants of road traffic and also to monitoring of the danger places on the roundabouts. There are results of analyses which were performed in 2010 and also comparative analysis of conflict situations and possible traffic accidents.

Keywords: Conflict Situation, Roundabout, Road Transport

1. Introduction

Road safety is the current focus of public debate. Dangerous places on the road are still a lot and any modification to increase safety is welcomed. Traffic designer can never deem his traffic solution as absolutely safe. And just the video-analysis of conflict situations can help designer, for example, to design reconstruction of some intersection with a lot of traffic accidents. Some dangerous hidden factors (which occur on the intersections) can be detected early and the designer can avoid his possible mistakes.

The usage of video-recording is very substantial and advantageous. It can be analyzed collectively and repeatedly. Disturbing influences of the road traffic (e.g. noise, dust etc.) and weather (e.g. temperature, wind, rain, etc.) are eliminated.

And what does the term "Conflict situation" mean? Conflict situation is a moment or a situation in road traffic when participants of road traffic are or can be endangered by other participants. The conflict situation predates every traffic accident. Every conflict situation is described by the symbol which includes description of participants of conflict situation, source of conflict situation and seriousness of conflict situation [1] – [3].

2. Selection of roundabouts for analysis of conflict situations

The video-recordings of traffic were made within the project [4] on selected roundabouts in the Czech Republic:

- Dukelska – Jeremenkova – Premyslovcu, Novy Jicin (NJ1),
- Premyslovcu – Sokolovska – Palackeho, Novy Jicin (NJ2),
- Sokolovska – Msgr. Sramka – Stefanikova, Novy Jicin (NJ3),
- Sokolovska – Bezrucova – Zborovska – gen. Hlado, Novy Jicin (NJ4),
- Zborovska – Machova – Karla Kryla, Novy Jicin (NJ5),
- Masarykova – parking Tesco, Valasske Mezirici (VM1),
- Masarykova – Hulince – Hrbitovni, Valasske Mezirici (VM3),
- Masarykova – Roznovska – Nadrazni, Valasske Mezirici (VM4),
- Masarykova – Zasovska – Vsetínska – Krizna, Valasske Mezirici (VM5),
- Vsetinska – Zerotinova – Sokolska, Valasske Mezirici (VM6),
- Ostravska – Zeleznicaru – U Nadrazi – Orlovska – Hl. trida – U Motelu, Havirov (HAV1),
- Zeleznicaru – U Nadrazi, Havirov (HAV2),
- Beskydska – parking Tesco, Frydek-Mistek (FM),
- Sokolska – 30. dubna, Ostrava (OV),
- Havlickova – Polepska – Jaselska – U Krizovatky – Dukelskych hrdinu, Kolin (KOL),
- Rysaveho – Pod Chodovem – Roztylska – U Kunratickeho lesa, Prague (PHA).

The roundabouts HAV1, FM and PHA are double-lane roundabouts and the others are single-lane roundabouts. The roundabouts NJ1 and VM1 have three legs, the roundabout KOL has five legs, the roundabout HAV1 has six legs and the others have four legs.

3. Video-Analysis of Conflict Situations

The volumes of traffic flows and their directions were detected from each recording. Video-analyses of conflict situations were performed using a methodology of the Folprecht's video-analysis of conflict situations [1].

* **Vladislav Krivda**
Department of Transport Constructions, Faculty of Civil Engineering, VSB – Technical University of Ostrava, Ostrava-Poruba, Czech Republic, E-mail: vladislav.krivda@vsb.cz

Every conflict situation is described by the symbol which includes three parts:
- one number – description of participants of conflict situation, e.g. *1* = pedestrian, *2* = car, *4* = pedestrian and car, *6* = two or more cars, *9* = other (one cyclist, cyclist and car etc.) [1],
- one or more letters – description of source of conflict situation, e.g. *n* = violation of rule "yield to ...", f_p = influence of pedestrian crossing, f_k = influence of near intersection, j_c = wrong ride of cyclist, *a* = aggression, *g* = giving priority against rule, *o* = restriction or danger in driving during change of the lane or during exiting the roundabout, *D* = danger of rear-end collision, j_o = wrong way of drive (very near curb) etc. [2], [3] (more see Chapter 4 or Tab. 4),
- one number (1 – 4) – description of seriousness of conflict situation.

The seriousness of conflict situation is described as follows [1]:
- the 1st level – potential conflict situations,
- the 2nd level – conflict situations when one or more participants are restricted,
- the 3rd level – conflict situations when one or more participants are endangered,
- the 4th level – traffic accident.

For example the symbol *6a3* means aggression (*a*) between two drivers of cars (*6*) and 3rd level of seriousness (*3*) – details see below or [1] – [3].

The resulting number of conflict situations was recalculated to coefficient of relative conflictness c_R:

$$c_R = \frac{N_{CS}}{V} \cdot 100 \quad [CS/100\ veh]$$

where:
N_{CS} – number of conflict situations (CS) per hour [CS/h]
V – hour traffic volume [veh/h]

The coefficient c_R is usually determined only for the conflict situations between two (or more) participants of road traffic.

We also distinguish several kinds of conflict situations (details see [1] – [3]):
- "own" conflict situation – a conflict situation which is related to traffic on the roundabout, its construction etc.,
- "non-own" conflict situation – a conflict situation which is influenced by other conflict situation in the vicinity (for example, on other intersection),
- "primary" conflict situation – a conflict situation which isn't caused by other conflict situation,
- "secondary" conflict situation – a conflict situation which is caused by other conflict situation.

Some video-recordings of conflict situations (WMV format) are on this web page: https://sites.google.com/site/krivda0ks/video-analyzy (in Czech). The list of selected conflict situations is in Tab. 1 – 3.

4. Conflict Situations (CS) versus Traffic Accidents (TA)

Some important conflict situations are described below, including considerations about the type of traffic accident, which can be caused by conflict situation. We distinguish several kinds of traffic accidents [4], [5]:
- crash with moving vehicle (head-on, side or rear-end collision),
- crash with parked vehicle,
- crash with obstacle (tree, traffic sign, crash barrier, curb, wall etc.),
- crash with pedestrian, tram etc.

The most important conflict situations (identified from video-analysis on the roundabouts):
- Violation of rule "yield to ..." (conflict situation *6n2* or *6n3*) – the conflict situation, when a vehicle entering the roundabout doesn't

The list of selected conflict situations on roundabouts in Novy Jicin (N_{CS} [CS/h], V [veh/h], c_R [CS/100 veh]) Tab. 1

Conflict situation*	NJ1		NJ2		NJ3		NJ4		NJ5	
	N_{CS}	c_R	N_{CS}	c_R	N_{CS}	c_R	N_{CS}	c_R	N_{CS}	c_R
9jc1	3	0.19	5	0.33	10	0.61	1	0.05	6	0.55
6f$_k$2	6	0.40								
6n2,6n3...	5	0.32			3	0.18	8	0.42	6	0.55
4f$_p$2	4	0.26	21	1.39	16	0.98	42	2,18	14	1.28
6g2	2	0.13	1	0.07			2	0.10	1	0.09
6D3	1	0.06	3	0.20	1	0.06	4	0.21	3	0.27
9jc2					4	0.25			1	0.09
6a2,6a3...							5	0.26		
V	**1547**		**1506**		**1630**		**1926**		**1094**	
c_R	**0.96**		**2.13**		**1.59**		**3.47**		**2.91**	

*) see above (or Chapter 4 and Tab. 4)

The list of selected conflict situations on roundabouts in Valasske Mezirici (N_{CS} [CS/h], V [veh/h], c_R [CS/100 veh]) Tab. 2

Conflict situation*	VM1		VM3		VM4		VM5		VM6	
	N_{CS}	c_R	N_{CS}	c_R	N_{CS}	c_R	N_{CS}	c_R	N_{CS}	c_R
9jc1			3	0.18	1	0.05	12	0.62	3	0.14
2jo1	23	1.78								
6f$_k$2	5	0.39								
6n2 ...			6	0.36	14	0.65	13	0.67	8	0.37
6n3 ...			4	0.24	3	0.14	3	0.15	4	0.19
4f$_p$2	1	0.08			5	0.23	12	0.62	45	2.13
6g2			2	0.12	2	0.09	7	0.36	5	0.24
6D3							2	0.10		
9jc2, 9jc3					1	0.05	3	0.15	2	0.09
V	**1290**		**1648**		**2141**		**1942**		**2115**	
c_R	**2.41**		**0.90**		**1.16**		**2.30**		**3.13**	

*) see above (or Chapter 4 and Tab. 4)

The list of selected conflict situations on the other roundabouts (N_{CS} [CS/h], V [veh/h], c_R [CS/100 veh]) Tab. 3

Conflict situation*	HAV1		HAV2		FM		OV		KOL		PHA	
	N_{CS}	c_R	N_{CS}	c_R	N_{CS}	c_R	N_{CS}	c_R	N_{CS}	c_R	N_{CS}	c_R
9jc1							1	0.06	5	0.18		
6fk2			14	0.85			10	0.63				
6n2,6n3...	10	0.27	4	0.24	12	0.43	1	0.06	28	1.03	6	0.21
4fp2	1	0.03	4	0.24			26	1.64	23	0.84		
6g2	19	0.51	11	0.67			3	0.19	10	0.37		
6D3					1	0.04			4	0.15		
9jc2			1	0.06			1	0.06				
6a2,6a3...	17	0.45					5	0.31	4	0.15	1	0.03
6o2,6o3...	11	0.30			16	0.58					2	0.07
6D4	1	0.03										
V	**3747**		**1648**		**2762**		**1590**		**2722**		**2884**	
c_R	**1.89**		**2.18**		**1.05**		**4.97**		**3.19**		**0.55**	

*) see above (or Chapter 4 and Tab. 4)

yield to a vehicle on circulating roadway. The situations 6n2 (or 6n3) occurred on all monitored roundabouts, especially on roundabouts VM4, VM5, HAV1, FM and KOL. This conflict situation can cause traffic accident of type "crash with moving vehicle (side collision)" (cause: against "YIELD TO").

- Stopping or decelerating of traffic on circulating roadway due to queue of vehicles before pedestrian crossing (conflict situation 4f_p2) – the pedestrian crossing near roundabout can cause a queue of vehicles which extends to circulating roadway. The traffic on roundabout is stopped or decelerated. Some vehicles go round the stopped vehicles using the truck apron (the truck apron or the curb of the central island can be damaged – see Fig. 1). This situation occurred on roundabouts VM4 and VM5 and especially on roundabout VM6. This conflict situation can cause traffic accident of type "crash with moving vehicle (rear-end collision)".
- Stopping or decelerating of traffic on circulating roadway due to queue of vehicles on other near intersection (conflict situation 4f_k2) – the other intersection (which is relatively near roundabout; usually other roundabout or intersection with traffic lights) can also cause a queue of vehicles which extends to circulating roadway. The traffic on roundabout is stopped or decelerated. This situation occurred on roundabouts NJ1, VM1 and HAV2 (near intersection is also roundabout) and on roundabout OV (near intersection is intersection with traffic lights). This conflict situation can also cause traffic accident of type "crash with moving vehicle (rear-end collision)".
- Wrong ride of cyclist on circulating roadway (conflict situation *9jc1* or *9jc2*) – the conflict situation, when a cyclist doesn't ride on the right side of the circulating roadway (but on center or the left side of the circulating roadway or even on the truck apron). The situations 9jc1 or 9jc2 occurred on roundabouts VM5 and

Fig. 1 Damaged truck apron and curb of the central island

NJ3. This conflict situation can cause traffic accident of type "crash with moving vehicle (rear-end collision)" or "crash with moving vehicle (side collision)".

- Giving priority against rule (conflict situation *6g2*) – the conflict situation, when a vehicle on circulating roadway yields to a vehicle entering the roundabout (against rule). The driver of vehicle on circulating roadway stops or decelerates and yields to vehicle on entry. The driver entering the roundabout needn't understand it, he starts to behave chaotically (slowly to drive on, to stop etc.). The vehicles can suddenly pull away together and crash. This situation occurred on all monitored roundabouts, especially on roundabouts HAV1, HAV2 and KOL. This conflict situation can cause traffic accident of type "crash with moving vehicle (side collision)" (cause: against "YIELD TO"). However, this conflict situation can also cause traffic accident of type "crash with moving vehicle (rear-end collision)" in a queue of vehicles entering the roundabout.
- Aggression (conflict situation *6a2* or *6a3*) – there is a lot of aggressive behavior on the roundabout, for example overtaking a queue of vehicles entering the roundabout. This situation occurred on roundabout with wide single-lane entries and especially on roundabout HAV1. This conflict situation can cause traffic accident of type "crash with moving vehicle (side collision)".
- Wrong way of drive – very close to the curb (conflict situation $2j_o1$) – the conflict situation, when a vehicle (usually truck) exiting the roundabout goes very close to the right curb (the curb can be damaged – see Fig. 2). This conflict situation can cause traffic accident of type "crash with obstacle (curb)".

Fig. 2 Damaged right curb (roundabout VM1)

- Restriction or danger in driving during change of the lane or during exiting the roundabout (conflict situations *6o2, 6o3* etc. – see Figs. 3 and 4). These conflict situations usually occur on double-lane roundabouts and can cause traffic accident of type "crash with moving vehicle (side collision)" (cause: "change of the lane").

Exiting the roundabout is very problematical especially on multi-lane roundabouts. Two accidents happened on monitored roundabouts. The first one happened on roundabout FM immediately before our measuring. The driver of the vehicle in the left lane wanted to exit roundabout, but the driver of the vehicle in the right lane wanted to move on the circulating roadway. This conflict situation (or more exactly the accident) is classified as *6o4* (see Figs. 4 or 5).

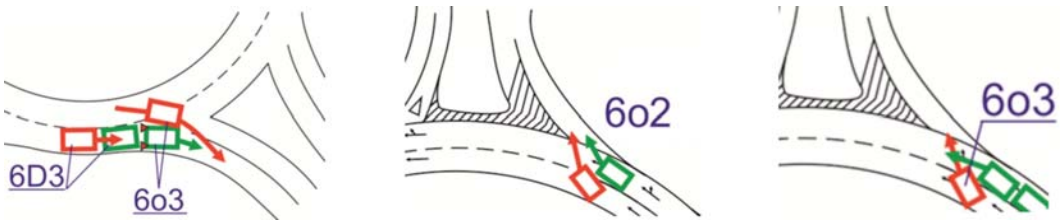

Fig. 3 Some conflict situations of type 6o2, 6o3 (red car restricted or endangered green car)

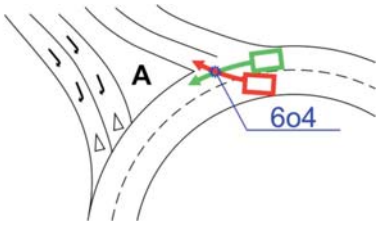

Fig. 4 Scheme of traffic accident 6o4

Fig. 5 Traffic accident 6o4

The second accident happened on roundabout HAV1 during our measuring (see Figs. 6 or 7). The vehicle *Veh1* on the circulating roadway crashed into the vehicle *Veh2* rear-end (conflict situation *6D4* – see Fig. 6). This accident was caused by previous "primary" conflict situation (*6o3* – see Fig. 6), when other vehicle had dangerously left the roundabout.

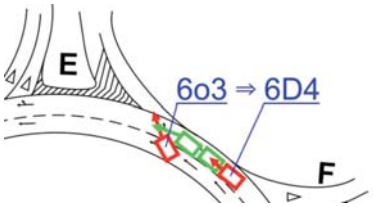

Fig. 6 Scheme of traffic accident 6D4

Fig. 7 Traffic accident 6D4

5. Conclusions

The most important monitored conflict situations are in Tab. 4. There are also types of traffic accidents which can be caused by the conflict situations.

The list of selected conflict situations and traffic accidents — Tab. 4

Conflict situation ==>	==> Traffic accident
6n2, 6n3 – Violation of rule "yield to ..."	"Crash with moving vehicle (side collision)" (cause: against "YIELD TO")
4f_p2 – Stopping or decelerating of traffic on circulating roadway due to queue of vehicles before pedestrian crossing	"Crash with moving vehicle (rear-end collision)"
6f_k2 – Stopping or decelerating of traffic on circulating roadway due to queue of vehicles on other near intersection ("non-own" conflict situation)	"Crash with moving vehicle (rear-end collision)"
9jc1, 9jc2 – Wrong ride of cyclist on circulating roadway	"Crash with moving vehicle (rear-end collision)" or "Crash with moving vehicle (side collision)"
6a2, 6a3 – Aggression	"Crash with moving vehicle (side collision)" or the others
2j_o1 – Wrong way of drive – very near curb	"Crash with obstacle (curb)"
6g2 – Giving priority against rule	"Crash with moving vehicle (side collision)" (cause: against "YIELD TO") or "Crash with moving vehicle (rear-end collision)"
6o2, 6o3 etc. – Restriction or danger in driving during change of the lane or during exiting the roundabout (see Figs. 3 and 4)	"Crash with moving vehicle (side collision)" (cause: "change of the lane")

These traffic accidents (see Tab. 4) are also the most frequent traffic accidents on the monitored roundabouts (see [4] or [5]). We can certify that we can make a prediction of number of traffic accidents (and their kinds) by the video-analysis of conflict situations. On the basis of this video-analysis the transport designer can make necessary adjustments of the roundabouts, which can lead to increase of traffic safety.

Some conflict situations (e.g. 6n2, 6a2 etc.) occur on all types of roundabouts, but on the other hand some situations occur only on some roundabouts. For example situations 6o2 or 6o3 (see Fig. 3) occur only on multilane roundabouts. At present this type of roundabouts is usually superseded by turbo roundabouts which certainly cause other conflict situations (due to difficult orientation of the drivers). Conflict situations 4f_p2, 9jc2 or 6f_k2 usually occur on urban roundabouts where there are a lot of pedestrians, cyclists and the intersections are close to each other. It's also necessary to realize that some conflict situations (e.g. 6g2) can cause the other secondary situations (e.g. 6D3) which can result in traffic accident (6D4).

The video-analysis is very good device to analysis of such conflict situations as $2j_o1$. Precise description position and source of this conflict situation can be a great inspiration for traffic designer to design reconstruction of monitored intersection.

In conclusion:

1. The usage of video-recording for analysis of conflict situations is very substantial and advantageous (above all, for possibility of repetition). It is an efficient device on the one hand for analysis of behavior of drivers, pedestrians etc. and on the other hand for monitoring of danger places on the roads, intersections etc.
2. Each modification (although with good intention) can cause the other problems (often more dangerous)!

This article is the result of the project implementation "The influence of structural elements geometry on the safety and fluency of operation in roundabouts and possibility of rise crashes prediction" (CG911-008-910 supported by the Ministry of Transport in the Czech Republic) [4].

References

[1] FOLPRECHT, J., KRIVDA, V.: *Traffic Organization and Control I (in Czech),* Ostrava : VSB-TU Ostrava, 2006. ISBN 80-248-1030-1.

[2] KRIVDA, V.: *Assessment of Effectiveness of Roundabouts (in Czech),* PhD Thesis, Ostrava : VSB-TU Ostrava, 2003. ISBN 80-248-0207-4.

[3] KRIVDA, V.: *New Findings in the Sphere of the Conflict Situations Analysis on the Czech Republic Road Traffic.* Transactions of the VSB-TU Ostrava, Mechanical Series. Ostrava : VSB-TU Ostrava, pp. 161–169, 2009. ISBN 978-80-248-1633-3, ISSN 1210-0471.

[4] MAHDALOVA, I. et all: *Final Report of Project CG911-008-910 "The Influence of Structural Elements Geometry on the Safety and Fluency of Operation in Roundabouts and Possibility of Rise Crashes Prediction" (in Czech),* Project of the Ministry of Transport, Czech Republic. Ostrava : VSB-TU, Ostrava, 2011.

[5] MAHDALOVA, I., KRIVDA, V.: *Analysis of Traffic Accidents on Roundabouts in the Czech Republic (in Czech),* Pardubice : Perner's Contact, No. I, vol. 5. WWW: <http://pernerscontacts.upce.cz/>, pp. 156–169, 2010. ISSN 1801-674X.

Benedikt Badanik – Milan Stefanik – Martin Matas *

USING FAST-TIME SIMULATIONS FOR DESIGNING AND OPERATING AIRPORT TERMINALS AS NODES OF INTERMODAL TRANSPORT

Ever growing traffic in air transport with associated capacity constraints brings problems to air passenger flows at airports. There is strong link between quality of airport ground access system and airport terminal operations. However, this aspect remains underestimated in the development plans of many airports all over the world, which results in underutilization of both planed and existing infrastructure. In efforts for improvement, the higher level of synchronization and coordination between air and ground transport needs to be achieved. For this purpose, a computer model enabling to simulate passenger flows within airport's catchment area has been developed by the Air Transport Department, University of Zilina. Thanks to this simulation model, it is possible to perform comprehensive operational, economic and environmental assessment of the innovative airport ground access concepts and thus facilitate designing and operating airports as nodes of intermodal transport.

Key words: Passenger flow model; design and operations of airport terminals; fast-time simulations; airport ground access; operational, economic and environmental assessment.

1. Introduction

Due to physical and nuisance constraints the airports have always been built far from the city centres and their operations have always been dependent on the ground transport [2]. As the passenger trip does not start or finish at the airport, the speed that is considered to be the primary advantage of the air transport is being reduced by ground portion of the trip. This fact influences the competitiveness of both airport and air transport especially on short-haul trips. When selecting the transport mode, the total time of transportation 'from door to door' is one of the most important decisive factors for passenger. The attractiveness of the airport and air transport at the same time significantly decreases if the time of access by surface transport exceeds a certain maximum time. For short haul trips this should not exceed 30 minutes, while two hours or more might be acceptable for long haul flights [1].

However, the airport competitiveness is not the only factor that is influenced by airport access/egress link:

- *Size of the catchment area:* The quality of ground transport can significantly influence the size of the catchment area and give an airport a competitive advantage over other airports in the region [1].
- *Airport's finances:* High share of individual car access trips requires investments into constructing multi-level car parks in the terminal buildings vicinity. On the other hand, revenues from parking fees represent an important part of airport revenues [1].
- *Terminal operations and capacity:* Access trip duration and access mode reliability significantly influences the arrival earliness pattern of passengers. This consequently has an impact on time spent by passengers in the terminal building prior to their departure and on utilisation of terminal facilities [3].
- *Environment:* Traffic generated by the airport has a major influence on the surrounding environment. This influence increases with the size and throughput of the airport, its proximity to the built up residential area and with the share of individual car access trips [4].

Despite these facts, the problems of airport ground access are still being underestimated. Many studies dealing with the problems of airport landside operations are focused mainly on the processing part of the airport terminal and consider the airport terminal to be an isolated system. Even most of airport landside operations models developed using either generic or dedicated simulation software packages (e.g. PaxSim, SLAM, WITNESS, ARENA or EXTEND) are designed for simulating the passenger and baggage flows only between curb-side and apron. Although this approach provides valuable data concerning capacity, delays or processing bottlenecks, in some cases, identified capacity constraints are only the symptoms of the actual problem. In order to identify the cause of the problem, it is necessary to consider the airport terminal as an integral part of much more complex regional, national or international transportation system.

In order to fill this gap in research and development, our research aims at developing passenger flow model that would be able to simulate passenger flows from the place of origin (e.g. home or office) to the airport and back. Thanks to this model, it is pos-

* **Benedikt Badanik, Milan Stefanik, Martin Matas**
Air Transport Department of the University of Zilina, Slovakia, E-mail:bedendikt.badanik@fpedas.uniza.sk

sible to consider airport as an integral part of the whole transport chain rather than isolated system (i.e. from curb to curb) and thus analyse and investigate the relationship between traffic flows within airport's catchment area and terminal operations. The result of our research and development is Airport Ground Access and Egress Passenger Flow model (AGAP model) that simulates passenger flows from door to curb. On top of that, the AGAP model in combination with some of airport landside operations models enables to simulate passenger flows within entire door-to-door transportation process. Thanks to this feature, the AGAP model represents a powerful tool allowing user to perform comprehensive operational, economic and environmental assessment of innovative airport ground access concepts.

2. Airport Ground Access and Egress Passenger Flow model

AGAP model has been developed using MS Excel and Visual Basic programming environment. As it has already been mentioned, the model enables to simulate passenger flows from the place of passenger's origin to the airport and back. Thanks to this airport ground access/egress passenger flow model, it is possible to simulate passenger flows within the airport's catchment area to and from the airport and to investigate the interactions between airport ground access/egress and airport terminal operations [8], [13], [14] and [15].

The Airport Ground Access and Egress Passenger Flow model is a stochastic microscopic computer-based model that simulates entire airport access/egress related traffic within airport's catchment area. Its scope begins at the place of passenger's origin/destination and ends in the airport terminal. The model consists of the following two modules (see Fig. 1):

(1) Air passenger trips generation module (see light grey area in Fig. 1): This module is responsible for simulating the demand distribution within the airport's catchment area. Based on the input data this module allocates passengers to particular flights, generates passenger groups and passenger distribution to the cities within airport's catchment area.

(2) Passenger transport mode choice module (see dark grey area in Fig. 1): This module is responsible for simulating passenger airport ground access/egress mode choice. Based on outputs from air passenger trips generation module this module selects the most favourable airport access/egress transport mode taking into account price, travel time and convenience. This module employs algorithm of passenger behaviour.

3.1 Air Passenger Trips Generation Module

A flight schedule is the source of primary input data for generation the air passenger trips. Before the flight schedule can be imported into the AGAP model, it has to be supplemented by additional information and all the data needs to be pre-processed to ensure they are in correct format. A completed flight schedule contains the following information on each flight:

- Flight number
- Scheduled and actual time of departure
- Destination airports
- Aircraft operator, aircraft type and seat capacity, load factor
- Indication if flight is international or domestic; scheduled or charter
- Indication if flight's destination is a holiday resort
- Share of business and leisure passengers in flight
- Possible times of arrival (assuming that passenger uses services of the same operator for both outbound and inbound flights)

Based on the information from the flight schedule (i.e. based on flight type, destination, aircraft capacity, load factor, and proportion of leisure and business passengers) the model allocates passengers to each particular flight. The characteristics related to passenger flows within airport's catchment area are then randomly generated and assigned to each passenger based on relevant probability distributions.

In the first step of the algorithm, the model generates the sizes of passenger groups. The air passengers often travel in groups of various sizes (e.g. families, couples, friends, business partners etc.). The group sizes are different for business and leisure passengers (see Fig. 2). Each passenger type has a probability distribution of the group size. These probability distributions are used to generate passenger groups for the flight. The algorithm generates the groups in the cycle until the number of passengers reaches the actual number of passengers in the each particular flight from the flight schedule.

In the second step, the model assigns the place of trip origin/destination to each group of passengers. The region of the trip origin/destination is randomly assigned to each passenger group based on probability distribution that reflects the distribution of air transport demand within the airport's catchment area. The city of the trip origin/destination is randomly assigned to each passenger group based on the population distribution within particular region. The assignment of region and city of passenger's origin/destination is proportional. It means that if a particular region has higher air transport demand than another one, the probability that the passengers are from this region is proportionally higher. Same analogy is used in the case of city assignment. It means that if a city within particular region has higher population than another one within the same region, the probability that the passengers are from this city is proportionally higher.

In the third step, model randomly generates length of passengers' stays in their flight destination. The following figures depict passengers' stay length distribution (see Fig. 3 and Fig. 4). This parameter is important for assigning proper inbound flight to each passenger. On top of that, this parameter directly influences parking fees at the airport, which has direct impact on transport mode choice.

All the above mentioned characteristics were identified to be the key factors influencing the airport ground access mode choice process. By assigning these characteristics to each passenger, the

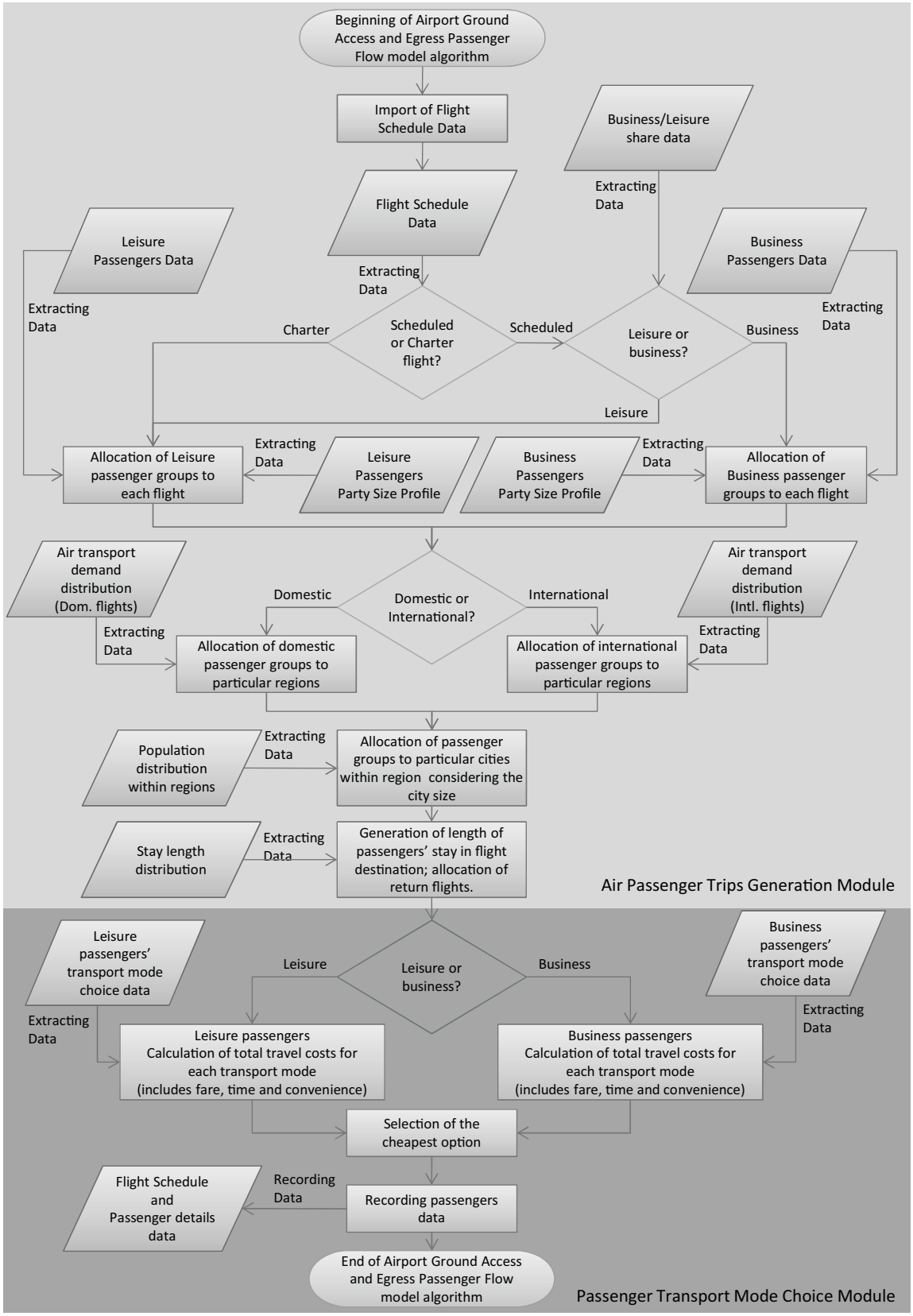

Fig. 1 Airport Ground Access and Egress Passenger Flow model Algorithm

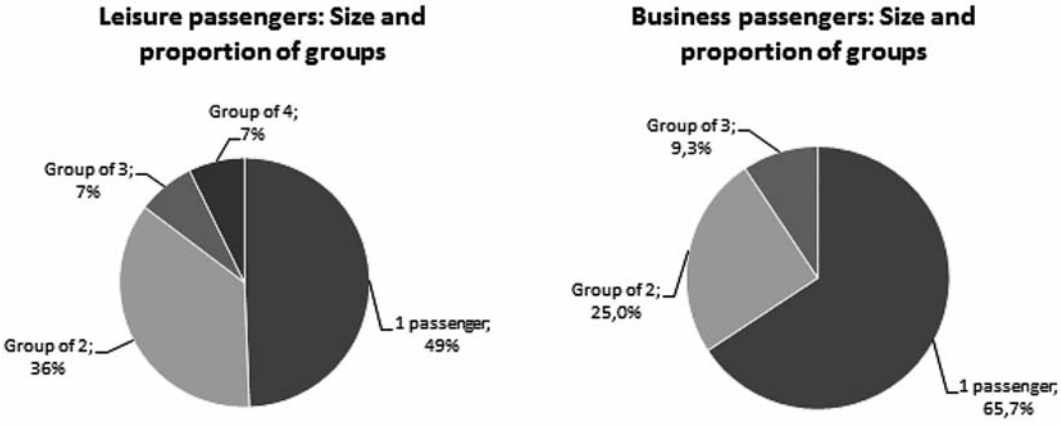

Fig. 2 Size and proportion of passenger groups (Source: Bratislava airport)

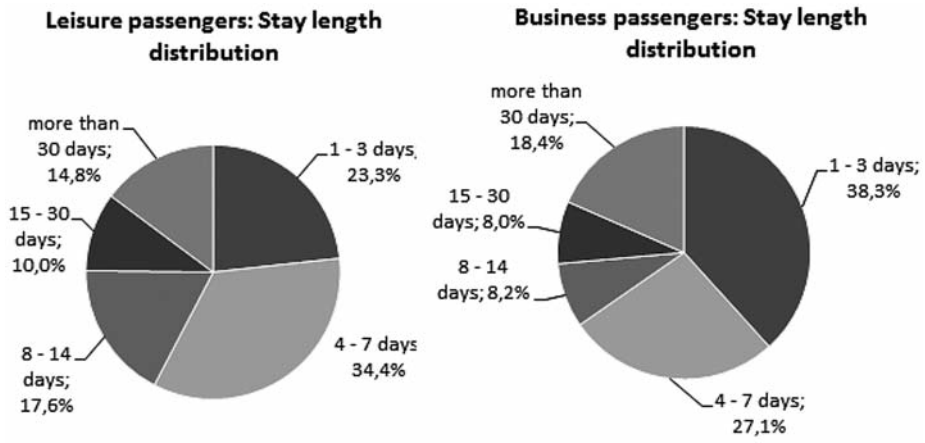

Fig. 3 Scheduled flights: Passengers' stay length distributions (Source: Bratislava airport)

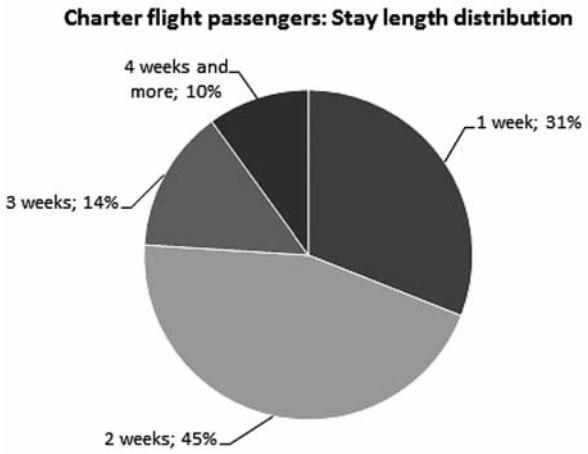

Fig. 4 Charter flights: Passengers' stay length distributions (Source: Bratislava airport)

Air Passenger Trips Generation Module defines a very complex passenger typology.

3.2 Passenger Transport Mode Choice Module

The algorithm of passenger transport mode choice that is used in the AGAP model is based on evaluation of the perceived costs of each transport mode. Thanks to this approach, it is possible to consider both quantitative and qualitative factors influencing the passenger mode choice. The AGAP model automatically selects the most favourable option in terms of price, travel time and convenience for each passenger.

The perceived costs of transport consist of the financial costs, time costs and transfer costs. The financial costs represent the money value needed to get from the place of origin to the airport and back including all related charges such as parking fees in case of car transport etc. The time costs represent a perceived value of in-vehicle travel time and excess travel time (i.e. waiting, walking, transfer time, etc.). The transfer costs represent a perceived value of additional physical and cognitive effort resulting from the transfer, and perceived value of risk of missing the connection. Both value of time and value of transfer were quantified based on average passenger income. Thanks to this approach, it was possible to con-

sider price sensitivity and time sensitivity of particular types of passengers (see Tab. 1).

Recommended Travel Time Values [16], [17] Tab. 1

Time component	Relative to wages
In-vehicle Personal (local)	50%
In-vehicle Personal (intercity)	70%
In-vehicle Business	120%
Excess (waiting, walking, or transfer time) Personal	100%
Excess (waiting, walking, or transfer time) Business	120%

The AGAP model evaluates perceived costs of the following airport access/egress transport modes:
- Individual car – 'Kiss and drive'
- Individual car – 'Park and fly'
- Taxi
- Public city transport
- National public transport + Taxi
- National public transport + Public city transport

Before AGAP model starts to calculate the perceived costs for particular airport access/egress modes, it has to calculate distances, travel times, waiting times and number of transfers for each airport access/egress option.

In the case of access/egress trips by individual cars (i.e. 'Kiss and drive' and 'Park and fly'), model gathers all the required information regarding distances and travel times from the database containing comprehensive information on road network within airport's catchment area. The time when passenger arrives at the airport before STD (Scheduled Time of Departure) of his/her aircraft is randomly generated by the model using normal probability distribution. The time when passenger leaves the airport after ATA (Actual Time of Arrival) of his/her aircraft is defined by fixed value that is estimated based on analysis of the arrival processes at particular airport.

The information related to access/egress trips by taxi are calculated and processed using same approach as in the case of individual car trips. The only difference is that in the case of taxi trip, the model randomly generates time that passenger spends by waiting for a taxi.

The information regarding national/urban public transport between particular parts of catchment area and airport are gathered from the actual public transport timetable database. The public transport timetable database contains information regarding travel times, service frequency, departure/arrival times and number of transfers for all public transport connections within the airport catchment area. The model selects the most favourable outbound and inbound connections from the database, considering the following factors:
- Passenger's itinerary defined by departure/arrival time of his/her flight;
- Price of the connection;
- Total travel and waiting times;
- Number of transfers.

The time when passenger arrives at the airport before STD of his/her aircraft is given by the public transport itinerary of particular passenger. The time when passenger leaves the airport after ATA of his/her aircraft is given by the arriving processes at the particular airport and by time that passenger spends by waiting for the public transport connection (calculated based on the public transport itinerary).

When the model compiles a set of traffic flow related information (i.e. distances, travel times, waiting times, transfers, dwell times in terminal etc.) for each airport ground access/egress option considering a specific needs and requirements of each particular passenger, it is ready to calculate perceived costs. The value of perceived costs for all of above listed airport access/egress transport modes is calculated using the following equation (1). The perceived costs are calculated for return trip as we assumed that passengers will use same transport mode for travelling to the airport as well as from the airport. We also assumed that when choosing airport ground access/egress mode, the passenger considers perceived costs of both outbound and inbound trip.

$$\textit{Perceived Costs} = \textit{Financial Costs} + \textit{Time Costs} + \\ + \textit{Transfer Costs} \ \text{[Eur]} \qquad (1)$$

Formulae for calculating particular elements of the equation depicted hereinbefore (i.e. for calculating financial costs, time costs and transfer costs) are significantly more complex. Moreover, each of considered airport ground access option has separate formula for calculating financial costs, time costs and transfer costs. For this reason, it was not possible to list all used formulae in this paper. On the other hand, the approach used for calculating these parameters was clearly described in the text hereinbefore. Detailed description of the Passenger Transport Mode Choice Module algorithm including all used formulae can be found in [15].

Assuming that airport access/egress ground transport mode with the lowest perceived costs would be the passenger's choice the AGAP model assigns the cheapest transport option to particular passenger. From statistical point of view, the selection of the cheapest option in terms of perceived costs is justifiable approach. However, we are aware that this approach does not fully reflect the actual process of transport mode selection as it automatically excludes more expensive options. In real life, the cheapest option represents the highest probability of choice and the most expensive option represents the lowest probability of choice. It means that any of considered options has probability of choice greater than zero. This issue is going to be solved within further research by incorporating a more sophisticated demand modelling algorithm into the AGAP model.

The main data output from the Airport Ground Access and Egress Passenger Flow model is an Excel spreadsheet where the

information about the passengers is stored. It includes the passenger ID number, place of origin, group size, transport time etc. The most important aggregate information includes:

- Total travel time
- Total distance travelled
- Travel costs
- Arrival earliness distribution of passengers

The travel time, distance travelled and travel costs are used as performance indicators necessary for the analysis of passenger flows within the airport catchment area and for comprehensive operational, economic and environmental assessment of the airport ground access/egress solutions. The arrival earliness pattern is key information for assessing the impact of airport ground access/egress on the airport terminal operations.

When performing operational, economic and environmental assessment of some airport ground access concept, the AGAP model simulates the airport access/egress part of the door-to-door transportation chain (i.e. between passenger origin/destination and entrance of the airport terminal). In order to investigate the impact of airport access/egress on passenger processing within the airport terminal, it is necessary to use some of airport landside operations models. In such a case, the outputs from AGAP model are used as inputs for airport landside operations model.

At this stage of research and development, the AGAP model is customised for simulating passenger flows within catchment area of Bratislava airport. Operation division and Marketing & Commerce division of the Bratislava airport supported this research initiative and provided us with all the data necessary for calibration and validation of the model.

3. AGAP model verification and validation

The model assumptions are based on extensive passenger survey at Bratislava airport (performed during summer season in 2003, 2004 and 2007) and also on operational data collection exercise that was performed at Bratislava airport and at Brno-Turany airport.

During the design process of the model we created a sample of 100 passengers (randomly generated). For these 100 passengers, we calculated all the parameters manually (e.g. group size, place of origin/destination within airport's catchment area etc.). During entire development process the functionality and accuracy of the AGAP model was verified using this testing sample of 100 passengers. Thanks to this verification process, we reduced the probability of creating the software bugs.

In order to validate used algorithms and verify assumptions that were taken into account the simulation results were compared with actual operational data. The AGAP model validation showed that the simulation results approximate the real operations. The simulation results accuracy was verified by means of the following parameters:

- Arrival earliness distribution of passengers (see Fig. 5);
- Proportion of airport ground access/egress transport modes (see Fig. 6).

As can be seen from the charts the simulation results correspond to the actual operational data.

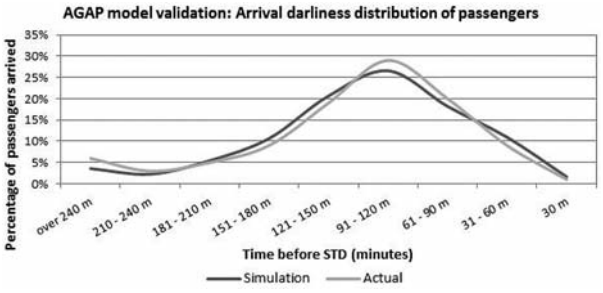

Fig. 5 AGAP model validation: Arrival earliness distribution of passengers

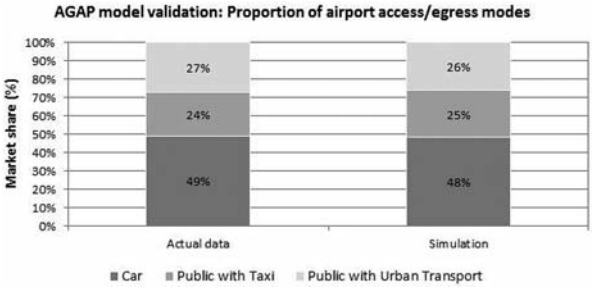

Fig. 6 AGAP model validation: Proportion of airport access/egress transport modes

4. Making AGAP model an efficient tool for airport design and planning

The operational capabilities of the AGAP model have already been used for operational, economic and environmental assessment of two innovative airport design concepts hypothetically implemented in the Bratislava airport environment:

'Pick-up/Drop-off' airport ground access concept: Using the AGAP model for simulation of passenger flows within the airport's catchment area and PaxSim model for simulation of passenger and baggage flows inside airport terminal, we compared current design of airport ground access/egress system at Bratislava airport with an innovative concept based on dedicated minibus network serving the entire catchment area. The minibus network was designed for collection, transportation and distribution of air passengers. Operation of minibuses within this network would be based on the analogy of collection, transportation and distribution of consignments within express carriers' regional distribution network. This principle would allow introducing a high-level coordination and synchronization between air and ground transport. The simulations

showed that the proposed 'Pick-up/Drop-off' airport ground access concept would significantly contribute to improvement of passenger flow efficiency and passenger processing efficiency, which would consequently be reflected in reduction of travel times, reduction of dwell times and reduction of travel costs. On the other hand, expected positive impact of more efficient passenger flows on the environment (based on simulation results) turned to be negligible [8], [13] and [15].

Airside-Landside separation concept: This concept is based on the physical separation of the landside from airside and connecting these two with the synchronised and coordinated high-speed transport means. Their idea is based on bringing the terminal areas back to the city while the runways could be built far from the city, where the capacity extension constraints are significantly lower than those in the city area. While this concept would potentially bring operational assets to future airports, our simulation proved that in terms of passenger flow efficiency the concept would not bring any significant benefits. The concept could even cause longer dwell times compared to conventional airport concepts [11], [12] and [14].

5. Conclusions and recommendations for future work

This paper describes and demonstrates the capabilities of the AGAP model that can be used for performing operational, economic and environmental assessment of future airport design concepts. This simulation model enables to perform fast-time simulation of door-to-door passenger flows and thus allows seeing the airport terminal as an integral part of regional, national or international transportation network. Thanks to this fact, it is possible to analyse the interactions between airport ground access/egress and passenger and baggage flows inside airport terminal building. The new method based on using the AGAP model reveals an innovative approach to performing comprehensive operational and environmental assessments of future airport design concepts.Using this new method, we have already performed an operational, economic and environmental assessment of two innovative airport design concepts. Thanks to microscopic simulation of door-to-door passenger flows we were able to conduct initial feasibility assessment of these concepts and identify their potential benefits and drawbacks.

More comprehensive validation of model outputs will enable using a developed simulation model as a decision making support tool in real operations.

Within further research, we will also focus on the following issues:

- Development of more sophisticated algorithms of passenger transport mode choice (e.g. current model assigns each passenger with the cheapest transport option, which does not fully reflect the actual passenger preferences);
- Integration of algorithms reflecting the probability of delay in both, air and ground transport.

Although algorithms incorporated in the AGAP model are generic and could be used for evaluation of airport ground access system at any airport, the model itself is customized for the Bratislava airport operational conditions. The simulation of passenger flows within airport's catchment area is very demanding in terms of availability of operational and statistical data. Moreover, data collected at one airport cannot be used for evaluating the airport ground access system at another airport as operational conditions at each airport are unique. Due to operational data availability, Bratislava airport was the number one choice when developing the AGAP model. Management of Bratislava airport was willing to cooperate with us in this research initiative and provided us with comprehensive set of required operational and statistical data. For this reason, in all studies that were conducted using the AGAP model, Bratislava airport was used as a case study.

We support research activities in Slovakia/Project is co-financed by EU Centre of Excellence for Air Transport ITMS 26220120065

References

[1] KAZDA, A., CAVES, R. E.: *Airport Design and Operations, Second Edition;* Elsevier, 2007
[2] M3 Systems, ANA, ENAC, LEEA: CARE II: The Airport of the Future: Central Link of Intermodal Transport? WP1: Review of current intermodality situation; EUROCONTROL Experimental Centre; October 2004
[3] ASHFORD, N., STANTON, H. P. M., MOORE, C. A.: *Airport Operations, Second Edition;* McGraw-Hill; 1997
[4] IATA: Airport Development Reference Manual, 9th Edition, IATA, 2004
[5] TETHER, B., METCALFE, S.: *Horndal at Heathrow?* Cooperation, Learning and Innovation: Investigating the Processes of Runway Capacity Creation at Europe's Most Congested Airports, The University of Manchester, UMIST, June 2001.

[6] NEUFVILLE, R., ODONI, A. R.: *Airport Systems: Planning, Design and Management,* McGraw-Hill, 2003.
[7] Preston Aviation Solutions, PaxSim Solutions User Manual, Preston Aviation Solutions Pty Ltd., 2006.
[8] STEFANIK, M.: *Problems of Airport Capacity Assessment,* Doctoral Thesis, University of Zilina, 2009.
[9] ASHFORD, N., STANTON, H. P. M., MOORE, C. A.: *Airport Operations, 2nd Edition,* McGraw-Hill, 1997.
[10] COKASOVA, A.: *Analysis of Passenger Viewpoints and of the Practical Shift in Air Rail Intermodal Transport,* PhD. dissertation, University of Zilina, 2006.
[11] MATAS, M.: *Future Airport Concept,* University of Zilina and Eurocontrol Experimental Centre; 2004
[12] MATAS, M., BROCHARD, M.: *The Airport of the Future or what can be the Airport in the Year 2020 and After?,* Eurocontrol Experimental Centre Innovative Research Activity Report; 2004.
[13] STEFANIK, M., BADANIK, B., MATAS, M.: Designing Sustainable Airport Ground Access/Egress Systems Supported by Fast-time Modelling; *J. of Civil Engineering and Architecture;* Vol. 4; No. 9; September 2010
[14] MATAS, M., STEFANIK, M., KROLLOVA, S.: Door-to-Gate Air Passenger Flow Model; 4th Int'l Conference on Research in Air Transportation, ICRAT 2010; Budapest; June 2010
[15] STEFANIK, M.: *Airport Landside Capacity: Making Airports Intermodal Transport Nodes;* Lambert Academic Publishing; January 2011.
[16] TCRP: *Report 78 - Estimating the Benefits and Costs of Public Transit Projects: A Guidebook for Practitioners;* Transit Cooperative Research Program; Transportation Research Board of the National Academies; 2002
[17] LITMAN, T.: *Valuing Transit Service Quality Improvements Considering Comfort and Convenience in Transport Project Evaluation;* Victoria Transport Policy Institute; 2008.

Martin Hrinko *

PREVENTIVE MEASURES AND ACTIONS OF THE POLICE OF THE CZECH REPUBLIC AGAINST URBAN VIOLENCE

The following article addresses the current problem of urban violence. The aim of the article is to outline the different preventive measures and actions of the Police of the Czech Republic taken in order to prevent urban violence. Moreover, various ways of documentation of illegal acts are presented. Having been the officer in charge during operations conducted against urban violence, the author also shares his practical experience.

1. Introduction

Regulation of safety measures against the illegal act of spectator violence (generally also known as urban violence) stems from the binding directive of the Police Headquarters No. 10/2009 entitled "Maintenance of internal order and security". The term "urban violence" comprises various forms of public and collective disturbance of public order in urban areas as well as signs of extremism (music production, radical groups' marches, etc.). The aforementioned directive governs the proceeding of the police when taking measures against negative events which may influence safety situation; when using disciplinary units, anti-conflict teams (ACT), spotters, etc.; when ensuring internal order and security; when ensuring organisation of disciplinary units, their armature, equipment as well as other material and technical provisions.

2. The origin and history of stadium violence

The history of football and football violence in particular can be probably traced back to the end of the 19th century. This gave rise to a first football association whose role, among others, was to solve riots at stadiums. Due to increasing violent conflicts, the association had to adopt adequate measures (e.g.: between the years 1895–1897 the English Football Association had to close up 21 football playgrounds and warned other 23 clubs of fans' misconduct. The situation, however, did not improve at the beginning of the 20th century; there were even events during which mass incursions of fans flooded the playgrounds. These were most frequently reactions to umpires' ruling and unsatisfactory performance of football players. During the interwar period, these incidents were no longer the centre of attention[1)]. Later, the 1950s became a historical milestone in the history of football fan clubs. The football season 1968–1969 brought about the emergence of large fan groups completely devoted to their teams. The groups did no longer count several, but rather thousands of members, who established their own rituals, symbology, hymns and cries. The worst thing about this new phenomenon was that the purpose of the fans' devotion to one football team or another was not primarily to support their favourite teams, but above all to assault the opposing team's fans and other participants on the day of the match. During the football match, these fans could be seen at their favourite spot – mostly right behind the goal or in the corners of grandstands (known as "End"; the Czech equivalent translates as "Mosh pit" into English). The common spectators often witnessed a violent incident also in the grandstands, as the radical fans of the two teams found pleasure in attacking the other team's "mosh pit".

3. The situation in the Czech Republic

The first incidents of football hooliganism in the Czech Republic can be traced back to the beginning of the 1980s. At that time, many fan clubs were founded and their members looked for enemies among the members of other fan clubs who would later, in the grandstands during the match, make a perfect target of their attack. Until then, no mass stadium violence could be seen at football matches in the Czech Republic. I remember the times when we used to go to watch a football match and support our favourite team properly. Our main aim was to watch the game, show some support, have a hot dog, maybe a beer. The football match between Sparta Praha and Dukla Banska Bystrica in 1985 was a real breakthrough in football hooliganism also outside of stadiums – the Sparta Praha fans vandalised a train on their way to Slovakia. The VB (a police force of the Czechoslovak Socialist Republic at that time) had to make the first intervention outside of stadium – at a train station. The event was later made into a film which documented football hooliganism in the republic. The film was entitled ´"Why?" and it raised many questions regarding the condemnable misconduct of the Sparta Praha fans. Unfortunately, this film also inspired other

* **Martin Hrinko**
Police CR, KRP Moravskoslezskeho kraje, Ostrava, Czech Republic, E-mail: martin.hrinko@seznam.cz

[1)] The violent incidents were described as „blaster of hot-heads" who have a low sense of self-control (King, 1997).

radical fans to organise mass tours to host cities to support their team. With respect to increasing violent incidents connected with football, there was a first fatal accident – one of the radical fans (who participated in a violent encounter of the Sparta Praha fans and the Pilsen fans) followed by police officers, knocked down an old lady at the train station in Pilsen. The next serious accident was caused by the Banik Ostrava fans who, when throwing stones at a train carrying the Sigma Olomouc fans, hit a random passenger. As a result of the accident, the woman went blind for life. Many other casualties were reported (their description and list of all of them would surely exceed the content of this work).

In reaction to this trend (the number of riots at stadiums was approximately the same as the number of riots outside of stadiums), the number of police safety measures accepted and the use of police forces and means increased. As a result, there was a lack of police forces and means during regular guard duties in the streets. Thus, the police on behalf of the Minister of the Interior called for change of legislation. The first amendment was probably imposed by Act No. 283/1991 Coll. on the Police of the Czech Republic, later amended by Act No. 273/2008 Coll. on the Police of the Czech Republic (efficient from 1.1.2009). Among others, this new act led to conclusion of an Agreement between the Football Association of the Czech Republic (abbreviated to FACR) and the Police of the Czech Republic. It regulates their cooperation, construction and technical equipment of the first and second league stadiums, ensurance of security standards, cooperation between the teams' organising service and the police, training and scope of activity of the organising service and common media policy. The Agreement also regulates duties of the subjects who participate in organisation of the match and ensure security. *The biggest responsibility for security at stadiums lies with the organising service.* If they are unable to deal with a certain situation, they may call the Police of the Czech Republic. The police officers are deployed at the proximity of stadium during a match; they ensure security outside the stadium and ensure safe transfer of the fans to the stadium. This newly imposed procedure provoked many discussions between the FACR officials and the Government, Ivan Langer (the Minister of the Interior, at that time) in particular. Especially, the common spectators were not sure whether their safety was guaranteed, as the security was to be ensured by a private security service, lacking the safety means, the training and the rights needed for execution of the duty. In the Czech Republic, the sports agenda lies in the hands of the Ministry of Education, Youth and Sports of the Czech Republic, which is the state central administrative authority for physical education, sport, hiking and sports representation of the State. Spectator violence agenda lies in the hands of the Ministry of the Interior of the Czech Republic, which is the state central administrative authority for domestic affairs, particularly for public order, other domestic affairs and security [1].

4. The Police and service regulations

Based on this directive, the Police convene the forces and means needed in order to ensure public order. Such organised convocation is called a safety measure, police measure or police action, depending on the extent of the measure being taken and on the number of forces and means convened.

„Safety measure" is according to the directive the first and the most extensive measure of the three. This type of measure is performed by the Police and other entities (e.g. § 3, Act No. 239/2000 Coll., § 240/2000 Coll.) in order to ensure internal order and security. The recent co-operation among the Integrated Rescue System units (IRS) during the football match between two top teams in the league – FC Banik Ostrava and FC Sparta Praha on 2 May 2010 can serve as an example. During the event, all the services of the Police of the Czech Republic were co-operating: the train escort department, the ACT, the disciplinary units, the heavy armoured personnel, the division of disciplinary and traffic service, the division of crisis management, the criminal police and investigation services, the district departments and the departments of transport. Also, the Municipal Police of Ostrava (the department of hippology, the operative intervention unit, the kynology unit, the municipal police stations), even the Fire Emergency Brigade, members of the Rescue Service teams and – last but not least – officers of Polish Policja were involved in the event. The specific football match is named purposedly in this article – the visiting team's fans' behaviour had to be repressed. During the course of the action, historically, the highest number of people were taken into custody. Having passed the screening, the 370 illegally acting fans were subsequently forced to return to Prague under further supervision of the police forces (see Figs. 1, 2).

Fig. 1 The fans of the visiting team are handcuffed for having repeatedly refused the orders of the police [1]

Such procedure taken by the Police of the Moravian-Silesian region represented a clear message to football fans – the police are able to supervise and accompany fans securely to the so-called "hazardous matches", so that common traffic and order in cities are not at risk (the police design routes through which, with the assistance from ACT members, the fans are directed). Understandably, the police also ensure security of the fans, so that fights among the fans of the two different teams are prevented. The police are ready to use forces and means needed to suppress any aggressive behaviour of the fans, who, when drunk, often irrationally seek to struggle with the police officers. From my personal experience,

many fans do not even care how their favourite team are playing or what the actual score is – instead, they tend to focus on how to organize fights with fans of the opposite team, so that they are not suppressed by the police forces.

Safety measure is directed by a Commander, who controls the staff. Both the Commander and the staff are chosen by order of the Chief of Police or the Chief of Regional Headquarters. According to its purpose, safety measure is usually performed by members of IRS units or members of various services of the Police of the Czech Republic available in the location.

Fig. 2 Fans accompanied by police officers are leaving Ostrava against their will [2]

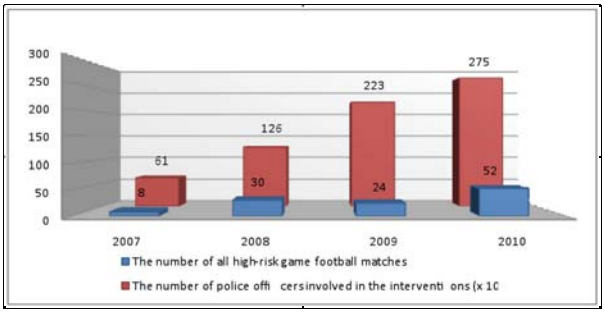

Fig. 3 An overview of all high-risk football matches, during which the order service assisted, and the number of police officers involved in the interventions.

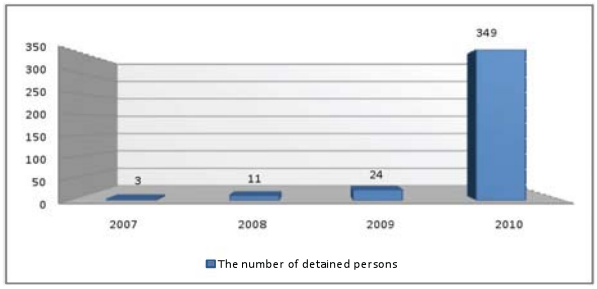

Fig. 4 An overview of the number of persons put under detention during safety interventions at or outside of stadiums in the Moravian-Silesian Region.

„Police measures" are in fact very similar to safety measures. However, other IRS units are generally not involved in the course of their action. During a police measure, various police services are combined in order to fulfill the purpose of the measure (e.g. during a foreigner residence check, the following services are involved: the Alien Police, the criminal police and investigation services, police officers from the district offices, etc.) Police measure is directed by a Commander, who is chosen by instruction or order of the Chief of Territorial Division or the Chief of Regional Headquarters.

„Police action" is a uniphase and temporary operation, during which police measures are performed and which cannot be ensured by common service in a certain area. Proceedings done during an operative elaboration as well as unexpected operations and measures taken to allow the performance of police tasks (e.g. inspections in restaurants, which are performed by forces and means of the relevant district department) are not considered a police action. Police action is directed by a Commander, who is chosen by instruction of the Chief of District Department or the Chief of Territorial Division.

5. Spotting

Spotters co-operate with local sports clubs and fans, they monitor hazardous fans and accompany and supervise "their" hazardous fans to and from sports matches. Spotters, who accompany fans, fall under the command of the Commander of the safety measure within the area where the match is played; during hazardous and international matches, the spotter is always a member of the Commander's staff. Spotters undergo a special training which prepares them for work with crowd, knowledge of the particular environment. They also have personal experience with hazardous fans, their behaviour and the potential risks, which might occur. The hazardous fans know their spotters. Spotters stand for a unique documentary team which monitors illegal acts of the fans by hand cameras. Such recordings then help when searching for specific unlawful acts and they represent a very useful supplement to helicopter monitoring of the events. Spotters´ shots are done mostly in crowds, from side stands, platforms, tribunes, etc. When shooting, spotters are dressed in civilian attire and they are usually members of the criminal police and investigation services. The shots taken by spotters very often help to prove offenders guilty. If an offender is proven guilty, the Commander tactically decides whether the offender will be taken into custody during the match, during the directed transit, in a means of transport or eventually the following day at the place of his permanent residence.

6. Anti-conflict team

The so-called anti-conflict team (abbreviated to ACT) is a new form of preventive action of the police used to prevent unlawful

conduct during mass public events where disturbance of public order is likely to occur. The establishment of anti-conflict teams was inspired by the Second division of the emergency order service in Berlin (also for other reasons besides the fact that the Berlin police are one of the best in Europe). The original inspiration by the French Crisis Corps' operation was inconvenient due to different rights the Corps possessed (compared with the Czech police). The establishment of anti-conflict teams was also encouraged by JUDr. Otakar Motejl (former public defender of rights – ombudsman) in his assessment report. He criticised the police for insufficient documentation of unlawful conduct committed during high-risk events. He assessed the specific police intervention in Tachov area as lawful, but inadequate. The establishment of three pilot anti-conflict teams in the Czech Republic was based *on the command of the Chief of Police No. 54/2006*. The Czech Republic is currently the second country in Europe to have these preventive police teams. At first, the teams were part of three regional police headquarters – the regional department of North Bohemia (in Ústí nad Labem), North Moravia (in Ostrava) and West Bohemia (in Pilsen). The choice of these three regions was not random, each of these regions experienced violent conflicts with the public. There were several techno parties in North Bohemia and West Bohemia, there are many radical, mostly football fans in North Moravia. Nowadays, also the rest of the Regional Headquarters of the Police of the Czech Republic are involved in the project. There were made some alterations of certain police procedure standards used during police interventions against large groups of people. The basis of the reform of this police procedure is prevention within the framework of tactical prevention interventions. The anti-conflict teams liaise with the police (the order service) and the participants of public events. Among others, their roles are:

- to anticipate aggressive conduct by the means of clear communication (and instruction);
- the members of the team intensely explain the purpose of the police interventions and, if needed, they discuss with citizens the possible problems which may arise from the situation;
- the members of ACT inform the participants of the event about lawful police measures which will be taken in case unlawful conduct occurs.

The members of ACT focus on their target groups (participants of the event, local inhabitants, spectators and the media). The members of ACT are entitled to inform the media about the most basic facts regarding their operation [3].

7. Ways of monitoring and documenting acts of urban violence

Besides helicopter monitoring and spotters' shooting of illegal acts, the police also use hand cameras to document both unlawful acts of offenders and action of disciplinary units of the Police of the Czech Republic. These records are shot by police officers of the documentary team of the disciplinary units. Moreover, the police can also use the recordings shot by municipal police stationary cameras or by the Mobile Monitoring Centre (MMC – Commander's truck equipped with cameras and thermovision).

8. Specific cases of mass behaviour

Situations where there exists danger of occurrence of mass behaviour (which requires more attention from the order service) can be divided into five categories. In the Czech Republic, judging from the number of the police interventions, the first come *spectator violence* interventions. Escalation of violence and disturbance of public order often occur during *demonstrations.* Last but not least, the order service intervenes during *mass cultural events, searches* and *short time safety interventions* aimed at vehicle checks (road traffic safety measures) or ensurance of public order (e.g. minors alcohol tests). Essentially, we can distinguish two types of public order surveillance – a coercive style and a consensual style. A coercive style can be characterised by visible presence of the order service and their early employment (paramilitary style). By contrast, a consensual style can be characterised by negotiations, non-violent intervention and communication, which precede the actual employment of the order service. Mass behaviour occurs most likely when the police use command and control' policy. By showing zero tolerance or escalating the forces, the police in fact paradoxically support the groups of people, who are very familiar with acting in the same way. This police style therefore increases influence of the violent groups of people. If the police use negotiation, violent incidents decrease, because the people who encourage and initiate violence do not get much support from other members of the group (unlike when the paramilitary attitude is used). Undoubtedly, the most renowned scientist who studied mass behaviour was Gustave Le Bon. According to his work, a crowd behaves irrationally. The crowd's characteristics are anonymity, mind infection, suggestibility. When being a part of a crowd one's control over their instincts, which they would normally suppress, decreases; their sense of responsibility is low. When being a part of a crowd one essentially becomes a robot, incapable of voluntary behaviour; one becomes a wild uncontrollable creature. The characteristics of a crowd are impulsiveness, changeability, provocativeness, incapability to think reasonably, lack of judgment and critical thinking, emotional exaggeration [4].

9. Summary

The phenomenon of spectator violence is certainly not a new one; it is known to have existed for a long time. Unfortunately, it needs to be said that this "English disease" which accompanies football also occurs in the Czech Republic. Consequently, during the high-risk football events, there is ever-present threat of incidents and need for appropriate safety interventions over the course of the fans' journey to and from the particular city, on the routes to and from the stadium, upon their entrance at the stadium and in the grandstands. Many media reports from football matches do not cover only the game itself, but also the football hooliganism caused before, during and after the match. Therefore, we can often see a report from a long-expected football match depicting police cordons and crowds of rioting fans, we can hear police car sirens wailing and it all seems to us as a vulgar and violent show in live broadcast.

The article described the problem to a phenomenon known as urban violence, which the Police of the Czech Republic gradually and increasingly effective fighting and looking for ways to combat this illegal activity. The interventions of the order service are very demanding and have a very complicated background which cannot be easily revealed to the public. This article attempts to offer at least a partial insight into the background.

In this article the author provides the reader with background work in police practice by starting the article writing from his own practical experience gained in commanding policemen and the establishment of labor and resources of many police actions.

References

[1] HRINKO, M.: *Legal aspects of spectator violence in practice (in Czech),* Monographs, Prague 2011: p. 67, Institute of Legal Studies, Prague

[2] Web page link [date accessed: 2.5.2010]: *Sparta football fans in Ostrava seen, lying on the road to the stadium (in Czech),* Novinky.cz, can be accessed online at: http://www.novinky.cz/domaci/199121-priznivci-sparty-fotbal-v-ostrave-nevideli-lezeli-na-silnici-pred-stadionem.html.

[3] Web page link [date accessed: 9.1.2011], ZAMEK, D.: Quo Vadis AKT, can be accessed online at: http://bezpecnostni-sbory.wbs.cz/clanky/1-2009/Quo_vadis_AKT-1.htm.

[4] JUNGWIRTOVA, J.: *The Police units and the Mob (in Czech),* Prague 2011: The Press Department of the Interior, magazine Policista, No. 1, supplement – pp. VII-X, ISSN 1211-7943.

COMMUNICATIONS – Scientific Letters of the University of Zilina
Writer's Guidelines

1. Submissions for publication must be unpublished and not be a multiple submission.
2. Manuscripts written **in English language** must include **abstract** also written in English. The submission should not exceed **10 pages** with figures and tables (format A4, Times Roman size 12). The **abstract** should not exceed 10 lines.
3. Submissions should be sent: **by e-mail** (as attachment in application MS WORD) to one of the following addresses: *komunikacie@uniza.sk* or *holesa@uniza.sk* or *vrablova@uniza.sk* or *polednak@fsi.uniza.sk* **with a hard copy** (to be assessed by the editorial board) **or on a CD** with a hard copy to the following address: Zilinska univerzita, OVaV, Univerzitná 1, SK-010 26 Zilina, Slovakia.
4. Abbreviations, which are not common, must be used in full when mentioned for the first time.
5. Figures, graphs and diagrams, if not processed by Microsoft WORD, must be sent in electronic form (as GIF, JPG, TIFF, BMP files) or drawn in contrast on white paper, one copy enclosed. Photographs for publication must be either contrastive or on a slide.
6. References are to be marked either in the text or as footnotes numbered respectively. Numbers must be in square brackets. The list of references should follow the paper (according to **ISO 690**).
7. The author's exact **mailing address of the organisation where the author works, full names, e-mail address or fax or telephone number,** must be enclosed.
8. The editorial board will assess the submission in its following session. In the case that the article is accepted for future volumes, the board submits the manuscript to the editors for review and language correction. After reviewing and incorporating the editor's remarks, the final draft (before printing) will be sent to authors for final review and adjustment.
9. The deadlines for submissions are as follows: September 30, December 31, March 31 and June 30.

COMMUNICATIONS

SCIENTIFIC LETTERS OF THE UNIVERSITY OF ZILINA
VOLUME 13

Address of the editorial office:
Zilinská univerzita
Office for Science and Research
(OVaV)
Univerzitna 1
SK 010 26 Zilina
Slovakia
E-mail: komunikacie@nic.uniza.sk,
pavel.polednak@fsi.uniza.sk

Each paper was reviewed by two reviewers.

Journal is excerpted in Compendex and Scopus

It is published by the University of Zilina in
EDIS – Publishing Institution of Zilina University
Registered No: EV 3672/09
ISSN 1335-4205

Published quarterly

Single issues of the journal can be found on:
http://www.uniza.sk/komunikacie